

HIGH THROUGHPUT PARTICLE SEPARATION USING DIFFERENTIAL FERMAT SPIRAL  
MICROCHANNEL WITH VARIABLE CHANNEL WIDTH

A Thesis  
Presented to  
The Graduate Faculty of The University of Akron

In Partial Fulfillment  
of the Requirements for the Degree  
Master of Science

Abdullah Al Amin

December, 2014

HIGH THROUGHPUT PARTICLE SEPARATION USING DIFFERENTIAL FERMAT SPIRAL  
MICROCHANNEL WITH VARIABLE CHANNEL WIDTH

Abdullah Al Amin

Thesis

Approved:

---

Advisor  
Dr. Jiang Zhe

Accepted:

---

Department Chair  
Dr. Sergio Felicelli

---

Committee member  
Dr. Francis Loth

---

Dean of the College  
Dr. George K. Haritos

---

Committee Member  
Dr. Marnie M. Saunders

---

Dean of the Graduate School  
Dr. George R. Newkome

---

Date

## ABSTRACT

Cell separation is one of the most required processes in the areas of clinical diagnostics, cellular analysis, biological and environmental microbiological processes. Continuous efficient separation of microparticles at relatively high throughput has been a challenge for Lab on Chip (LOC) devices used in biological and environmental applications. In this thesis, a differential area Fermat spiral microfluidic device that is capable of high throughout particle separation is investigated. The device employs a differential area by varying width along with a Fermat spiral microchannel to maintain force ratio close to unity at relatively higher flow rate that facilitates focusing and separation of microparticles at higher throughput. Numerical investigations were performed to validate the performance of the proposed device. Consequently, experiments are performed and it is shown that using the differential Fermat design with particle diameter to channel height ratio of  $0.08\text{--}0.16$ ; the device can continuously sort  $4.6\mu\text{m}$  and  $9.94\mu\text{m}$  spherical particle at a flow rate of  $700\mu\text{L}$ . To demonstrate the capability of high throughput separation of differently sized microparticles, numerical simulation of particle trajectories was performed at a flow rate of  $\sim 1700\mu\text{L}/\text{min}$ .

## DEDICATION

*I dedicate this work to all the graduate students who works day and night to graduate  
with their long cherished graduate degree.*

## ACKNOWLEDGEMENTS

I would like to thank God to provide me with the energy and opportunity to go through the graduate school. My family and friends were my place to resort during the difficult graduate school days. I would also like to extend my gratitude to my advisor Dr. Jiang Zhe for his supervision. I would also like to thank my committee members Dr. Francis Loth and Dr. Marnie M. Saunders for their guidance. I also wish to express my gratitude to Dr. Li Du, Mr. Yu Han and Mr. Xiaoliang Zhu for their prompt support concerning any issues I have encountered throughout the course of this study.

## TABLE OF CONTENTS

	Page
LIST OF FIGURES .....	ix
CHAPTER	
I. INTRODUCTION .....	1
1.1 Overview.....	1
1.2 Motivations .....	4
1.3 Thesis objectives.....	5
1.4 Specific goals .....	7
1.5 Organization of thesis.....	7
II. LITERATURE REVIEW.....	9
2.1 Inertial focusing in a straight channel .....	9
2.2 Inertial focusing in curved channel .....	12
2.2.1 Generation of Dean vortex .....	13
2.2.2 Focusing and separation using Dean vortex .....	15
2.2.3 Spiral microfluidic channel.....	20
III. MODELING OF PARTICLE SEPARATION IN CURVED CHANNEL.....	29
3.1 Proposed differential Fermat spiral microchannel .....	29
3.1.1 Device design and description.....	30
3.1.2 Force analysis .....	32

3.1.2.1	Formation of Fermat spiral.....	33
3.1.2.2	Variation of channel width .....	35
3.1.2.3 ..	Variation in Dean number and average Dean velocity along the flow direction .....	36
3.1.3	Force ratio as a measure of device performance .....	39
3.1.4	Numerical investigation of Dean vortex in a curved channel.....	42
3.1.5	Explanation of the device design .....	50
3.2	Basic theory and modeling equations .....	55
3.2.1	Steady state fluid flow .....	56
3.2.2	Discrete phase modeling.....	57
3.2.3	Calculation of coefficient of lift ( $C_L$ ) .....	59
3.2.4	Validation of numerical simulation.....	62
3.2.5	Simulation result .....	64
3.3	Simulation result at high flow rate.....	67
IV.	EXPERIMENTAL DEMONSTRATION.....	70
4.1	Overview.....	70
4.2	Device microfabrication .....	70
4.2.1	Fabrication of SU-8 mold.....	71
4.2.2	Fabrication of PDMS microchannel .....	74
4.2.3	Plasma bonding of PDMS-Glass substrate.....	76
4.3	Experiments.....	78
4.3.1	Sample preparation .....	79
4.3.2	Experimental setup .....	79

4.3.3	Experimental results .....	81
4.4	Future work .....	87
4.4.1	Bioparticle separation.....	87
4.4.2	TPE-Glass microfluidic system. ....	88
V.	CONCLUSION .....	91
	BIBLIOGRAPHY .....	94
	APPENDIX.....	101

## LIST OF FIGURES

Figure	Page
2-1 Uniformly distributed particles take an equilibrium position of 0.62D from the channel center when flowing through a straight channel.....	11
2-2 Equilibrium position of particles inside a straight channel at the inlet, the red particles were randomly mixed, but as the flow progresses they take an equilibrium position at 0.62D from the centerline. ....	11
2-3 Dean vortices generation on a curved channel.....	14
2-4 Numerical quantification of a Dean velocity profile.....	15
2-5 Forces acting on particles inside a curved channel .....	17
2-6 Scaling of summation of forces on differently sized particles.....	18
2-7 Dean velocity profile along the channel mid-plane from the outer wall towards the inner wall of 85 $\mu\text{m}$ width curved microchannel.....	19
2-8 Inertial focusing of particle in an asymmetric curved channel .....	20
2-9 Separation in an 180° circular bent. Green circles represents larger particles and blue circles represents smaller particles. ....	21
2-10 Three turn spiral microfluidic channel as reported by Gregoratto et al. ....	22
2-11 Five turn Archimedean spiral with bifurcated inlet and outlet.....	23
2-12 Double spiral microchannel with trifurcated outlet to separate a series (three different diameters) of particles.....	25
2-13 Schematic of the focusing streak at different channel Reynolds number for different channel geometry. The blue lines represent 4.4 $\mu\text{m}$ and green lines represent 9.9 $\mu\text{m}$ particles. (Sketch of the experimental result by Martel et al.[72]) .....	27
3-1 Device schematic with inlet and outlet location shown in the picture. The velocity profile at the outlet is also shown.....	32

3-2 Variation of radius along the angular coordinate of the Fermat spiral microchannel.	34
3-3 The width of the designed spiral channel as a function of angular location from inlet to outlet.	35
3-4 Dean number as a function of the flow rate for different microchannel designs. 1) with variable channel width; the channel width is varied from 50 $\mu\text{m}$ at the inlet to 200 $\mu\text{m}$ at the outlet, 2) with constant channel width; the channel width is kept constant throughout the entire channel from the inlet to outlet.	36
3-5 Variation of average Dean velocity with increasing flow rate. For the constant width microchannel, the average Dean velocity is relatively higher compared to variable channel width microchannel.	38
3-6 Force ratio comparison for a constant width (100 $\mu\text{m}$ ) and variable width (50~200 $\mu\text{m}$ ) at the outlet of a Fermat spiral microchannel for 9.94 $\mu\text{m}$ particles at various flow rates.	40
3-7 Variation of force ratio with channel Reynolds number.	41
3-8 Meshing on a circular bend. The inlet and outlet faces are meshed with 5 $\mu\text{m}$ elements. Then the curved channel is mapped with the face meshes along the four curved edges. Total number of elements are 112500.	43
3-9 Eighteen different flow profile at the outlet of a circular bent with constant channel width of 200 $\mu\text{m}$ . The inlet flow velocity is written below each picture. As the inlet velocity increases the Dean vortex intensity increases, the distortion in flow profile becomes visible as the flow profile shifts right of the channel cross section.	45
3-10 Variable circular bend with inlet width of 50 $\mu\text{m}$ and outlet width of 200 $\mu\text{m}$ . Inlet and outlet faces were meshed with 5 $\mu\text{m}$ sized element. The mesh elements were then mapped along the four curved edges to complete the meshing. Total number of elements are 40986	47
3-11 Flow profile of a variable width circular bent at the outlet. Inlet flow velocity is placed at the bottom of each picture.	48
3-12 Average Dean velocity with respect to inlet Reynolds number	49
3-13 Variation of Dean force along the channel length. From the inlet to outlet. Solid black line- variable width, red and green 50 $\mu\text{m}$ and 200 $\mu\text{m}$ channel width. Flow condition 700 $\mu\text{L}/\text{min}$ . Forces calculated for 9.94 $\mu\text{m}$ diameter spherical particles..	52
3-14 Variation of force ratio along the flow direction from the inlet to outlet. The radial location at the inlet is zero radians and at the outlet is ~69 radians	53

3-15 Mesh elements of a Spiral microchannels.....	56
3-16 Dean velocity profile at the outlet of differential Fermat spiral channel with inlet flow velocity of 3m/s.....	57
3-17 Coefficient of restitution on wall boundary condition for DPM modeling .....	58
3-18 Inertial lift along the non-dimensional channel location as extracted from Asmolov[61] .....	60
3-19 Coefficient of lift values for varying channel Reynolds number. ....	61
3-20 Validation of numerical method by comparing the simulation results with an existing device spiral microchannel on particle separation. The first two pictures are taken from Bhagat et al[18] at the outlet (flow rate 10 $\mu$ L/min) and the third picture is obtained from Fluent simulation at outlet under exactly the same conditions under which the experiments were conducted. Blue dots represent 1.9 $\mu$ m and red dots represent 7.32 microparticles.....	63
3-21 Channel location where images were taken. ....	65
3-22 Simulated particle trajectories for 4.5 $\mu$ m (blue) and 9.94 $\mu$ m (red) flowing through the device at a flow rate of 700 $\mu$ L/min. ....	66
3-23 Particle streamline of five different particles of diameter ranging from 5 $\mu$ m, 6 $\mu$ m, 7 $\mu$ m, 8 $\mu$ m and 10 $\mu$ m (the colors are shown to the right) at flow rate 1700 $\mu$ L/min at the outlet of the differential Fermat spiral channel. ....	68
4-1 Printed photolithography mask of the design.....	71
4-2 SU-8 patterning flow diagram of a silicon wafer. This patterned SU-8 mold will act as a die for PDMS mold .....	73
4-3 PDMS-Glass chip fabrication.....	75
4-4 Image of fabricated devices before connecting necessary tubing and syringe pumps. Inlet and bifurcated outlet are shown.....	77
4-5 Image of the devices. (a) Device overview at full scale (b) Near the inlet reservoir (c) at the first half of the channel (d) at the center S-junction (e) at the second half of the spiral (f) at the bifurcated outlet .....	78
4-6 Experimental setup of the particle separation process .....	80
4-7 Experimental result presented with numerical simulation at different location of microchannel. ....	81

4-8 Line scan at the outlet of a differential Fermat spiral microchannel. The blue lines represent the streams of $4.5\mu\text{m}$ , and the green lines represent the streams of $9.94\mu\text{m}$ particles.....	83
4-9 Simulation result of mixture of five different sized diameter particles.....	85
4-10 TPE Glass microchip fabrication flow chart.....	90

## CHAPTER I

### INTRODUCTION

#### 1.1 Overview

Cell separation at high throughput has been a recent interest in science and technologies, especially in the areas of clinical diagnostics[1], cellular analysis[2,3], biological[4–6] and environmental microbiological[7] processes. There are a variety of available approaches for high throughput separation that are effective and efficient. Among all these numerous techniques, some of the most focused areas include magnetic sorting[8], dielectrophoresis[9], electrophoresis[10], surface acoustic wave (SAW)[11,12], pinched flow fractionation[13–15], serpentine microchannel[16], hydrodynamic filtration[17], inertial microfluidics in curved micro-channel[18–21] and hydrophoretic filtration[22]. Because of these notable drawbacks of existing micro-particle separation devices i.e. performance degradation of the membrane filter[23–25], membrane fouling[22], clogging and/or contamination hazards[26], long processing time in sedimentation techniques[27], limited throughput in field flow fractionation[28], limitation of manipulating live cells because of externally applied excitation forces in dielectrophoresis[29], the demands for continuous, membrane-less, uninterrupted, high throughput, low-cost microparticle separation devices are urgent. Among numerous

advantageous approaches, microchannels with curved designs, utilizing inertial lift and Dean vortices[30] has shown the potential to separate microparticles ranging from  $1.9\mu\text{m} \sim 60\mu\text{m}$ [5,18,31] that can separate 20,000 ~ 555,000 cells per second[5,32,33]. They have proven efficient in separating blood cells and serum and thus opened a new path for biological assays[34]. As the generated inertial lift and Dean Force has proven effective in separating microparticles, the driving forces drew much attention from researchers. The new findings have been strongly influencing the microchannel designs and thus evolved several different curved microchannels i.e. spiral microchannels[18,35–37], Fermat spiral microchannel[5,38,39], differential spiral channel[20], spiral channel with various cross-sectional geometry[40], multi-orifice[41,42], centrifugation in 180° bent[43] and sinusoidal shaped asymmetric curved channels[19,44].

The advent of Dean Force application in particle separation showed potential for microchannels at low flow rates[44] ( $<1500\mu\text{L}/\text{min}$ ) but it requires special attention in channel design as uncontrolled increase in Dean force introduces mixing rather than particle focusing. Initially, some groups focused on reducing this disturbing vortices by varying the channel curvature radius and hydraulic diameter ( $D_h$ ),[45] concentrating solely on centrifugal[43] and shear induced drag force domination to separate particles based on their density and size. By limiting the Dean Vortices below the mixing Dean number range, continuous large volume of dilute suspension of particle separation using an Archimedean spiral was first demonstrated by Gregoratto et al.[45]. To minimize the secondary disturbing Dean Vortices, they opt to choose a high aspect ratio micro-

channel design. This technique of minimizing Dean Vortices to separate particle based on their size and density has been followed by several groups while experimenting with different geometric dimensions, channel curvature and hydraulic diameter[43]. Lately, several groups have figured out the advantage of maintaining a balance between inertial lift and Dean Drag to favor particle separation based on the particle dimension dependence of these forces[18,46]. After several groups had reported particle focusing by equilibrating these driving forces in asymmetric curved channels and spiral channels[47–51] with a particle diameter to channel hydraulic diameter ratio (particle confinement ratio)  $\geq 0.07$ [42,44], researchers intensified their investigations with spiral channel designs, with an aim to focus particles in a single stream. Different groups have reported the separation successfully and focusing of micro-particle ranging from  $1.9\mu\text{m} \sim 40\mu\text{m}$  particle [18,31,35,52], using 4~6 loops using Archimedean Spirals[36,46,47,53]. There were some other types of curved channel particle separation devices designed based on multi-orifice[41], centrifugation in  $180^\circ$  bent[43], etc. All these microchannel designs were capable of separating microparticles to a reasonable separation distance at a moderate flow rate. However, there was ample room for improvement in terms of flow rate and separation distance. At a point, Seo et al.[38,39] introduced a double spiral microchannel; at the center of this microchannel, flow direction changes from clockwise to counterclockwise to help compact the wide band of particle streamlines into a narrower one. Since the continuous investigation in passive curved microfluidic or spiral microfluidic channel provided scholars the understanding

that hydraulic diameter has an important role in particle focusing, several groups investigated irregular cross section[40] and microchannel width variation[20].

These spiral microfluidic channels[18–21] utilize the continuous effects of inertial lift forces and Dean vortices[30]. They have shown the potential to separate microparticles by size [5,18,31] at a moderate flow rate. A recent study has proven the feasibility of using this type of device in separating blood cells from serum[2,4,34,54,55]. These capabilities of Archimedean microchannels show promise as a solution to the problem of high throughput focusing and separation of particles as small as  $2\mu\text{m}$ [47].

## 1.2 Motivations

Cells in biological fluids from animals and humans contain important information that are critical for human health. There are normal cells and unwanted cells (such as rare cells and circulating tumor cells) in the biological fluids once they are infected. Isolation and analysis of these unwanted cells from normal cells plays an important role in disease diagnosis and prognosis, because unwanted cells are typically the underlying reasons of these diseases and infections. Many technologies have been utilized to isolate the rare cells from the biological samples; these methods typically suffered from low throughput and reasonable efficiency that restricts them from using it in real time[56]. The underlying reason behind the inability of real-time operation is clear, the restriction in throughput and separation efficiency. Because, typically high separation

efficiency is essential such as in circulating tumor cell (CTC). In the case of CTC, they are found at a rate of 1-100[57] cells in 1mL of blood. The number of cells is relatively low, but it is more than enough to cause metastatic cancer and the cause of 90% of cancer deaths[58–60]. For this type of biological fluidics assay, high throughput with high efficiency is the key to successfully diagnose, separate and analyze the rogue cells. These requirements present a challenge of analyzing a large volume of sample in a very short time with acceptable accuracy. Hence, to assist in diagnosing and separating cells from a large volume of sample the necessity of microfluidic devices has arisen. Design and improvement of such a device would save much time, effort and money & prove vital to clinical assessment.

### 1.3 Thesis objectives

The objective of the thesis is to achieve particle separation at relatively higher Reynolds numbers and flow rates. To achieve this goal a new spiral microchannel consisting of a differential Fermat spiral design with varying channel hydraulic diameters was microfabricated and tested. The use of varying channel hydraulic diameters facilitates balance of the Dean Drag force and the inertial lift forces on microparticles at higher Reynolds number and hence assists in particle focusing at high flow rates. The use of differential Fermat spiral structures reduces the bandwidth of particle streaks, increases the separation distance of particle streaks, and simplifies the loading and unloading of

particle separation. Finally, demonstration of the device's capability of separating microparticles by size at high Reynolds and high flow rates by experiments and numerical work is shown. To demonstrate its capabilities of particle focusing, and particle separation at  $700\mu\text{L}/\text{min}$  experimental results are presented.

To attain particle separation at higher flow rate, the work of this thesis focuses on a differential Fermat spiral channel with variable channel width to control the sharp rise in Dean Drag force. Such a design enables force balance and particle focusing/separation at high Reynolds number and flow rates. Upon successful implementation of the proposed microchannel, the device would enable separation of microparticles with high throughputs as required by rare cell separation and assessment. In particular, such an advanced cell particle separation component would be helpful in developing lab-on-chip instruments for real-time detection of CTC and other unwanted cells which are typically present at low concentration. In addition to high throughput separation, the proposed device have also been demonstrated to have high separation resolution, i.e., separation of particles with small size difference is reported. This feature will be useful for separating rare cells that have similar sizes to normal cells in the biological fluids. With its high throughput and high separation resolution, along with its compact size and low power consumption, this microchannel is expected to benefit cell separation and real-time biological assessments.

#### 1.4 Specific goals

- a. Design and fabricate a differential Fermat spiral microchannel device with gradually increasing channel width that is capable of separating microparticles.
- b. Conduct force analysis to quantify the advantages of microchannels with variable channel width spiral microchannels compared to constant channel width.
- c. Perform numerical analysis using commercially available software package Fluent to predict the present microchannel's functionality and suggest further modifications.
- d. Test the device with a binary mixture of particles and record fluorescence images to demonstrate the device's performance.
- e. Demonstrate the device's capability to separate microparticles at higher Reynolds numbers using numerical simulation.

#### 1.5 Organization of thesis

The rest of this thesis organization is as the following: The background behind particle focusing in straight and curved microchannels is presented in chapter II. Fundamental force analysis, flow field simulation and particle trajectory simulation are discussed in Chapter III. Chapter IV elaborates the microchannel fabrication, an experimental setup, sample preparation and testing results that demonstrate the designed microchannel is

capable of separating microparticles by size at high Reynolds numbers and high flow rates. The limitations of the proposed design and further plan to overcome the shortcomings along with improvements are also addressed in chapter IV. Conclusions are pointed in Chapter V.

## CHAPTER II

### LITERATURE REVIEW

#### 2.1 Inertial focusing in a straight channel

When fluid flows through a straight channel, a parabolic flow profile is developed because of the viscous nature of the fluid. In this parabolic flow profile as we move away from the center of the channel, the velocity tends to reduce and thus generates a velocity gradient. Moreover, because of this velocity gradient, inertial lift force ( $F_{SL}$ ) is generated on the suspended spherical[61]. There is also wall induced inertial drag ( $F_{WL}$ ) that pushes the particle away from the channel wall. The net force of  $F_{SL}$  and  $F_{WL}$  is called the inertial lift force,  $F_L$ . The variation of magnitude of the lift force is related to the dimensionless particle Reynolds number ( $R_p$ ).

$$R_p = R_c \frac{a_p^2}{D_h^2} \quad (2-1)$$

Where,  $R_c$  is the dimensionless channel Reynolds number, an indication of flow disturbance through a micro-channel, and is defined as,

$$R_c = \frac{U_m D_h}{\nu} \quad (2-2)$$

In the equation (2-2)  $a_p$  is the particle diameter,  $U_m$  is the maximum channel velocity,  $D_h$  is the channel hydraulic diameter defined as  $(2wh)/(w+h)$ ,  $w$  and  $h$  are the channel width and height respectively.  $\nu$ , the fluid kinematic viscosity is defined as  $\mu/\rho$  ( $\mu$  is the dynamic viscosity, and  $\rho$  is the fluid density). The magnitude of the inertial lift force was derived by Asmolov[61] assuming  $R_p < 1$  as,

$$F_L = \frac{\rho U_m^2 a_p^4 C_L}{D_h^2} \quad (2-3)$$

Where,  $\rho$  is the fluid density,  $U_m$  is the maximum flow velocity which has been approximated as  $2 \times U_f$  ( $U_f$  is the average flow velocity)  $a_p$  is the particle diameter,  $D_h$  is the hydraulic diameter of the microchannel. The lift coefficient  $C_L$  on a neutrally buoyant particle inside a straight microchannel was derived by Asmolov[61] and approximated  $\sim 0.5$  by Di Carlo[44].

In addition, Stokes drag force is exerted on a moving particle, and it can be calculated by

$$F_D = 3\pi\mu a_p U_s \quad (2-4)$$

Here  $U_s$  is the relative velocity between the particle and the fluid.

There is an equilibrium position inside a straight channel where the inertial lift force and the Stokes shear Drag balances. The equilibrium position is the location where suspended neutral particles are focused (Figure 2-1). Segre et al[62,63] quantified the

equilibrium position to be 0.62 times of the characteristic diameter, which has been verified by other research groups[64,65].

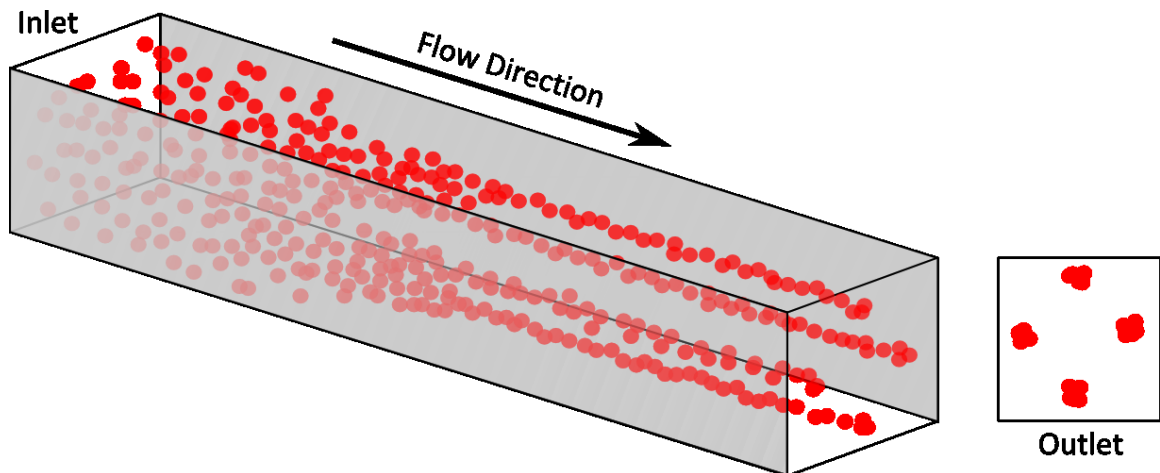


Figure 2-1 Uniformly distributed particles take an equilibrium position of  $0.62D$  from the channel center when flowing through a straight channel.

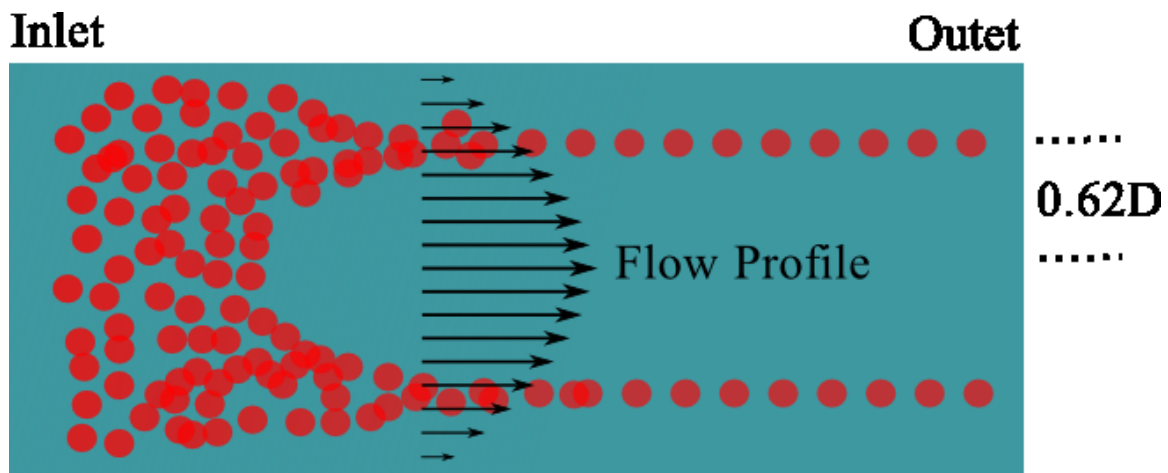


Figure 2-2 Equilibrium position of particles inside a straight channel at the inlet, the red particles were randomly mixed, but as the flow progresses they take an equilibrium position at  $0.62D$  from the centerline.

For better visualization of the particle trajectories, 2D plane was considered through the microchannel as shown in Figure 2-2. At the inlet, the particles are evenly distributed. As the particles advance in the flow direction, they tend to find an equilibrium position at a distance  $0.62D$  from the channel centerline where the shear lift force and the wall shear is neutralized by each other.

## 2.2 Inertial focusing in curved channel

With the introduction of curvature, a secondary counter-rotational flow, Dean flow[30] occurs, which is symmetrically divided equally on both top and bottom of the channel mid-plane[66]. This Dean flow generates the Dean drag ( $F_D$ ), which circulates particles from the mid-plane to the top and bottom wall, positioning microparticles at the equilibrium position where the acting forces, inertial lift force ( $F_L$ ), and Dean drag ( $F_D$ ) force are balanced. In a curved channel, Dean drag force ( $F_D$ ), depending on the aspect ratio of the channel cross section, can be effectively manipulated to adjust the equilibrium position of particles.

### 2.2.1 Generation of Dean vortex

When fluid is flowing through a curved channel, based on the radius of the curvature, centrifugal force takes into effect, and the flow velocity closer to the outer wall is greater than the flow velocity at the inner wall. As the fluid near the outer wall moves with relatively large velocity, an apparent vacuum at the inner wall is generated immediately in front of the flow and the fluid closer to the outer wall shows a tendency to move towards the inner wall. This circulatory flow from the outer curved wall to the inner wall is named as Dean vortex. Because of this fluid motion, it generates a drag force on a neutrally travelling particle inside the curved channel. This rotating or swirling flow profile is observable in 3D and can be effectively used to focus particles. This rotating vortex is characterized by a dimensionless number, Dean number (De)

$$De = Re \sqrt{\frac{D_h}{2R}} \quad (2-5)$$

Where, R is the radius of the curvature of the channel. This rotational flow induces Dean Drag ( $F_D$ ) and assuming Stokes drag; the magnitude is quantified as,

$$F_D = 3\pi\mu\overline{U_D}a_p \quad (2-6)$$

The average Dean velocity  $\overline{U_D}$  in the equation is approximated by Ookawara et al[67]. in a circular bend as

$$\overline{U_D} = 1.8 \times 10^{-4} De^{1.63} \quad (2-7)$$

This equation is an empirical equation and is valid for a circular bend. For a spiral microfluidic channel or another curved channel the quantification might be different and is still under investigation by research groups. Therefore, the Dean force acting on a particle is approximated from the equation (2-6) which takes the form

$$F_D \sim \rho U_m^2 a_p D_h^2 R^{-1} \quad (2-8)$$

Here, R is the radius of the curvature of the curved channel that is included in the equation (2-5) for Dean number.

Figure 2-3 shows the visualization of a typical Dean vortices generated in a 270° circular bent microchannel from a numerical simulation using commercially available software package ANSYS Fluent. The cross section of the circular bent is a square with a side of 100μm. The radius of the curve is 1mm. It clearly shows the Dean vortices are generated inside a 270° bent. An expanded clear flow profile with Dean Flow direction is shown in figure 2-4

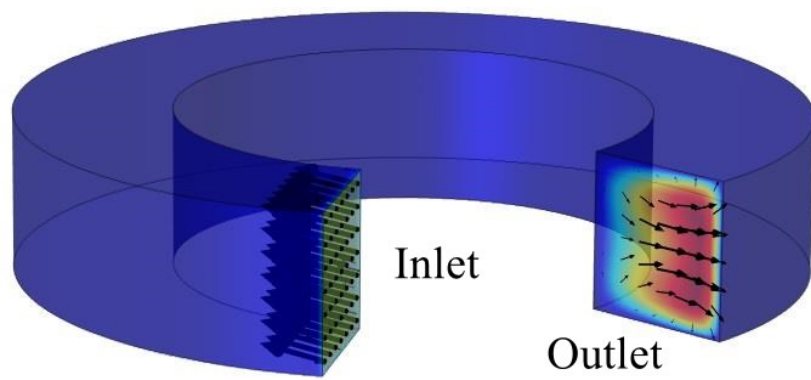


Figure 2-3 Dean vortices generation on a curved channel

The generated vortices, depending on the channel curvature and flow velocity, can be effectively controlled to alter the focusing position of the particle streamlines.

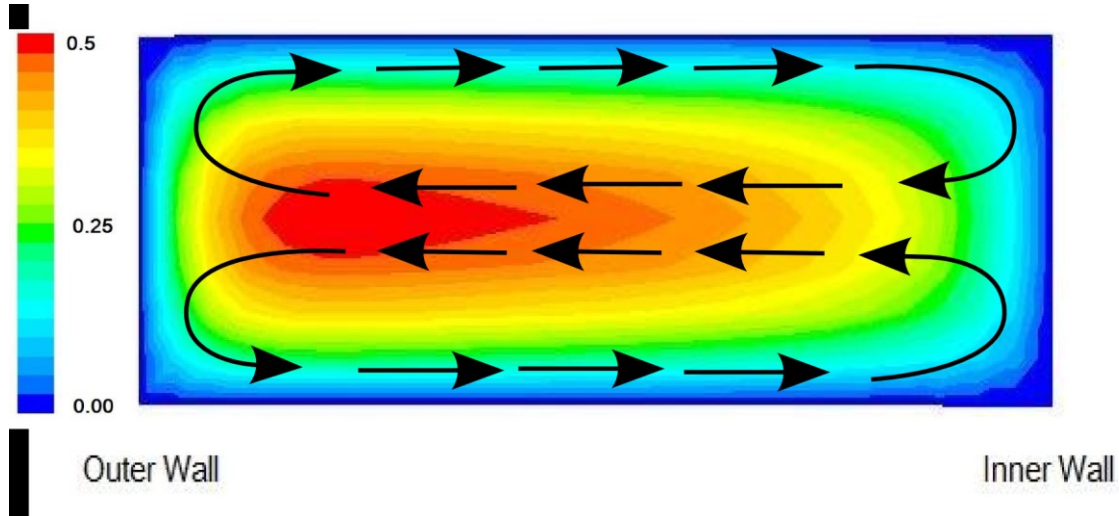


Figure 2-4 Numerical quantification of a Dean velocity profile.

### 2.2.2 Focusing and separation using Dean vortex

As the viscous inertial lift force and Dean drag forces have been cautiously examined by many researchers[30,67,68], it is evident that they are largely dependent on the particle diameters suspended on the fluid. Thus, particles with different diameters are subjected to different magnitudes of  $F_D$  and  $F_L$ , and find their equilibrium position at different distances from the channel center. Hence, there is a potential to separate micro-particles based on their size difference by manipulating the competition between  $F_D$  and  $F_L$ . In an attempt to enhance the force balance to further facilitate the particle separation, some groups have focused on manipulating the channel geometry to vary

the hydraulic diameter to control the interplay between Dean drag and inertial drag.

[20,69] As the aspect ratio decreases, Dean drag becomes comparable to inertial drag,

[69] which makes it possible to focus and separate particles at Dean number as high as

25[20].

In summary, if a particle is travelling through a curved channel filled with fluid streams,

there are shear lift forces ( $F_{SL}$ ) caused by the parabolic shear flow, the wall shear force

( $F_w$ ), the Dean Drag force caused by the velocity gradient from the curved channel ( $F_D$ ),

the weight of the particle suspended on fluid stream ( $F_{wt}$ ) and the buoyant force ( $F_B$ ).

The interaction of these forces are balanced at some point, and that is the position

where the particles get focused. The direction of the forces acting on a suspended

particle in a curved channel is schematically shown in Figure 2-5.

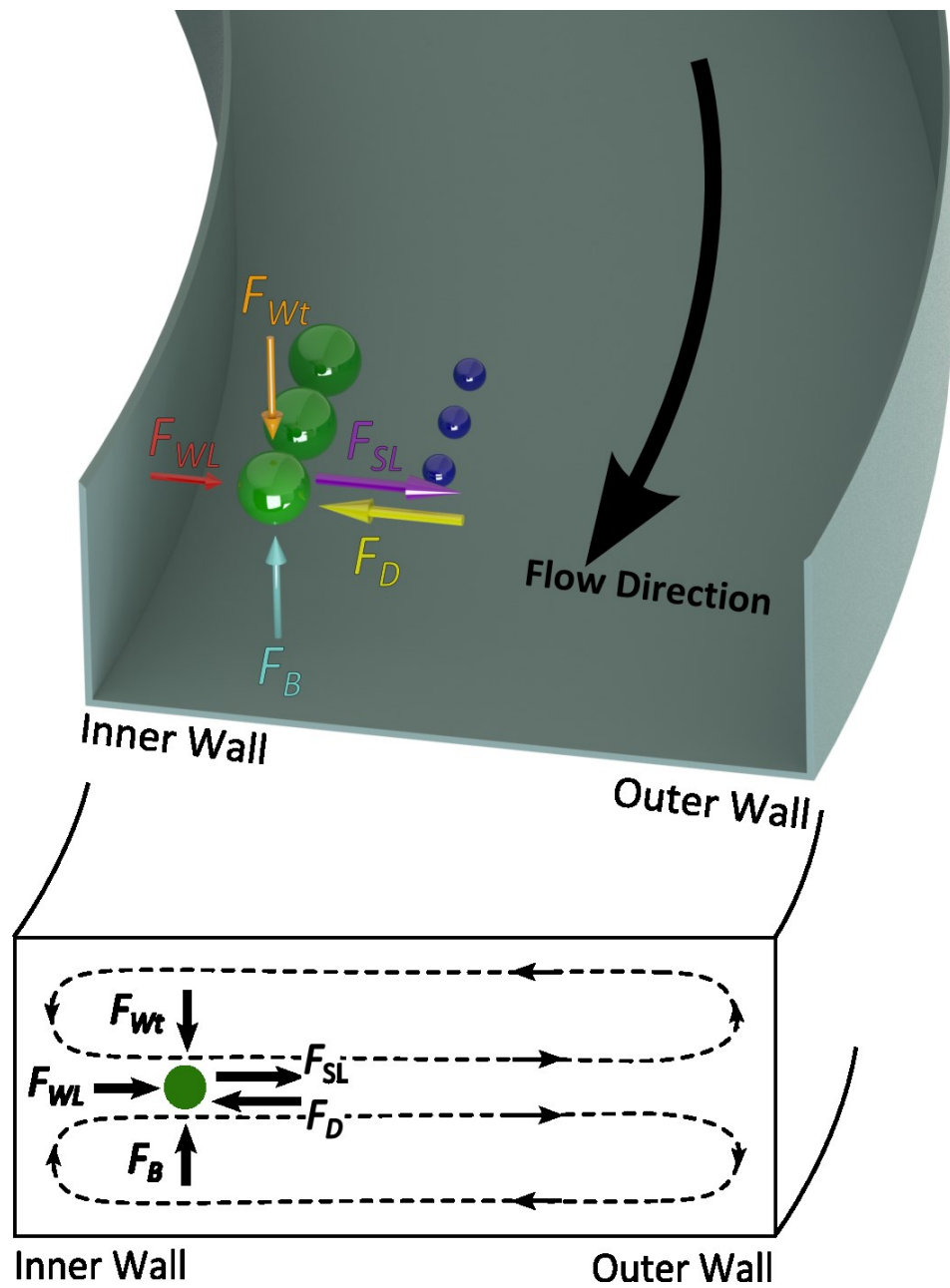


Figure 2-5 Forces acting on particles inside a curved channel

From the equation (2-3) and (2-6) it is observed that the two forces scale differently based on particle diameter. The inertial lift force scales as the fourth power of the

particle diameter whereas the Dean Force scales as the first exponent of the particle diameter. Therefore in terms of the inertial lift force and Dean Drag force, the larger particles always face the larger magnitude of the force compared to the smaller particles. As such their neutral position is different based on the particle diameter. This phenomenon is explained in schematic in figure 2-6

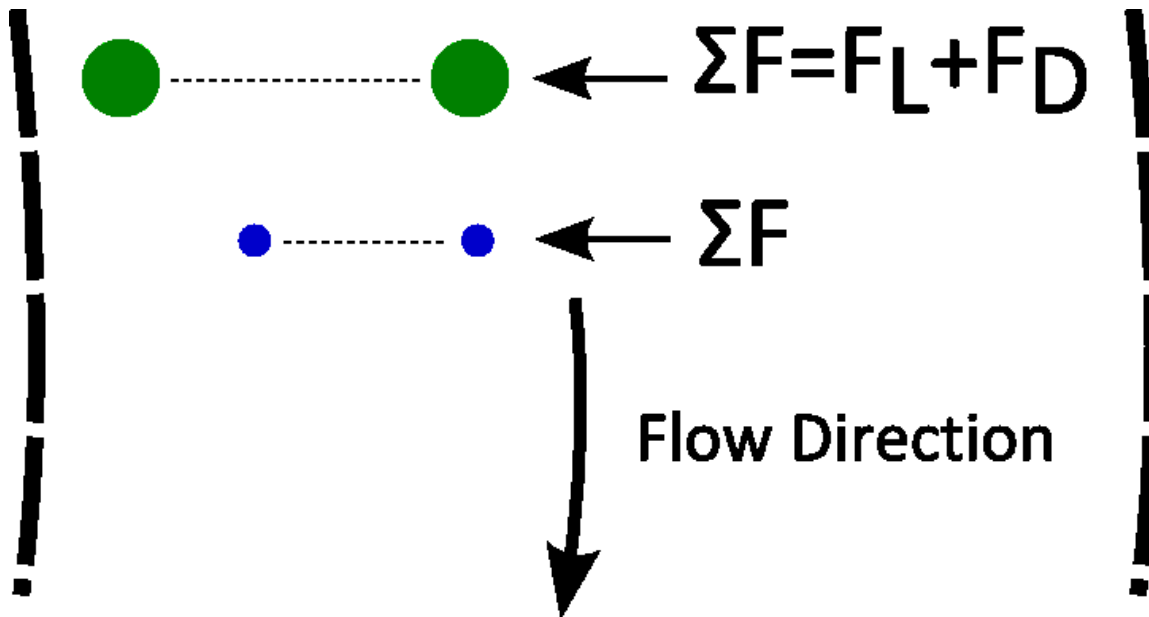


Figure 2-6 Scaling of summation of forces on differently sized particles

In figure 2-6 both the larger and smaller particles are presented with red circles. The sum of all the forces (Dean Drag force and inertial lift force) act on the particle at a specific instant. As these forces scale down depending on the particle diameter, the magnitude of force changes as a function of particle diameter. The force magnitude is directly proportional to diameter. Therefore the displacement of the larger particles

from the channel centerline is larger. Hence larger particles are focused much closer to the inner wall than the smaller particles.

As Dean vortex has an important role in focusing particles inside a curved channel, to have an overview of how the Dean vortex varies along the channel width, numerical data was extracted from a simulation of a circular bent at the outlet. The outlet width was 80 $\mu$ m, and the velocity at the mid-plane of the channel is plotted from outer to the inner wall in Figure 2-7.

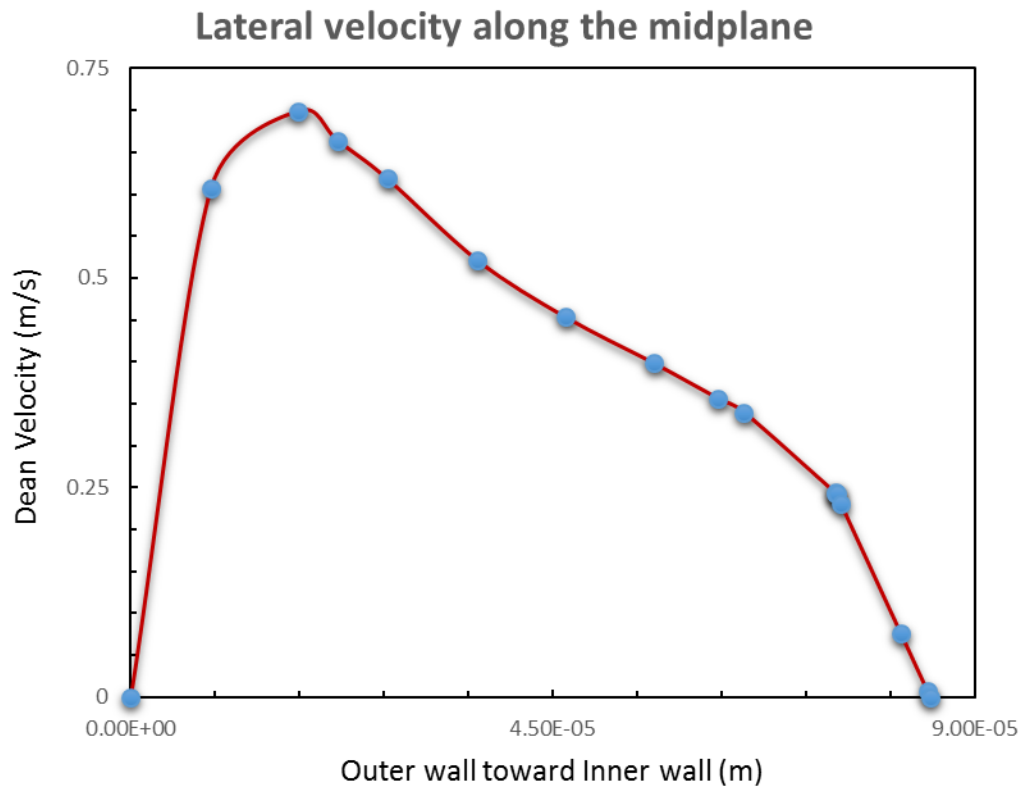


Figure 2-7 Dean velocity profile along the channel mid-plane from the outer wall

towards the inner wall of 85 $\mu$ m width curved microchannel.

From the figure above, it is observed that the lateral flow velocity namely the Dean Velocity is relatively larger near the outer wall. That means the Dean Force should also be larger closer to the outer wall. Therefore; the focusing position is always near the closer wall and away from the outer wall. If the force is higher, the particle displacement will be larger.

### 2.2.3 Spiral microfluidic channel

To take advantage of the curved microchannel, several researchers tried to utilize the Dean force as a means of focusing and separating microparticles. The first idea of spiral microfluidic channel came from an asymmetric s-shaped curved channel[44] for continuous separation of microparticles that operated at Reynolds number of 90. A schematic of the device and the focusing trend is shown in figure (2-8). At this flow rate, they can separate microparticles ranging from  $2\sim 10\mu\text{m}$ . [44] But the major drawback is their relatively low flow rate and the narrower separation distance.

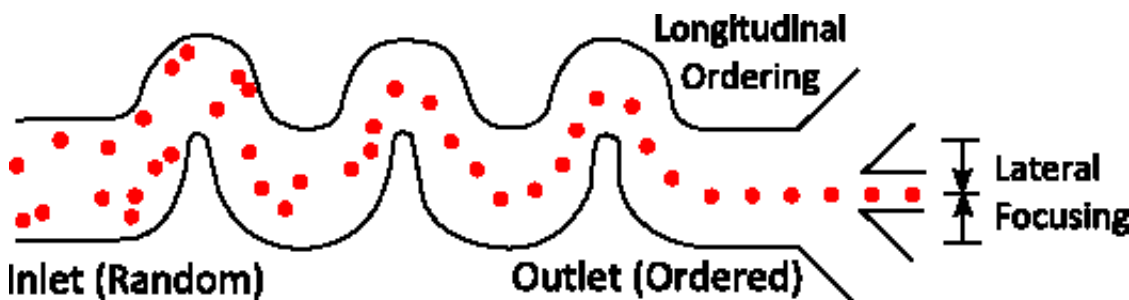


Figure 2-8 Inertial focusing of particle in an asymmetric curved channel

In an attempt to separate microparticles, circular bend was tested and reported by several groups. [21,43] A 180 degree bend[21,43] was demonstrated to separate microparticle at a flow rate of  $150\mu\text{L}/\text{min}$ . At this flow rate,  $3$  and  $10\mu\text{m}$  particles were separated but the flow rate remained a major drawback in real time particle separation. The device schematic is presented in figure (2-9). These types of devices are more dependent upon centrifugation than the Dean Force. Therefore, inside the channel centrifugal force is usually dominant, and the larger particles are focused near the outer wall rather than the inner wall. This device worked well in separating microparticles from a binary mixture but with increasing flow rate, the Dean Force continues increasing and overcomes the centrifugal force. This Dean Force restricts circular bent devices from functioning at higher flow rates.

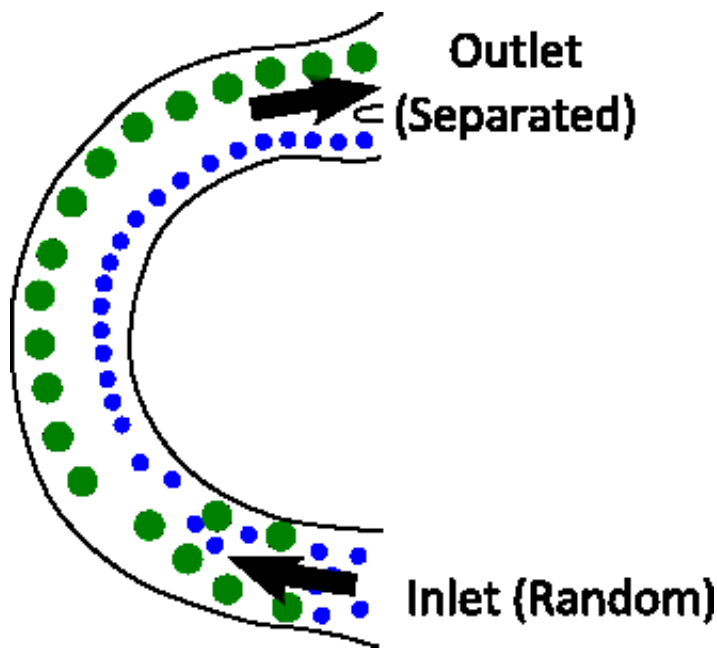


Figure 2-9 Separation in an  $180^\circ$  circular bent. Green circles represents larger particles and blue circles represents smaller particles.

With an attempt to decrease the Dean number, researchers then focused on decreasing the channel curvature gradually to control the rise of Dean number. One solution to the problem came in the form of a spiral channel where the radius of curvature increases from the center towards the periphery. Therefore the spiral microfluidic channel was first demonstrated by Gregoratto et al.[45] in 2007 with a very high aspect ratio channel. The research group was focusing on centrifugal force more than the Dean vortex. Later Sollier et al.[43] demonstrate that a spiral channel consisting of ten turns was able to separate microparticles with a flow rate of  $300\mu\text{L}/\text{min}$ . A schematic of the three turn spiral microfluidic channel is shown in figure 2-10

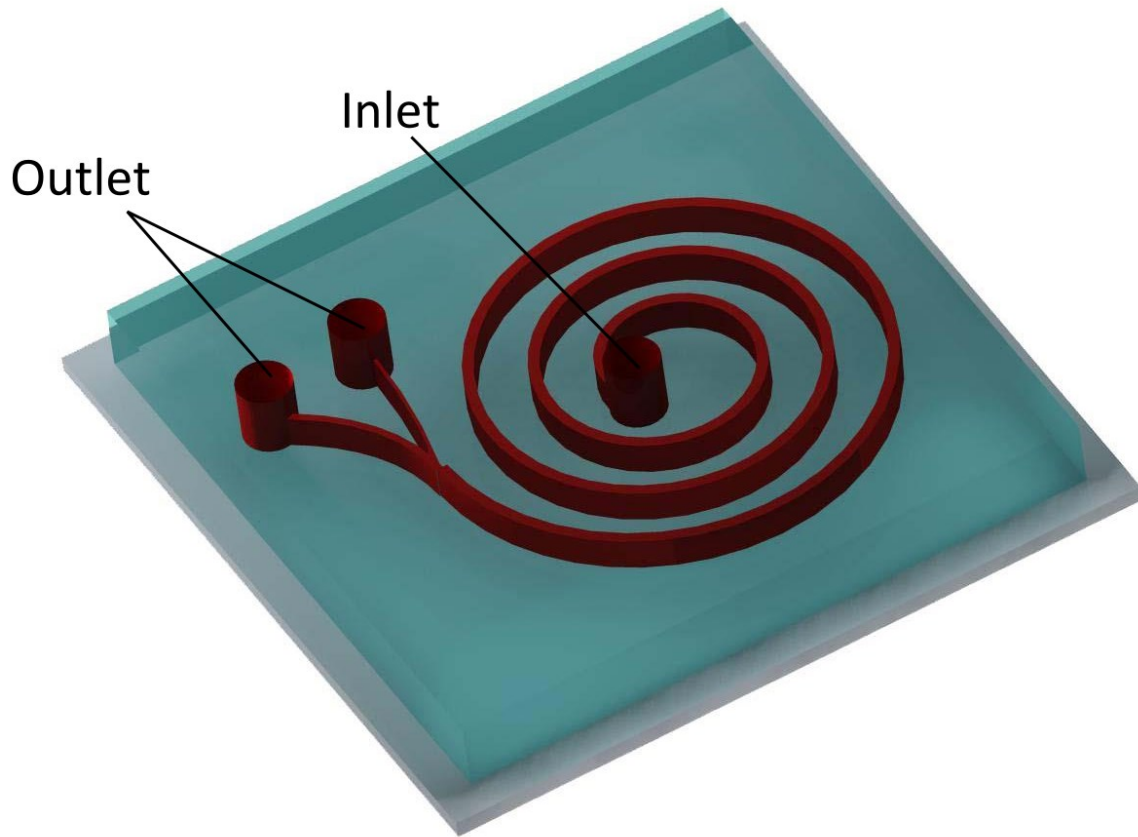


Figure 2-10 Three turn spiral microfluidic channel as reported by Gregoratto et al.

Additional research has aimed to enhance the flow rate and throughput of the devices, continued endeavor pushed researcher to think out an alternative. Later people figure out a way to control the Dean vortex to assist in focusing particles in spiral microchannels. The first utilization of Dean vortex to focus and separate microparticle was demonstrated by Bhagat et al.[18] with a five turn spiral channel with two inlets and bifurcated outlet. They showed it was possible to use Dean Force to focus particle of diameter  $10\mu\text{m}$  at a flow rate of  $\sim 415\mu\text{L}/\text{min}$ . The device schematic is presented in figure 2-11

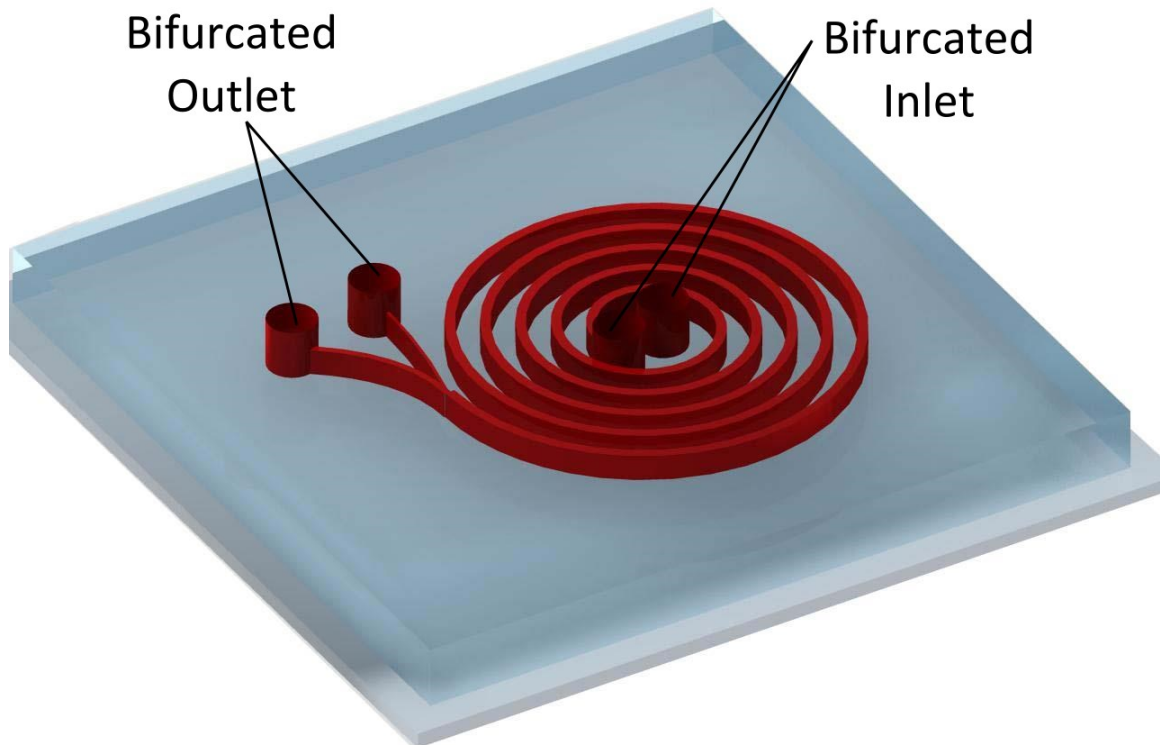


Figure 2-11 Five turn Archimedean spiral with bifurcated inlet and outlet.

To compact the focusing streak width of the microchannel, a double spiral microchannel in the form of Fermat spiral was introduced. The Fermat spiral channel was capable of operating at a flow rate of  $165\mu\text{L}/\text{min}$  that demonstrated separation of  $3\mu\text{m}$  and  $10\mu\text{m}$  particles[38]. In those early days, the particles were separated without focusing. Restricting the device functionality in binary mixtures. Although, there were asymmetric curved[19] channels capable of separating a series of five different particles ranging from  $3\sim9\mu\text{m}$  at a flow rate of  $0.9\text{mL}/\text{min}$  there was no high flow rate multiple particle separation devices.

Kuntaegowdanahalli et al.[35,46] was the first to demonstrate the focusing and separation of three different sized particle stream ( $10, 15, 20\mu\text{m}$ ) and proved the capability of spiral channel as a potential solution to cell sorting and cell separation applications. The capability of handling multiple mixtures of particles is a significant advantage of the spiral microchannel over other separation devices capable of only separating binary mixture of particles.

As the investigation intensified, researchers tended to understand the Dean vortex more and studied its effect on the channel hydraulic diameters to push the operating flow rate limit. To take the advantage of varying hydraulic diameter to control the Dean vortex, Russom et al.[20] designed a differential spiral microchannel and demonstrated microparticle separation ( $3 \& 10\mu\text{m}$ ) at a flow rate of  $3000\mu\text{L}/\text{min}$  with a corresponding Reynolds number of 155. This device proved the capability of the spiral microchannel to

be operated at higher flow rates. Also, spiral microchannels have shown the potential to separate larger microparticles in the range of  $40\text{--}60\mu\text{m}$  at flow rate of  $3000\mu\text{L}/\text{min}$ [48]. These discoveries confirmed the spiral channel capabilities at higher flow rate and for a wide range of particles ( $2\mu\text{m}\text{--}60\mu\text{m}$ ) if the channel is designed carefully. Since, bio particles are relatively uniform with respect to their diameter successful separation of bio particles were demonstrated using spiral microchannels[5,36,70,71].

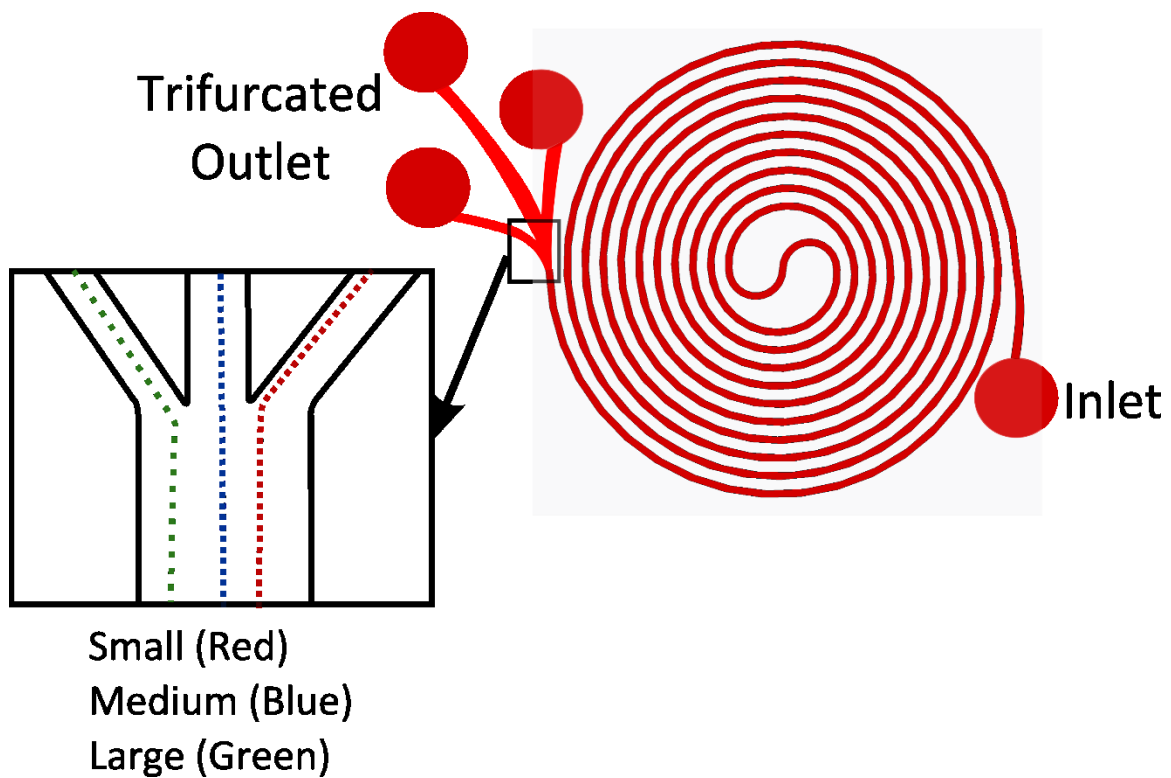


Figure 2-12 Double spiral microchannel with trifurcated outlet to separate a series (three different diameters) of particles.

With the recent trend of demonstrating the separation of bio-particles for clinical applications, several new ideas evolved. Among them, a double spiral microchannel with constant cross section as shown in figure 2-12 was reported by Sun et al.[70]. This group effectively separated CTC cells at a flow rate of  $\sim 450\mu\text{L}/\text{min}$  that corresponds to  $3.33\times 10^7$  cells/min. After all these promising research, it was necessary to understand the focusing dynamics inside the curved and spiral channels. Martel and Tonar[69] attempted to run analysis for different aspect ratio microchannels and reported the effect of different Dean number on focusing of microparticles. They tried to re-establish the force ratio term[44] proposed early by Di Carlo[44] as an indication of the initiation of focusing inside a microchannel. However, for several different aspect ratio, the force ratio appeared to vary widely and deviated away from unity at different flow conditions. They proposed a corrected velocity to be included in the calculation of force ratio, which showed a reasonable approximation as an indication of particle focusing as the force ratio tends to unity. They proposed that if the channel aspect ratio is smaller the focusing can withstand a higher flow rate and Reynolds number. Based on their finding, to increase the flow rate and separation efficiency, some research groups went on experimenting with the hydraulic diameter of the channel.

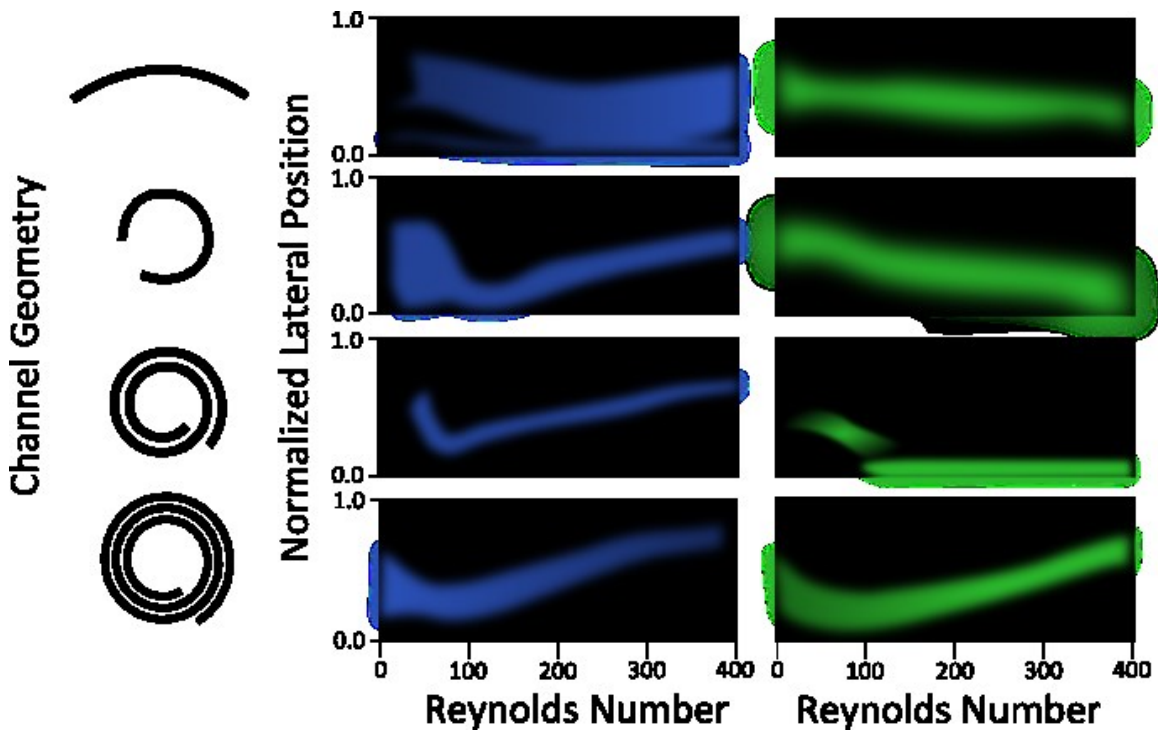


Figure 2-13 Schematic of the focusing streak at different channel Reynolds number for different channel geometry. The blue lines represent  $4.4\mu\text{m}$  and green lines represent  $9.9\mu\text{m}$  particles. (Sketch of the experimental result by Martel et al.[72])

In another investigation, (figure 2-13) they investigated the focusing position for different channel geometries for different channel Reynolds numbers. Martel et al.[69] reported if the spiral turns are increased the larger particles tend to get focused near the inner wall while the smaller particles tend to stay near the centerline of the channel. This trend was not valid at higher Reynolds number for all the geometries. At higher Reynolds number the particles whether small or large move closer to the channel centerline. Therefore even if the particles are focused, the separation is difficult. This finding suggests that to focus and separate microparticles at higher Reynolds number, manipulating the channel hydraulic diameter is necessary. Trapezoidal cross-sections

has also been evaluated to optimize the focusing distance and streak width[40][20] came up with an idea to vary only the channel width to manipulate the aspect ratio to attain higher flow velocities. Recently, Martel et al.[72] addressed some other parameters in particle focusing and showed a strong correlation between particle confinement ratios, curvature ratios, and particle focusing and equilibrium position. With these new findings, several research groups are still trying to improve the flow rate and separation distance. An example of such a device was reported by Geng et al.; [73] where they combined the filtration technique with a spiral microchannel to handle more cells per minute. However, the device opens up the channel fouling problem. Therefore the particle separation area still lack a high throughput improved resolution high-efficiency devices. In an effort to solve this problem, a new type of device is proposed, analyzed and demonstrated in this thesis.

## CHAPTER III

### MODELING OF PARTICLE SEPARATION IN CURVED CHANNEL

In the quest to design a device capable of focusing particles at higher flow rates and with reasonable resolution, several design criteria were evaluated, and a unique design was proposed and analyzed. First, preliminary calculations by basic governing equations were conducted to prove the validity of the design, Secondly, the design was modeled in parametric CAD software; Thirdly, the CAD geometry was imported into ANSYS workbench to generate mesh and assign boundary and initial conditions. The Navier-Stokes equation and Discrete Phase Modeling was then solved for the channel geometry.

#### 3.1 Proposed differential Fermat spiral microchannel

With the demonstration of a curved microchannel is capable to separate microparticles at moderate flow rate, [43–45,47] several research group started investigating curved channels. The most primitive design of a curved channel was a half circular microchannel that was capable of effectively separating two particle streams at the

bifurcated outlet[43,68]. The asymmetric curved microchannels were the first of their kind to use Dean vortex to focus microparticles[44]. With the asymmetric curved channel the potential of Dean vortex in particle focusing was realized. At a point, spiral[47] microchannels started to gain popularity because of their efficient and effective separation. To reduce the focusing streak width, Seo et al.[38,39] incorporated micro-channels consisting of two spirals wound in a different direction connected by an S-shaped junction at the center. To further improve the operating flow rate Russom et al.[20] showed that if the cross-sectional area varied for a spiral microchannel, the particles tend to stay focused even at higher flow rates. To further improve the flow rate further trapezoidal[40] cross-sectional area was proved effective. Therefore, the combination of these two features, double spiral (Fermat Spiral) and varying width proved beneficial to achieving high flow rate for microparticle separation. These two criteria were considered in the design of the current device.

### 3.1.1 Device design and description

Figure 3-1 shows the design of the microchannel, which consists of five turns of a spiral wound in a counterclockwise direction initially and another five turns in a clockwise direction connected by an s-shape junction at the center. The channel width varies from 50 $\mu\text{m}$  (at the inlet) to 100um in the s-shaped junction at the center, and then to 200 $\mu\text{m}$  (at the outlet). The channel depth is a constant 60 $\mu\text{m}$ , and the channel spacing between

adjacent loops is 390 $\mu$ m. The minimum radius of curvature is 1.1mm at the center while the maximum radius of curvature is 6.2mm at both the inlet and the outlet. The S-shaped junction connecting the two spiral microchannels at the center consisted of two small half circles. The radius of each half circle is 1.1mm with a constant channel width of 100 $\mu$ m. Two outlet reservoirs are used to collect separated microparticles. Figure 3-1 shows the junction of the two spirals at the center connected with two half circles.

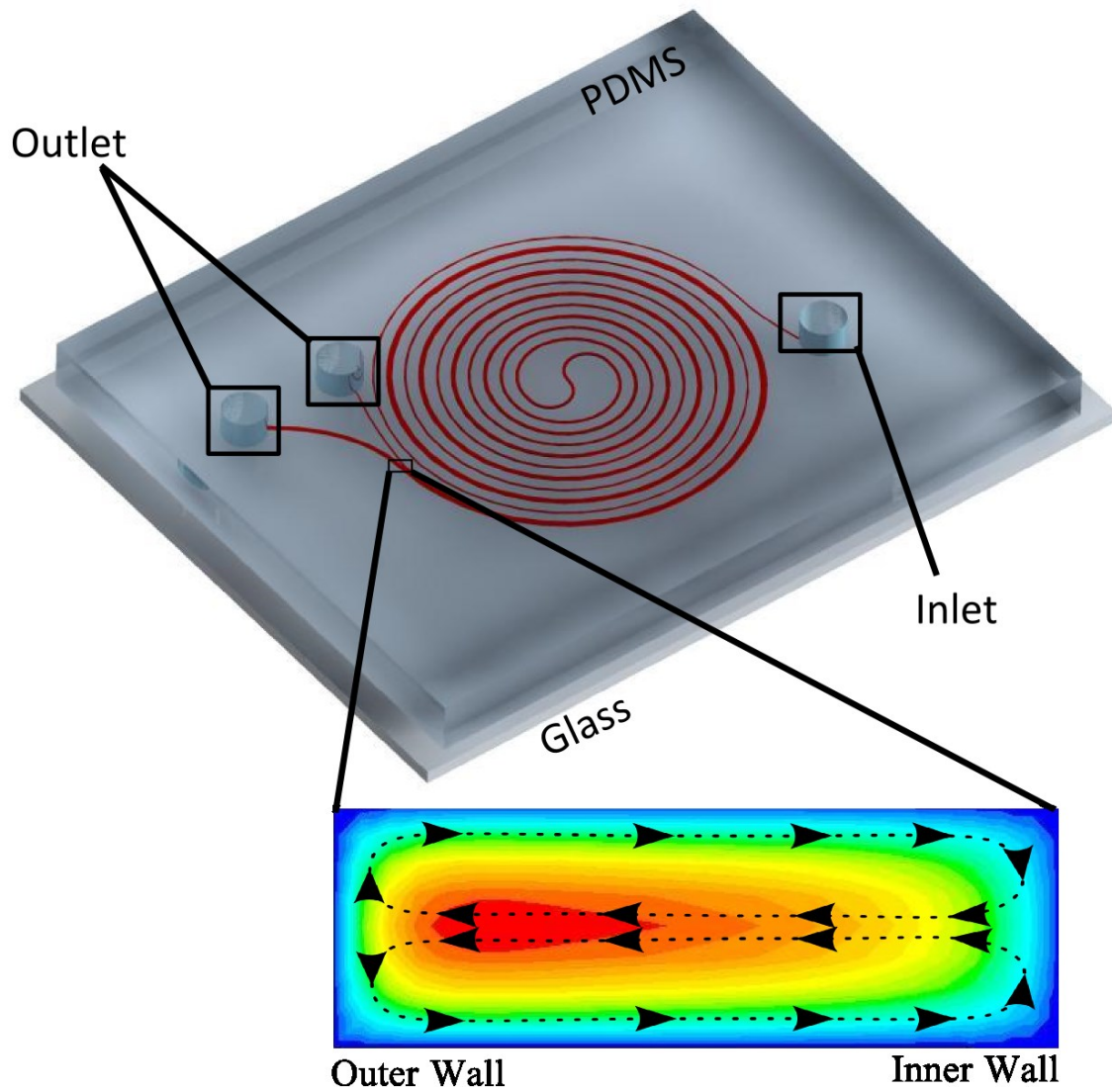


Figure 3-1 Device schematic with inlet and outlet location shown in the picture. The velocity profile at the outlet is also shown.

### 3.1.2 Force analysis

The proposed device design was first analyzed with force governing equations for Dean number, Reynolds number, flow velocity, inertial lift force and Dean Drag force. These analyses show the advantage of the design over other spiral microchannels.

### 3.1.2.1 Formation of Fermat spiral

As described in the device design section, the minimum radius of curvature is 1.1mm at the center while the maximum radius of curvature is 6.2mm at both the inlet and the outlet. For a ten turn spiral channel if the polar co-ordinate is utilized, the equation of an Archimedean spiral channel with outer radius of 6.2mm and inner radius of 1.1mm becomes,

$$R_{in}(\theta) = 0.0062 - 0.0001623\theta \quad (3-1)$$

Here,  $\theta$  represents the angular position in the polar coordinate and  $R_{in}(\theta)$  is the radius at corresponding angular position. This equation validates as  $R_{in}(0) = 0.0062$  and  $R_{in}(10\pi) = 0.0011$

Similarly at the center, the radius stays constant to 1.1mm at the center the equation becomes

$$R_c(\theta) = 1.1 \times 10^{-3} \quad (3-2)$$

Again from the center to the outer periphery the radius is increasing from  $1.1 \times 10^{-3}$ m to  $6.2 \times 10^{-3}$ mm, the new equation is the conjugated form of the equation (3-2) and takes the form

$$R_o(\theta) = -0.00502 + 0.00016\theta \quad (3-3)$$

When, all these three equations are combined for all conditions from inlet to the outlet of the channel the radius at an arbitrary theta angle can be expressed as

$$R(\theta) = \begin{cases} 0.0062 - 0.0001623\theta & \text{for } 0 \leq \theta \leq 10\pi \\ -0.00502 + 0.00016\theta & \text{for } 12\pi \leq \theta \leq 22\pi \\ 1.1 \times 10^{-3} & \text{otherwise} \end{cases} \quad (3-4)$$

Equation (3-4) is plotted in Figure 3-2 to demonstrate the variation of radius along the angular axis of polar coordinate.

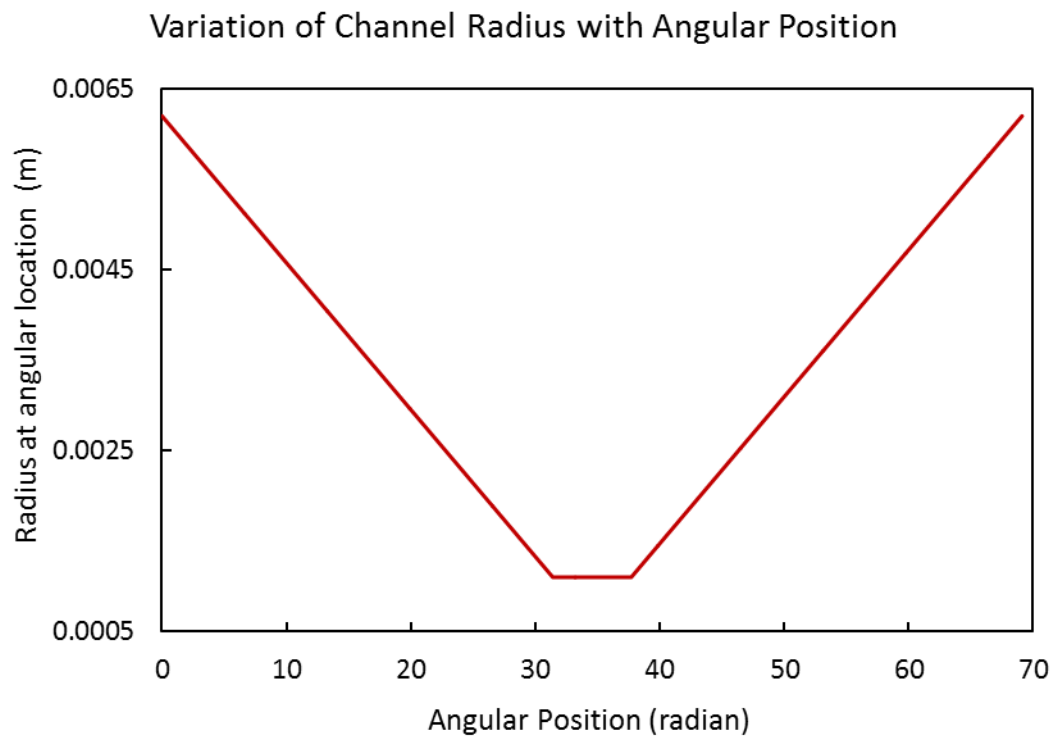


Figure 3-2 Variation of radius along the angular coordinate of the Fermat spiral

microchannel.

### 3.1.2.2 Variation of channel width

For the proposed design, the channel width varies from inlet to outlet from 50 $\mu\text{m}$  to 200 $\mu\text{m}$  with width being constant at the center S-junction. The process is similar to the one used to develop the radius variation of the channel (Section 3.1.2.1) and the variation of width is plotted in figure 3-3. The equation in the final form is

$$W(\theta) = \begin{cases} 0.00011 - 0.0098\theta & \text{for } 0 \leq \theta \leq 10\pi \\ 0.000078 + 0.0196\theta & \text{for } 12\pi \leq \theta \leq 22\pi \\ 100 \times 10^{-6} & \text{otherwise} \end{cases} \quad (3-5)$$

Equation 3-5 is plotted below to show how the channel width varies from the inlet to outlet.

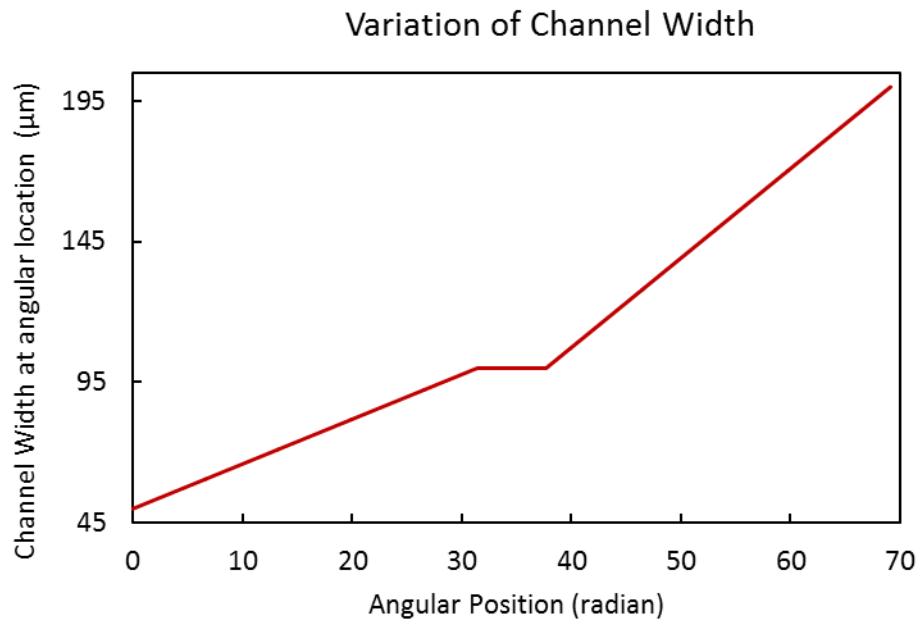


Figure 3-3 The width of the designed spiral channel as a function of angular location from inlet to outlet.

### 3.1.2.3 Variation in Dean number and average Dean velocity along the flow direction

Dean number along the flow direction is calculated using equation (2-5) and is plotted in figure 3-4. An average Dean velocity is calculated at the outlet of the channel for different flow conditions using equation (2-7) to compare the variations of Dean number in different geometries. Dean numbers for two different microchannel designs are plotted. The first microchannel has a constant channel width of 50 $\mu\text{m}$ ; the second microchannel width is varied along the flow direction from the inlet (50 $\mu\text{m}$ ) to outlet (200 $\mu\text{m}$ ) while the width remains 100 $\mu\text{m}$  at the center in the S-junction.

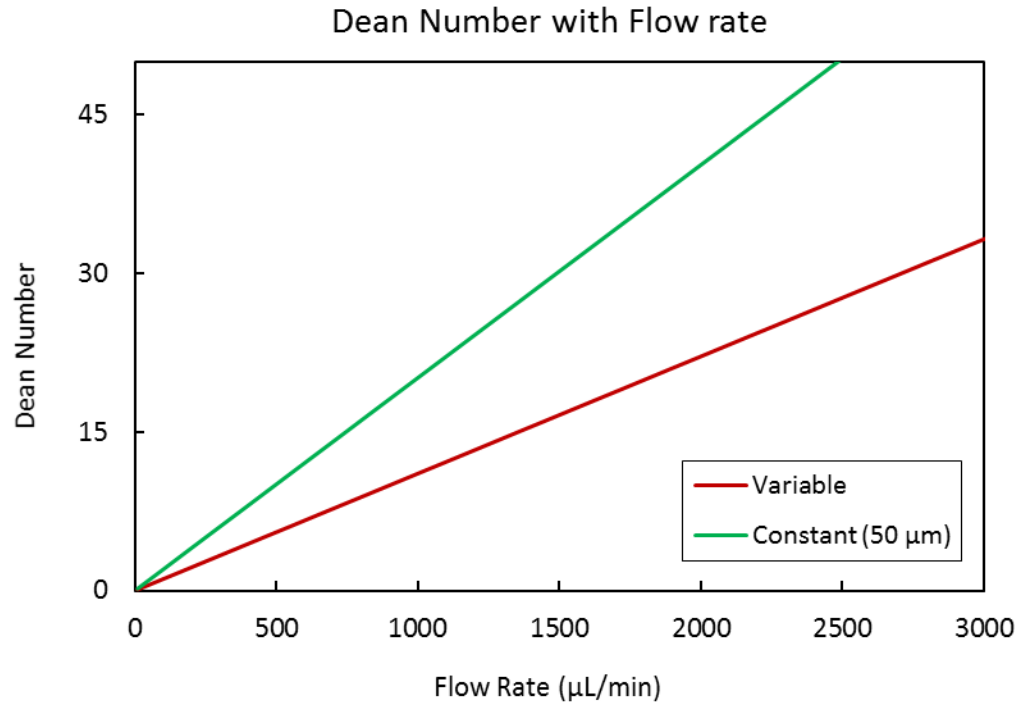


Figure 3-4 Dean number as a function of the flow rate for different microchannel designs. 1) with variable channel width; the channel width is varied from 50 $\mu\text{m}$  at the

inlet to 200 $\mu\text{m}$  at the outlet, 2) with constant channel width; the channel width is kept constant throughout the entire channel from the inlet to outlet.

From figure 3-43-4 it is observed that the Dean number at higher flow rate is relatively lower if the channel width is gradually increased compared to the one with constant width. As discussed previously in the focusing and separation section of the literature review, it is accepted that if the Dean number increases and goes beyond 30[20], the focused stream of particle is expected to break down and get defocused. A relatively lower Dean number at higher flow rate ensures the device's capability to focus particle at higher flow rate. In the proposed design as the channel width is increased gradually this helps control the sharp increment of Dean number and thus the Dean drag force.

Another important parameter to investigate is the average Dean velocity. As described by Ookawara[68], the average Dean velocity is a measure of disturbance velocity. Smaller particles usually follow the streamline of the Dean vortex. Hence, if the velocity is larger, the disturbance is greater meaning higher Dean velocity perturbs the focusing of particles. The equation 2-7 was used to calculate the average Dean Flow velocity, which is, plotted in figure 3-5 for visualization.

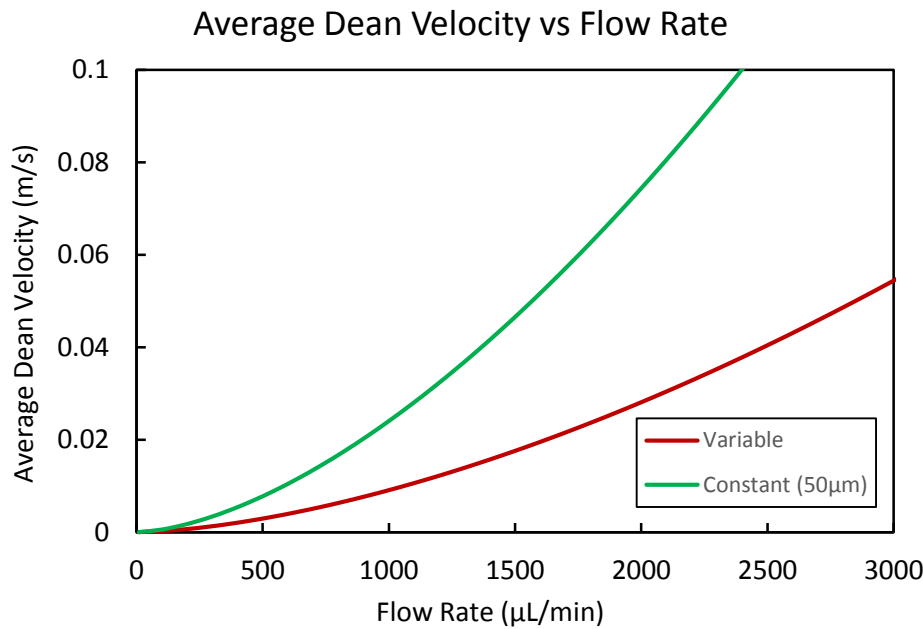


Figure 3-5 Variation of average Dean velocity with increasing flow rate. For the constant width microchannel, the average Dean velocity is relatively higher compared to variable channel width microchannel.

The plot shows that as the flow rate increases, the general trend is that the Dean velocity also increases. However, if the channel width is also increased along the flow direction, the increment in average Dean Velocity is relatively lower. This facilitates to reduce the disturbance at higher flow rate caused by the Dean vortex. Hence varying hydraulic diameter helps in focusing microparticles at higher flow rate by reducing the magnitude of average Dean Velocity.

### 3.1.3 Force ratio as a measure of device performance

In an attempt to characterize the device performance, several parameters are considered, among them force ratio was proposed by Martel et al.[69]. The force ratio is defined as

$$R_f = \frac{F_L}{F_D} = \frac{\rho G^2 C_L a^3}{3\pi\mu U_{Dean,avg}} \quad (3-6)$$

Martel et al.[69] investigated the force ratio and demonstrated that when the force ratio is close to unity, the particle focusing is much favorable. However, channel with different cross-section and aspect ratio seemed to have different force ratio values that is different than unity while maintain the force balance[74]. The problem arise with the prediction of  $U_{Dean,avg}$  at different aspect ratio and different flow condition. There is no suitable equation available to simply calculate the  $U_{Dean,avg}$  and use that in equation (3-6). Nevertheless, the investigation showed that, if the  $U_{Dean,avg}$  could be calculated by numerical simulation using commercially available software packages such as COMSOL or ANSYS. When the force ratio is calculated it is seen that it is always less than two when the particles are focused. As a measure of device performance, the force ratio is plotted for varying and constant width microchannel for different flow condition in figure (3-6)

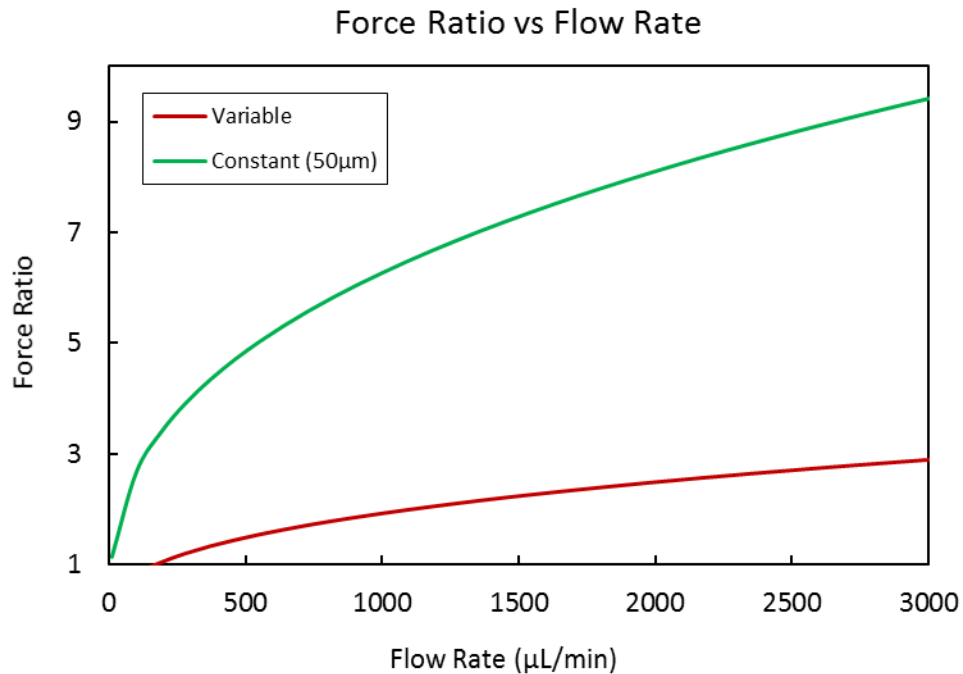


Figure 3-6 Force ratio comparison for a constant width (100 $\mu\text{m}$ ) and variable width (50~200 $\mu\text{m}$ ) at the outlet of a Fermat spiral microchannel for 9.94 $\mu\text{m}$  particles at various flow rates.

From the figure (3-6) an increasing trend in force ratio is observed as the flow rate goes on increasing. However, for the channel with constant channel width (100 $\mu\text{m}$ ) the force ratio values are rising more steeply compared to a variable width (width varying from 50 $\mu\text{m}$  to 200 $\mu\text{m}$ ). As mentioned by Martel et al.[69], force ratio values are an indication of focusing of particles inside a microchannel, this figure shows that the force ratio values are better (more close to unity) for variable channels.

In the real scenario, the design of a microchannel depends on the particles that are to be focused or separated. In other words, the channel dimensions might vary from  $50\mu\text{m}$  to several millimeters depending on the necessity. Therefore, it is always better to look at the variation of force ratio with respect to the channel Reynolds number. To study the variation in the tendency of force ratio at various Reynolds numbers, figure 3-7 is plotted with Reynolds number along abscissa and force ratio along ordinate.

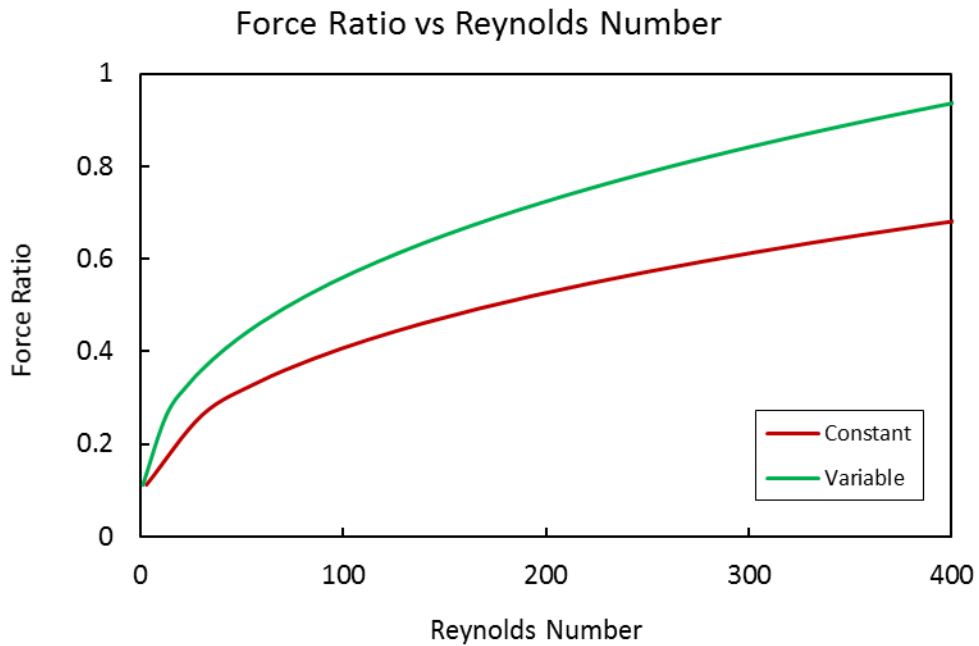


Figure 3-7 Variation of force ratio with channel Reynolds number.

It is observed from the plot that as the channel Reynolds number increases, the force ratio tends to unity. It appears that at higher Reynolds number the force ratio for constant width channel is far off from the unity. It indicates that the Dean force is

dominating over the inertial lift force and obtaining a focusing is difficult. Once the force ratio is close to unity, force balance is reached, and the particles migrate to equilibrium positions. From figure 3-7 it is observed that at higher Reynolds number the Dean force is dominant if the channel cross section is maintained constant, which may break down focused particle streams. However, if the channel cross section is increased gradually, the force ratio increases faster, meaning that the Dean Drag force increases not as fast as in the microchannel compared to constant width cross sections. This balancing helps particles find an equilibrium position and get focused at higher channel Reynolds number.

### 3.1.4 Numerical investigation of Dean vortex in a curved channel

To understand the Dean vortex generation and approximate Dean velocity for different inlet flow condition, numerical investigation was performed. As this works focuses on varying the hydraulic diameter, two different types of channel were considered. The first one is a 270° bend circular channel with a constant 200 $\mu\text{m}$  channel width, and the other one is 270° bend circular channel, width of which varies from 50 $\mu\text{m}$  to 200 $\mu\text{m}$ . The inlet and outlet width was chosen carefully to match with the inlet and outlet of the proposed design. The two different devices were studied at different flow condition. The velocity profile at the outlet was analyzed to understand the effect caused by varying the width of the channel dimension.

The constant circular bent was meshed with rectangular mapped mesh element with an element size of  $5\mu\text{m}$ . After the meshing is complete, the geometry and the meshes are shown figure 3-8

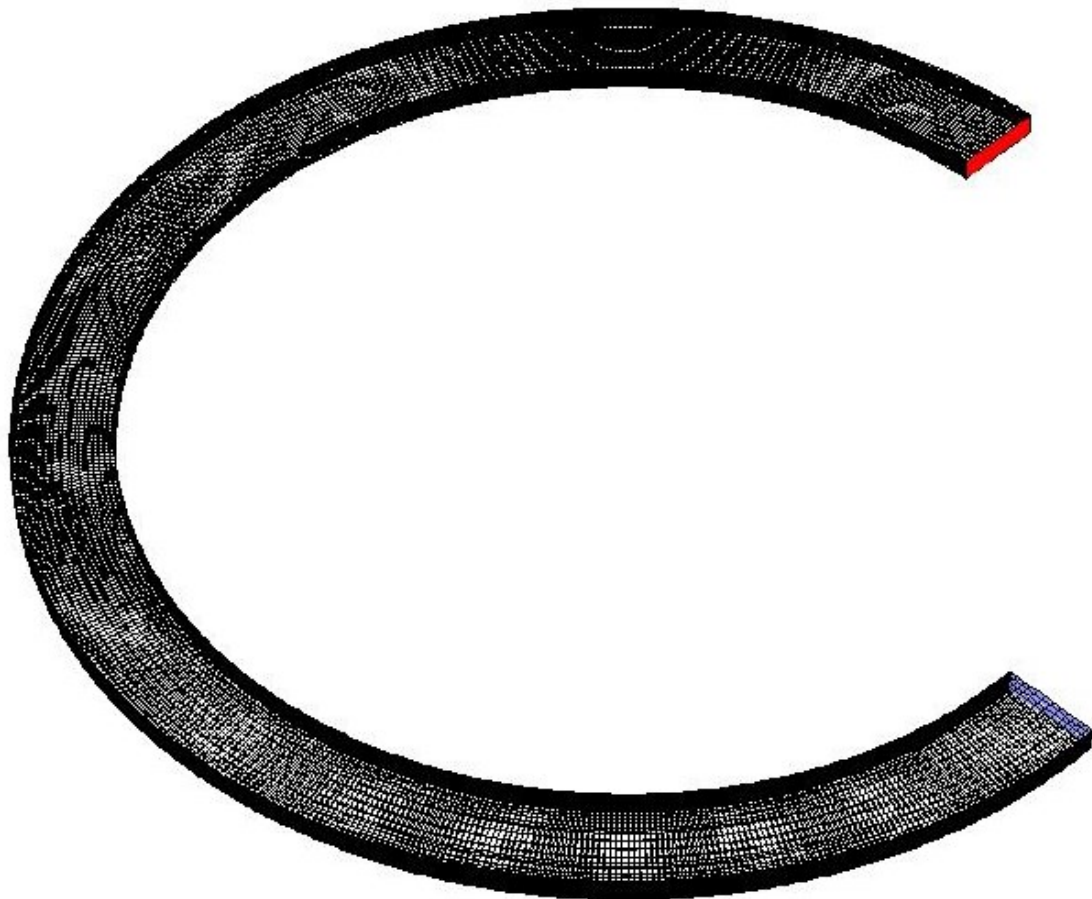


Figure 3-8 Meshing on a circular bend. The inlet and outlet faces are meshed with  $5\mu\text{m}$  elements. Then the curved channel is mapped with the face meshes along the four curved edges. Total number of elements are 112500

After the meshing had been completed, the channel was solved for eighteen different inlet velocity condition starting from 0.1m/s and ending at 3.0m/s. The flow profile at the outlet of the channel is shown in figure 3-9 for comparison.

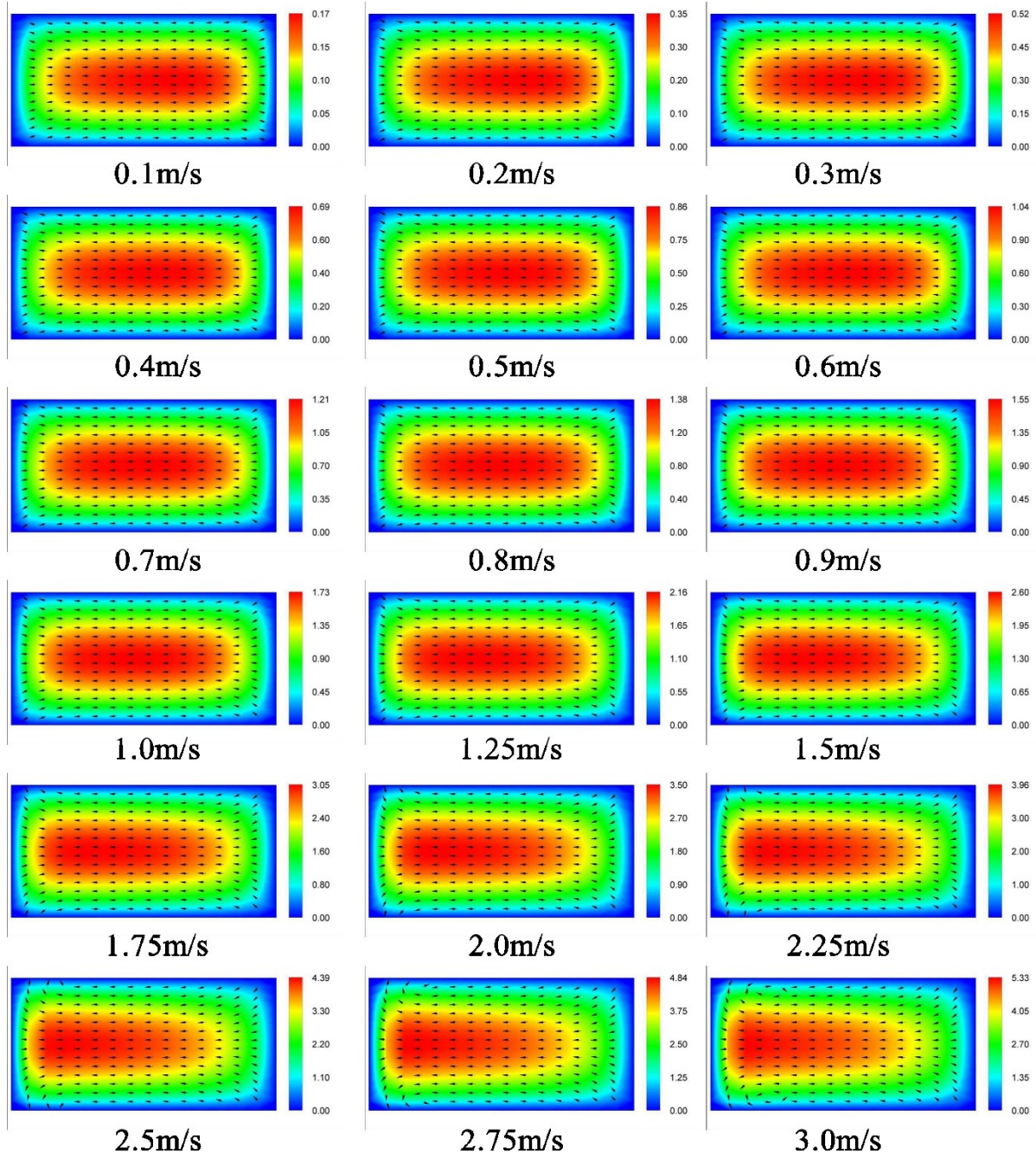


Figure 3-9 Eighteen different flow profile at the outlet of a circular bent with constant channel width of 200 $\mu$ m. The inlet flow velocity is written below each picture. As the inlet velocity increases the Dean vortex intensity increases, the distortion in flow profile becomes visible as the flow profile shifts right of the channel cross section.

From the above flow profiles, it is seen that the flow becomes distorted more as the velocity increases. At low flow rate, the velocity was nearly symmetric about the mid-plane in both horizontal and vertical direction. As the flow increases, the flow velocity near the outer wall increases and the symmetry about the horizontal axis becomes distorted. When the flow becomes more distorted by the Dean vortex, Dean drag force dominates over inertial lift force. At this point focusing breakdown occurs.

To compare the result of the constant width circular bend, another variable width circular bend was numerically investigated. The bend starts with a channel width of 50 $\mu\text{m}$  and goes on increasing up to 200 $\mu\text{m}$  at the outlet. The CAD model was imported in ANSYS and meshed with mapped rectangular 5 $\mu\text{m}$  elements.

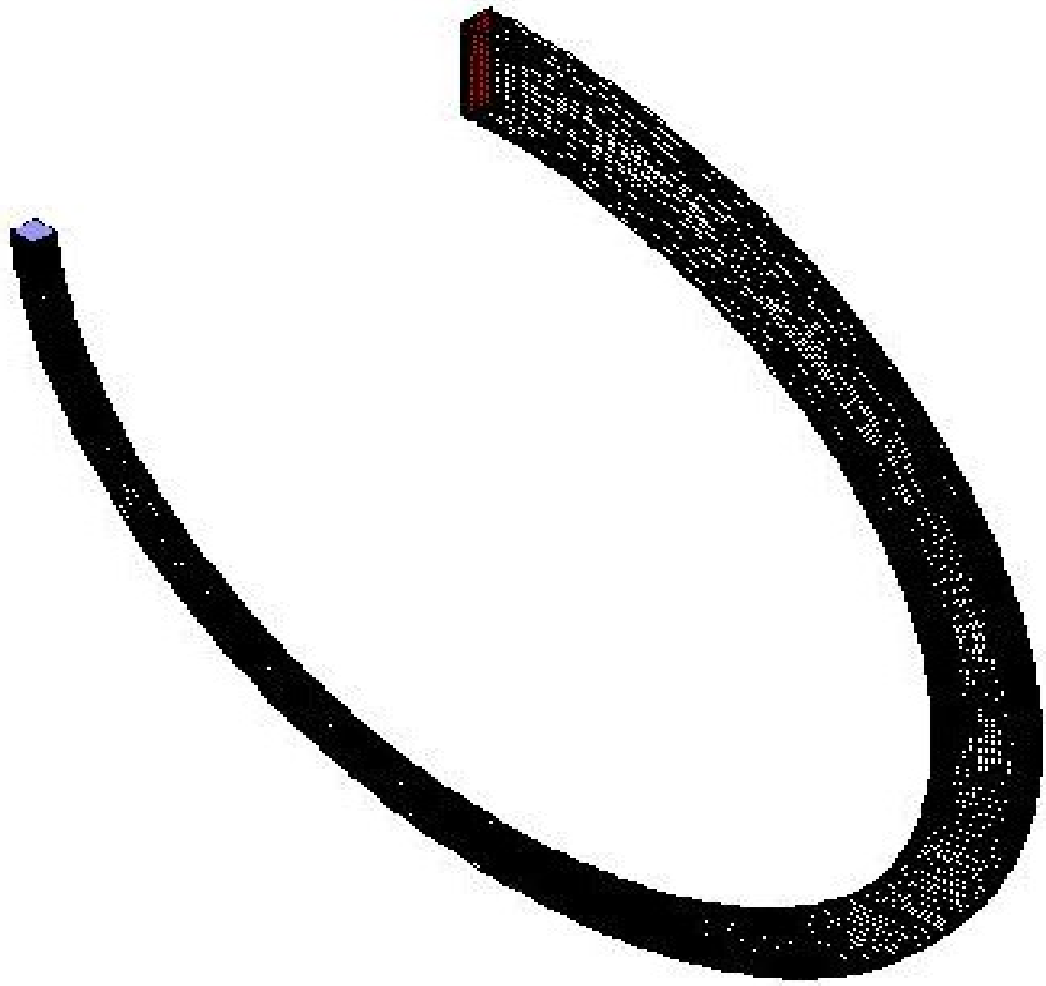


Figure 3-10 Variable circular bend with inlet width of  $50\mu\text{m}$  and outlet width of  $200\mu\text{m}$ . Inlet and outlet faces were meshed with  $5\mu\text{m}$  sized element. The mesh elements were then mapped along the four curved edges to complete the meshing. Total number of elements are 40986

This microchannel was also solved in ANSYS for eighteen different inlet flow condition starting from  $0.1\text{m/s}$  and ending at  $3.0\text{m/s}$ . The result is presented in figure 3-11

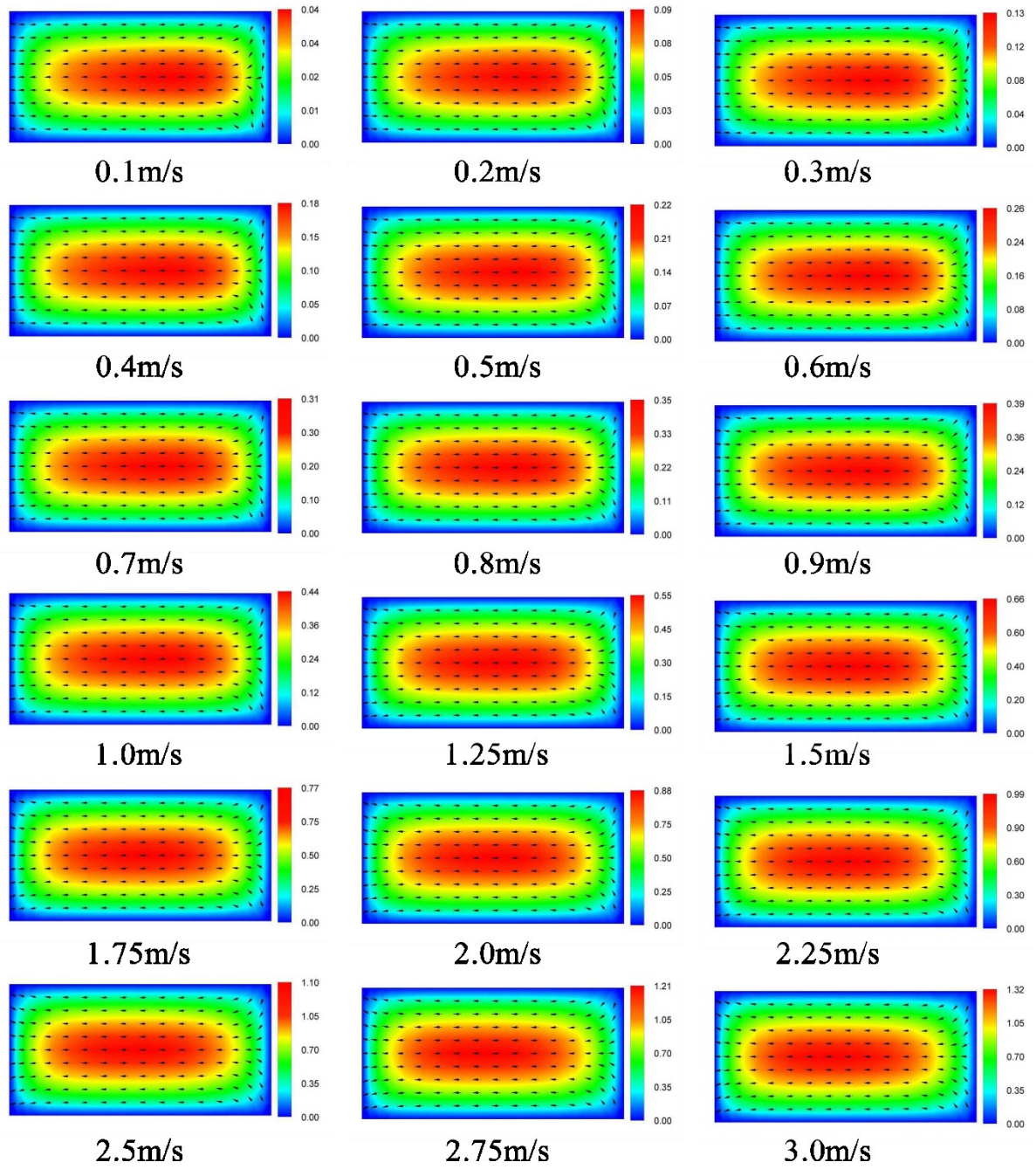


Figure 3-11 Flow profile of a variable width circular bent at the outlet. Inlet flow velocity is placed at the bottom of each picture.

Figure 3-11 shows that even the inlet flow condition stays the same as constant bent; the flow profile does not show any extensive Dean vortex (typical average Dean Velocity 0.0003m/s instead of 0.0006m/s; corresponding Reynolds number of 6) and flow distortion even at flow rate as high as 3.0m/s. This helps in maintaining the focusing at higher flow rate for variable width microchannels.

To visualize the Dean Flow velocity affected by the channel width, the average Dean velocity with channel Reynolds Number is plotted in figure 3-12.

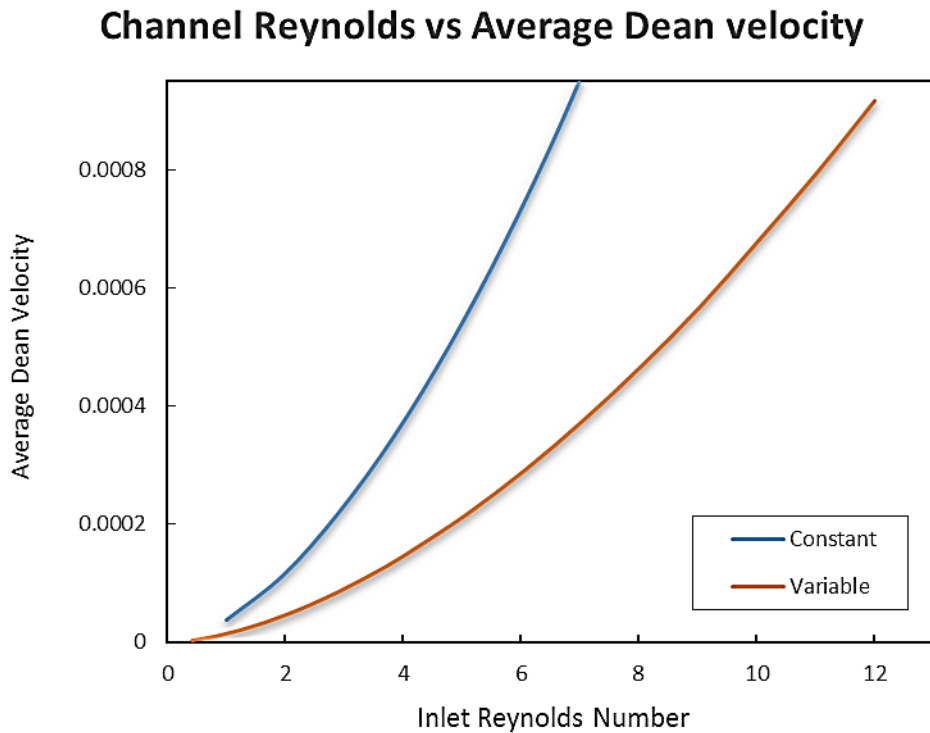


Figure 3-12 Average Dean velocity with respect to inlet Reynolds number

From the figure, it is clear that the variable channel cross section is advantageous over the constant channel width, because as the channel Reynolds number increases, the average Dean Velocity increases sharply in microchannel with constant width compared to microchannel with variable width. This indicates that it is possible to prevent the Dean number from increasing sharply even at higher flow rate, which results in particle defocusing.

### 3.1.5 Explanation of the device design

Studies by some research groups[18,38,45] indicated that the key for particle focusing/separation in spiral channel is the force balance between inertial lift force and Dean drag force. To date, many spiral microchannels for particle separation used uniform channel dimensions. One disadvantage of the uniform design is that the Dean Drag forces increase faster than lift force. At high flow rate, Dean Drag force is dominant, making it difficult for microparticles to reach a force balance at high Reynolds numbers and are likely to break down the focused stream. To enhance the force balance at high flow rate, that will facilitate the particle separation, in this work a spiral microchannel was used that has a gradually increased hydraulic diameter to control the interplay between Dean drag and inertial drag [20,69]. With such a design, Dean drag force becomes comparable to inertial drag even at high Reynolds number, [69] facilitating focusing and separation of particles at high Reynolds number[20].

In the first half of the Spiral microchannel, as the flow progresses from the inlet to the S-shaped junction, the curvature of the channel ( $1/R$ ) increases, leading to increasing Dean number and the Dean drag force. However, at the same time, because the channel width increases, the flow velocity decreases; hence as the curvature increases along the flow direction, the increments in Dean number and Dean drag force are not as large as in a spiral channel with constant channel width. While quickly increased Dean drag force at a high Reynolds cause breakdown of focused particle streaks [69] in microchannels with constant cross sections, the use of a spiral microchannel with gradually increasing channel width has advantage in focusing microparticles at higher Reynolds numbers and flow rates.

In the S-shaped junction at the center, when particles enter the 1<sup>st</sup> half circle, both particles are focused in the streaks near the inner wall[37,53,69,72,75]; at the center of the S-shaped junction, because the flow direction was switched from counter-clockwise to clockwise[38,39], the Dean force and inertial force changed directions; the outer wall becomes the inner wall. As a result, in the 2<sup>nd</sup> half circle of the S-junction, the focused particle streaks were focused again toward the “new” inner wall. This transition is beneficial for mitigating against dispersion and diffusion effects of particle motions and also assists in compacting the bandwidth of focused particle streaks[39].

After the S-junction, the flow advances towards the outlet. Along the flow direction, the Dean number and the Dean drag force reduces because of the reducing curvature and

the increasing channel width. Hence, at higher Reynolds numbers/flow rates, the present microchannel design facilitates in maintaining force balance between the Dean Drag force and the inertial lift force. Different sized particles are focused at different equilibrium positions according to their sizes. At high Reynolds numbers, using the design with increasing channel width, larger particles are focused near the inner wall, while the smaller particles are affected more by the Dean effect and tend to move away from the inner wall of the channel[20,72] which helps in increasing the separation distance between particle streaks.

To visualize the advantages of varying the channel cross section, the Dean force acting on  $9.94\mu\text{m}$  particle is plotted in figure 3-13.

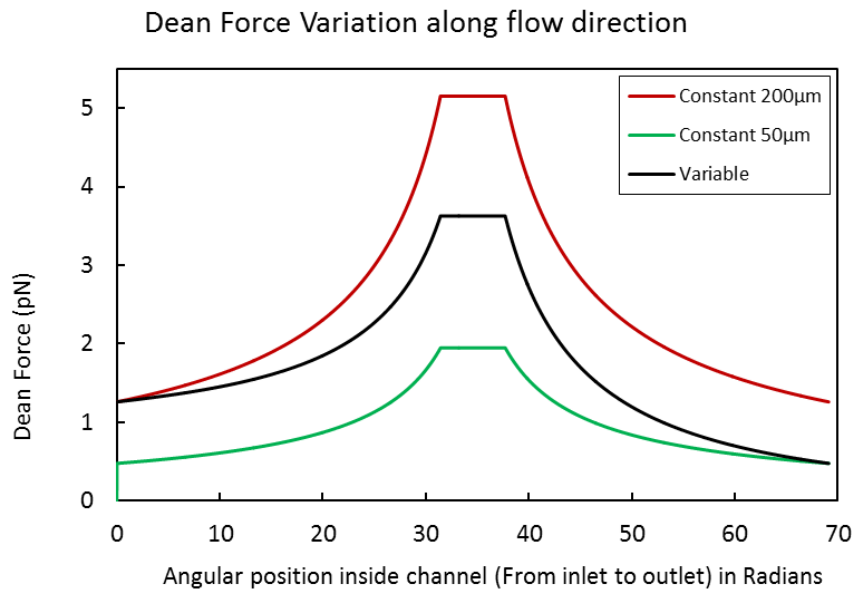


Figure 3-13 Variation of Dean force along the channel length. From the inlet to outlet. Solid black line- variable width, red and green  $50\mu\text{m}$  and  $200\mu\text{m}$  channel width. Flow condition  $700\mu\text{L}/\text{min}$ . Forces calculated for  $9.94\mu\text{m}$  diameter spherical particles.

Figure 3-13 shows the Dean force inside the proposed microchannel. The calculations are performed using equations (3-5) and (2-6). From figure 3-13 it is observed that the Dean Force at the first half of the microchannel increase slowly compared to both the constant width microchannel. At the center inside the S-junction, the Dean Force is constant. After the S-junction, at the second half of the spiral channel, the Dean force is decreasing faster-compared to both the constant width microchannel. This gives the advantage to restrict the Dean Force to go beyond the focusing limit and help separating two stream of microparticles.

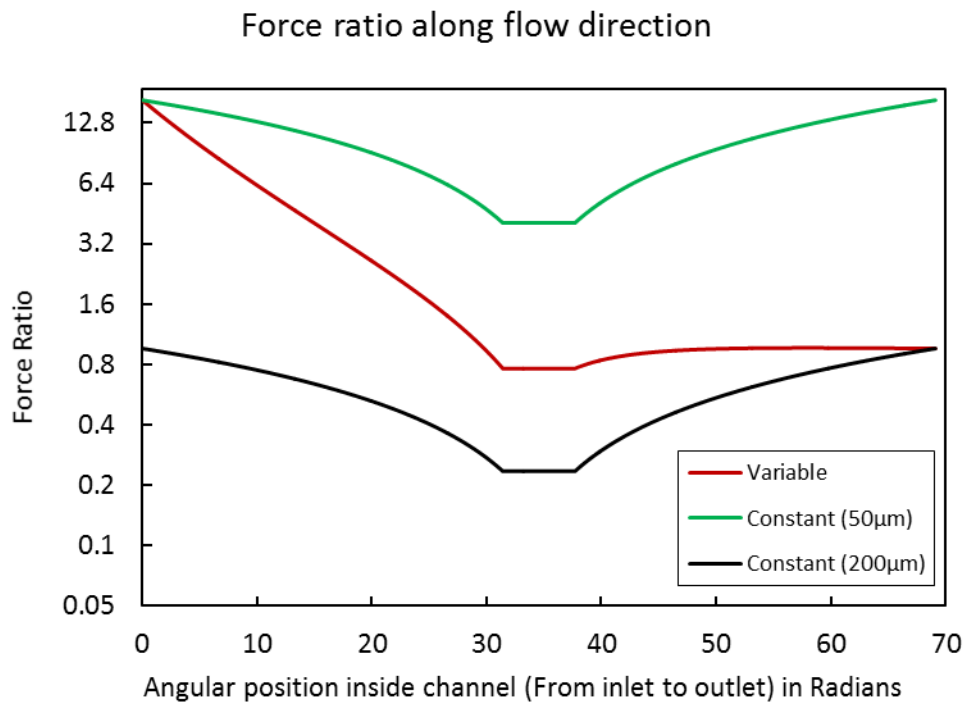


Figure 3-14 Variation of force ratio along the flow direction from the inlet to outlet. The radial location at the inlet is zero radians and at the outlet is  $\sim 69$  radians

To better visualize the advantage of varying the hydraulic diameter of Fermat Spiral microchannel, the force ratio is plotted and compared with constant (two different widths) width microchannel. The result is plotted in figure 3-14 which indicates that the force ratio is significantly closer to unity for variable width microchannel than the other two throughout the channel from the inlet to outlet. Most importantly, after the S-junction, the force ratio almost remains close to unity. Throughout the second half of the spiral microchannel, the force ratio stays constant. This helps particles to find their equilibrium position because the magnitude of the force is staying the same. This is a primitive indication of the device's functionality at higher flow rate.

While the force analysis shows the advantages of restricting the Dean Force inside the microchannel of the current design, the calculations and plots do not directly show the particle separation behavior using the proposed design. In an attempt to study the particle separation behavior, in the next section (section 3.2), a complete numerical simulation of the device is presented. Commercially available flow solver ANSYS was utilized to solve for steady-flow condition, and Discrete Phase Modeling (DPM) is used to trace the particle trajectories. The simulation details are presented, and results are discussed in section 3.2.3.

### 3.2 Basic theory and modeling equations

In order to design and model the geometry of the proposed device, CREO parametric was used to build the 3-D model of the spiral microchannel using sweep blend feature along a set of datum curve defined by equations in cylindrical co-ordinate. The spiral datum curve was defined by the parametric relation of  $r$  and  $\theta$  on a plane.

$$x = (a + b \cdot t) \cdot \cos(360 \cdot n \cdot t) \quad (3-7)$$

$$y = (a + b \cdot t) \cdot \sin(360 \cdot n \cdot t) \quad (3-8)$$

In the above equations 'n' defines the number of turns while  $a$  and  $b$  defines the initial distance from the coordinate and the spacing between the adjacent turns.

After the 3D model was generated, the geometry was then imported into ANSYS Workbench, and the inlet and outlet faces were meshed using element of size  $5\mu\text{m}$ . The entire geometry was then mapped using the surface mesh along the curved edges of the Differential Fermat Spiral microchannel. Once all the mapped meshing criteria was assigned, the geometry is meshed with  $\sim 1.8$  million quad elements. A magnified view of part of the geometry is presented in figure 3-15.

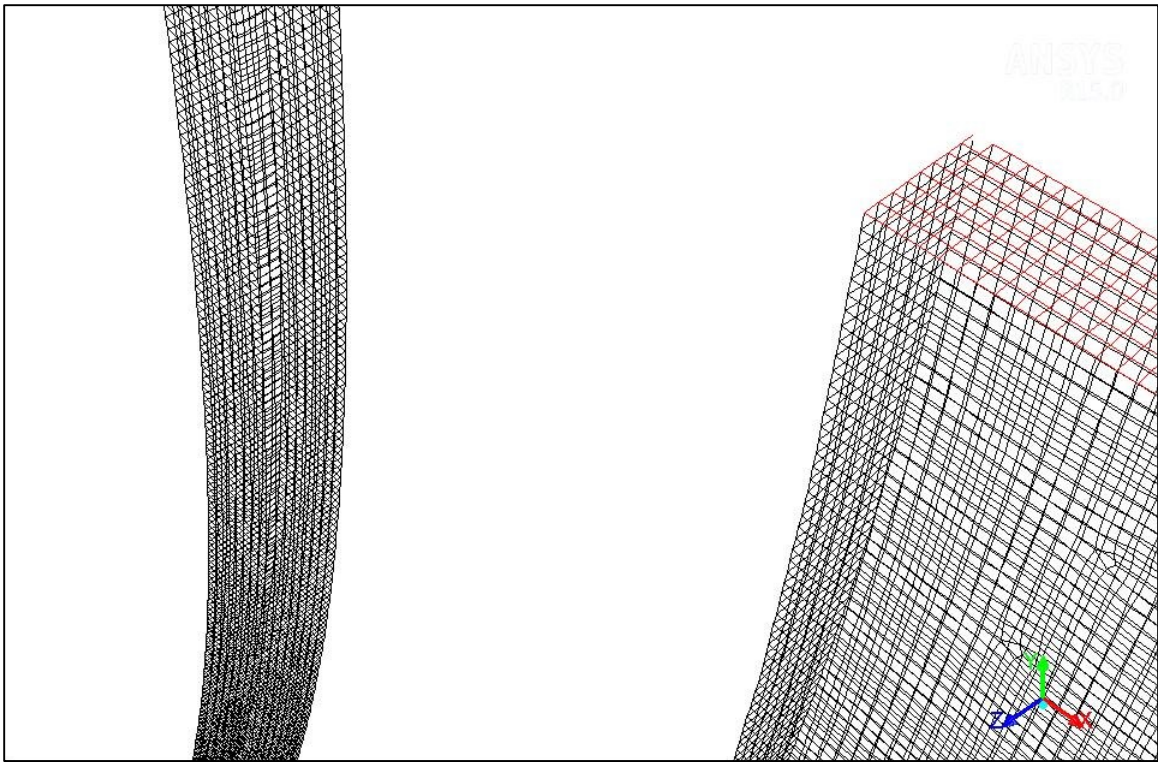


Figure 3-15 Mesh elements of a Spiral microchannels

### 3.2.1 Steady state fluid flow

The meshed geometry were then imported into Fluent (version 14) to simulate the flow field. Inlet velocities, calculated from corresponding flow rate or Reynolds number, were applied as the inlet boundary condition. Non-slip boundary conditions were set on all channel walls; atmospheric pressure was applied at the outlet. To solve the fluid flow inside the channel, Coupled scheme for pressure-velocity coupling and MUSCLE scheme for the momentum equation was employed to solve the Navier-Stokes equations. The solution converges after about ~300 iterations and flow field solution became the input

to Discrete Phase Modeling (DPM). Once the flow field was solved, the velocity profile and velocity vector at the outlet of the spiral channel is plotted (figure 3-16) The flow field shows a Dean vortex as predicted by W. R. Dean[30].

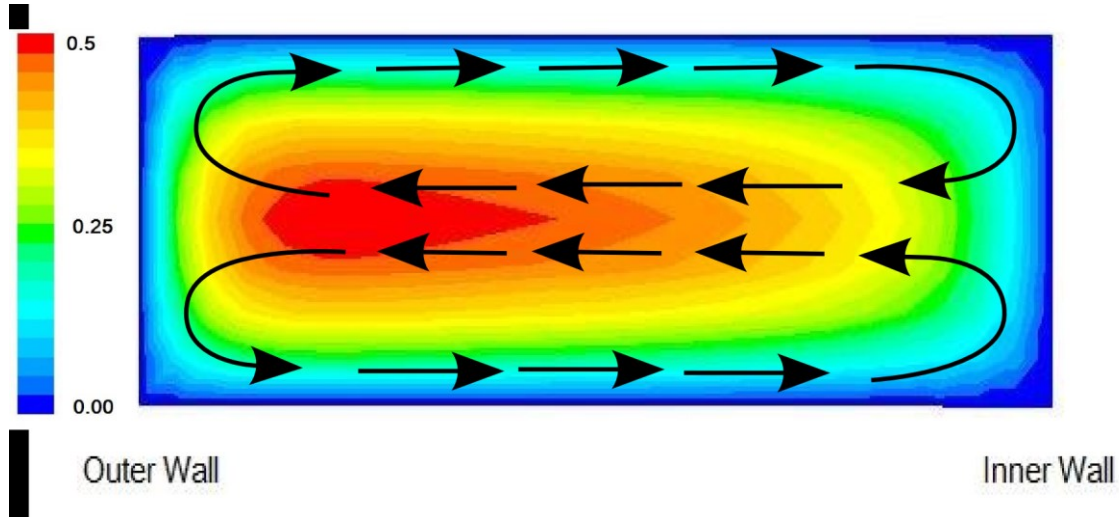


Figure 3-16 Dean velocity profile at the outlet of differential Fermat spiral channel with inlet flow velocity of 3m/s

### 3.2.2 Discrete phase modeling

After a steady state flow solution was solved, two sets of ( $4.5\mu\text{m}$  and  $9.94\mu\text{m}$ ) particles were introduced normal to the inlet surface; in every node one particle of each size was released. The collision of the particles with the walls was assumed perfectly elastic. Hence, the coefficient of restitution were assumed unity.

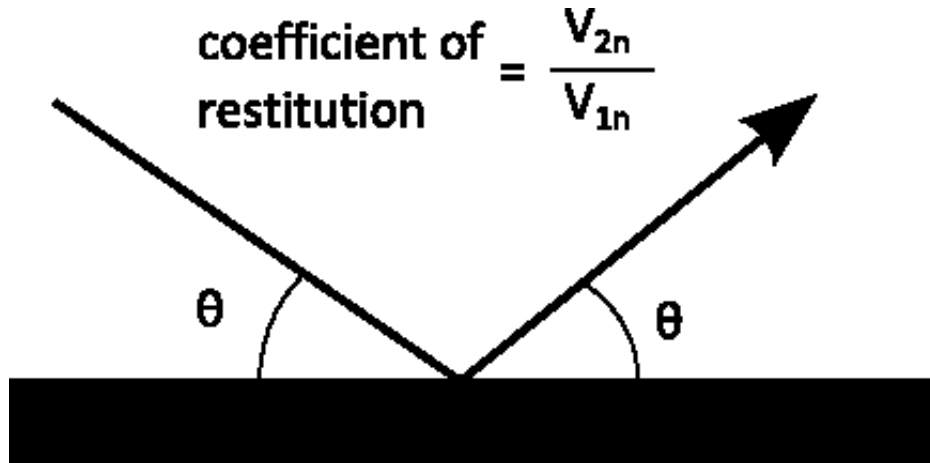


Figure 3-17 Coefficient of restitution on wall boundary condition for DPM modeling

The particle trajectories were calculated from the forces acting on them (Newton's second law). The force balance equates the particle inertia in Lagrangian reference frame:

$$\frac{d\bar{v}_p}{dt} = F_{Dr}(\bar{v} - \bar{v}_p) + \frac{\bar{g}(\rho_p - \rho)}{\rho_p} + F \quad (3-9)$$

In the equation,  $F_{Dr}$  is the drag force caused by the velocity variation between fluid and particle.  $F_{Dr}$  is defined as

$$F_{Dr} = \frac{18\mu}{\rho_p a^2} \frac{C_D Re_s}{24} \quad (3-10)$$

Here,  $C_D = a_1 + \frac{a_2}{Re_s} + \frac{a_3}{Re_s^2}$  and the values of  $a_1$ ,  $a_2$  and  $a_3$  are proposed by Morsi and Alexander[76]. In equation (3-9)  $F$  is the additional acceleration term that includes force required for a particle to accelerate through fluid medium and also the inertial lift force proposed by Asmolov[61].

$$F = \frac{1}{2} \frac{\rho}{\rho_P} \frac{d(\bar{v} - \bar{v}_p)}{dt} + \frac{F_L}{\frac{1}{6} \pi a^3 \rho_P} \quad (3-11)$$

In the equation,  $F_L$  is calculated using equation (2-3), where  $C_L$  is a function of Reynolds number and channel location. The inertial lift force was assigned using a User Defined Function (UDF) in ANSYS. The code was then compiled and built to generate a library file that ANSYS can recognize. The files were then loaded in Fluent 14. After the generation, library files are imported, the UDF becomes available to be selected as body force.

The  $\frac{\bar{g}(\rho_P - \rho)}{\rho_P}$  term in equation (3-9) was negligible for particle density that is very much close to the surrounding fluid, which was the case for polystyrene suspended in water ( $\sim 1.05 \text{ g/cm}^3$ )

After all the necessary forces were included in the model using fluent default options and by writing UDF, the particle trajectories were solved for different flow rates. For all the particles to complete the trajectories, it requires 300,000 time steps in DPM modeling.

### 3.2.3 Calculation of coefficient of lift ( $C_L$ )

The lift coefficient in equation (2-3) varies with channel Reynolds number and the location inside the microchannel. In mathematical form, lift coefficient is written as

$C_L = f(Re, x_L)$  where,  $x_L$  is the particle location inside the channel. The average value of  $C_L$  was proposed by Di Carlo[44] as  $\sim 0.5$  for a Reynolds number close to 90. For different Reynolds number the value can be estimated from Asmolov's[61] derivation. In his article, Asmolov provided a plot of inertial lift for neutrally buoyant particle along the particle location inside the microchannel for various Reynolds number.

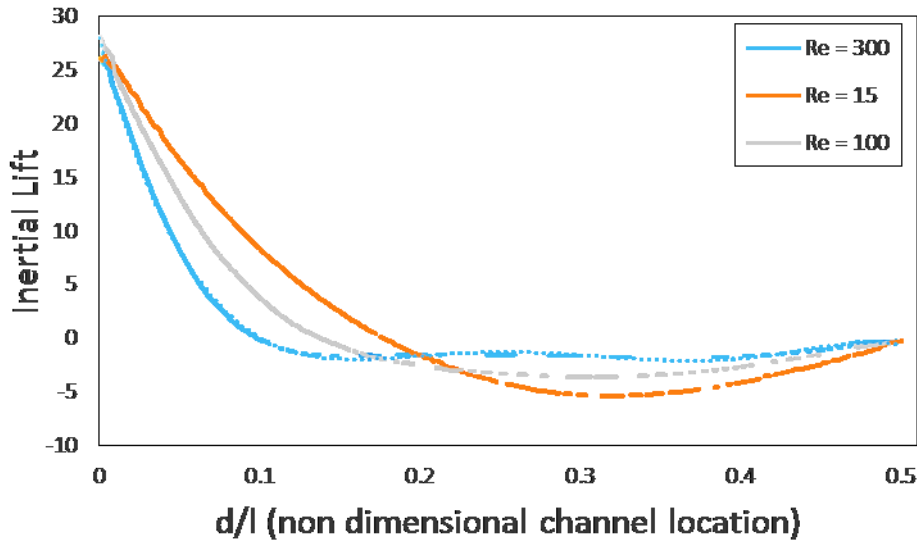


Figure 3-18 Inertial lift along the non-dimensional channel location as extracted from Asmolov[61]

From the graph, inertial lift can be calculated in the form  $F_z R_c^{\frac{1}{2}} \varepsilon^{-3}$ . Again, Asmolov quantified the inertial lift force as a function of lift coefficient as  $F_z = \varepsilon^3 C_L$ . Comparing these two equations, the  $C_L$  values can be calculated for a specific channel Reynolds number. In order to find the average value of  $C_L$ , a polynomial approximation is made at a specific Reynolds number and using calculus, the average value of the function is calculated for desired Reynolds number. After the  $C_L$  values are find out for different

Reynolds number, they are then plotted on graph with an intention to find out a power fit.

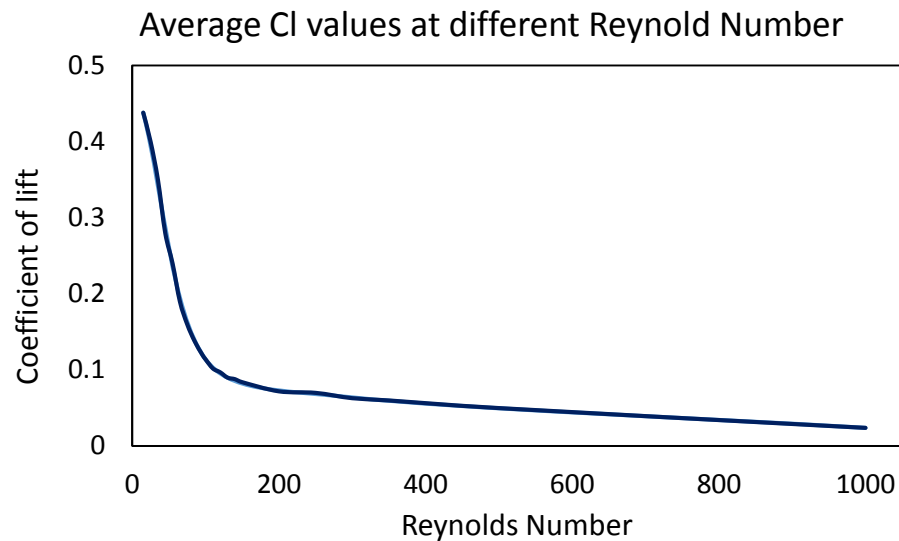


Figure 3-19 Coefficient of lift values for varying channel Reynolds number.

From figure 3-19, an equation is extracted that relates  $C_L$  values to different channel Reynolds number. The equation is in the form

$$C_L = 3.4368Re^{-0.714} \quad (3-12)$$

Asmolov provided  $C_L$  values for Reynolds number starting from 15~1000. For numerical simulation Reynolds number approaches zero at the proximity of no-slip wall boundary conditions. To handle such irregularities, a constant  $C_L$  value of 0.5 is assumed for Reynolds number less than 15.

### 3.2.4 Validation of numerical simulation

To validate the numerical method we simulated a particle separation device with experimental data[18] using the same geometry and other operating conditions in ANSYS Fluent. The particle separation device proposed by Bhagat et al.[18] consists of five turn spiral microchannel. The channel width was 100 $\mu\text{m}$  and height was 50 $\mu\text{m}$ . The adjacent spacing between two microchannel walls was about 250 $\mu\text{m}$ . The initial radius of the channel was 3mm and the total length of the channel was  $\sim$ 13cm. 1.9 $\mu\text{m}$  and 7.32 $\mu\text{m}$  particles, used in the experiments, were utilized for this numerical simulation. The Dean number inside the channel was 0.94 with a corresponding flow velocity of 0.13 m/s.

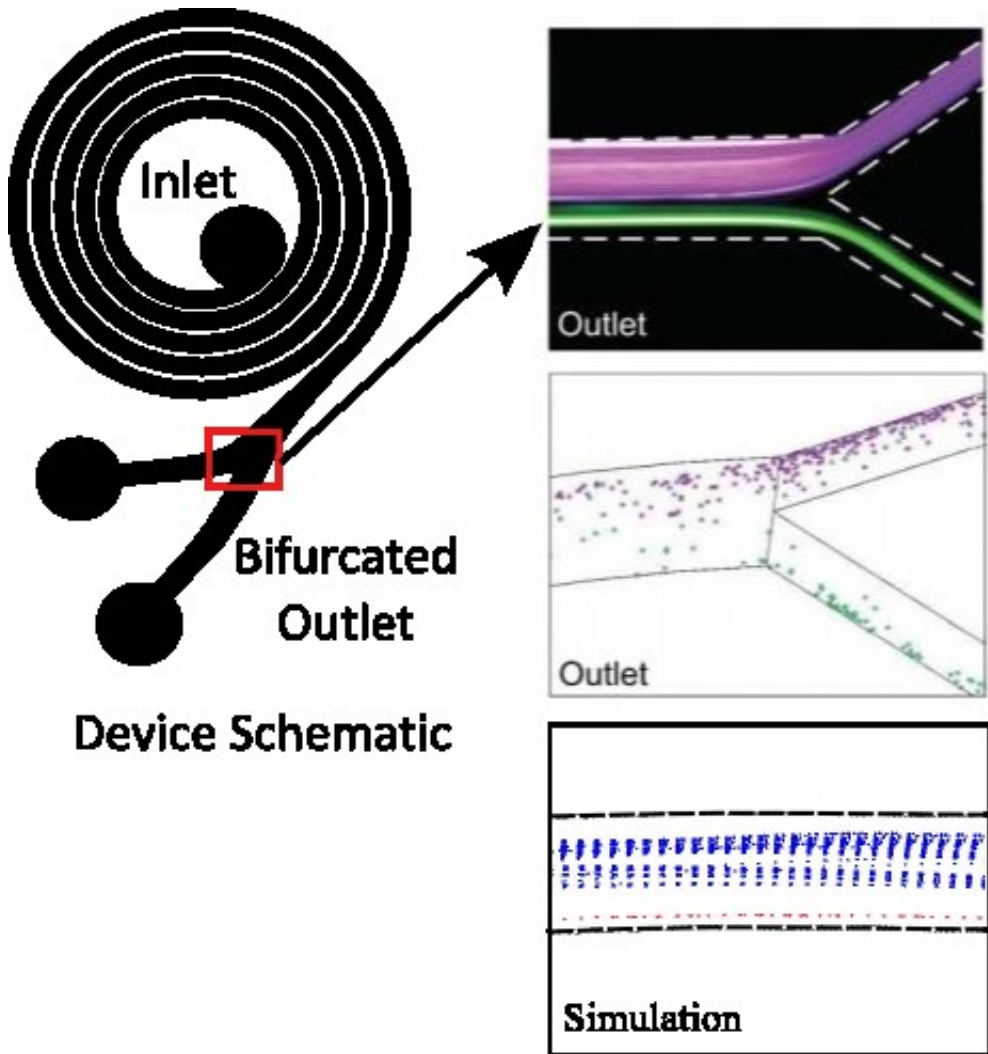


Figure 3-20 Validation of numerical method by comparing the simulation results with an existing device spiral microchannel on particle separation. The first two pictures are taken from Bhagat et al[18] at the outlet (flow rate  $10\mu\text{L}/\text{min}$ ) and the third picture is obtained from Fluent simulation at outlet under exactly the same conditions under which the experiments were conducted. Blue dots represent  $1.9\mu\text{m}$  and red dots represent  $7.32$  microparticles

From figure 3-20 it is observed that the simulation and experiment is in good agreement. At the specified flow rate the smaller  $1.9\mu\text{m}$  particles were observed to stay closer to

the outlet of the microchannel and the larger  $7.32\mu\text{m}$  particles were observed to stay near the inner wall. The larger particles were also seen to follow a compact streak width. All these demonstrations were qualitatively compared with the simulation model, and a good match is observed. This ensures the validity of the model and confirms further experimentation as valid.

### 3.2.5 Simulation result

After the simulation was complete, the particle trajectories were recorded at specific location of the microchannel as shown in the figure 3-21 (same locations it was done for the experimental observations). The results are presented in figure 3-22.

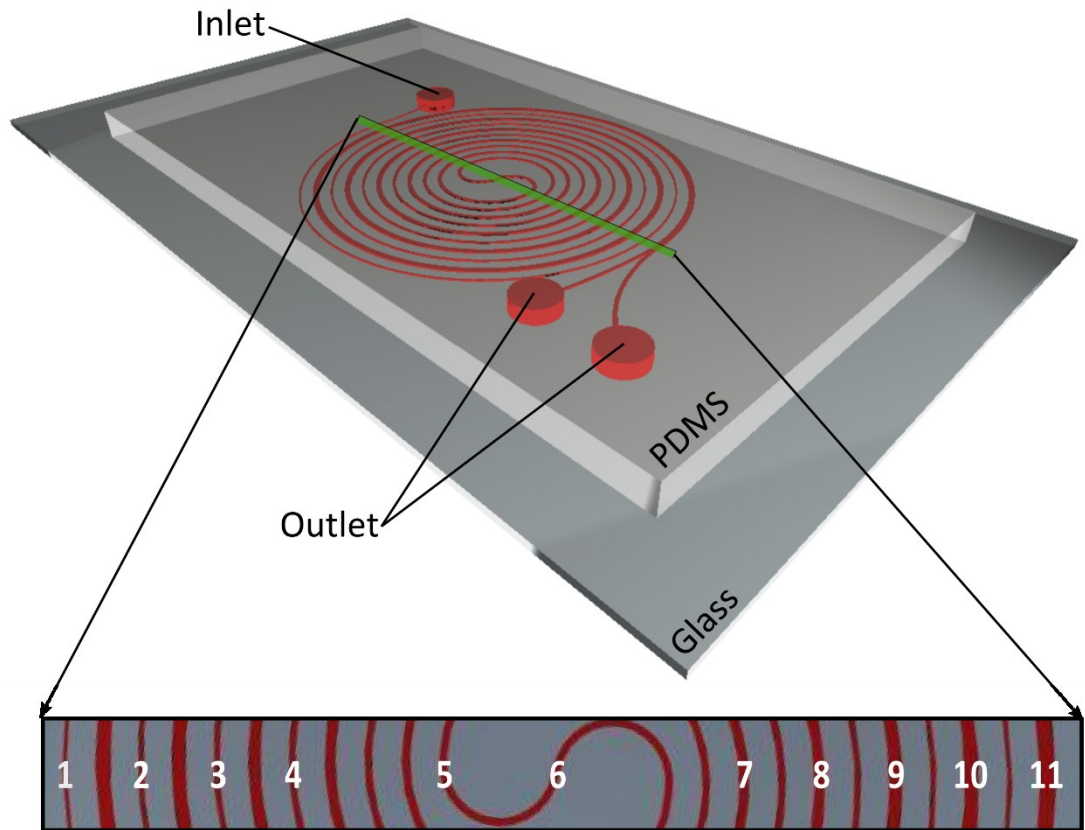


Figure 3-21 Channel location where images were taken.

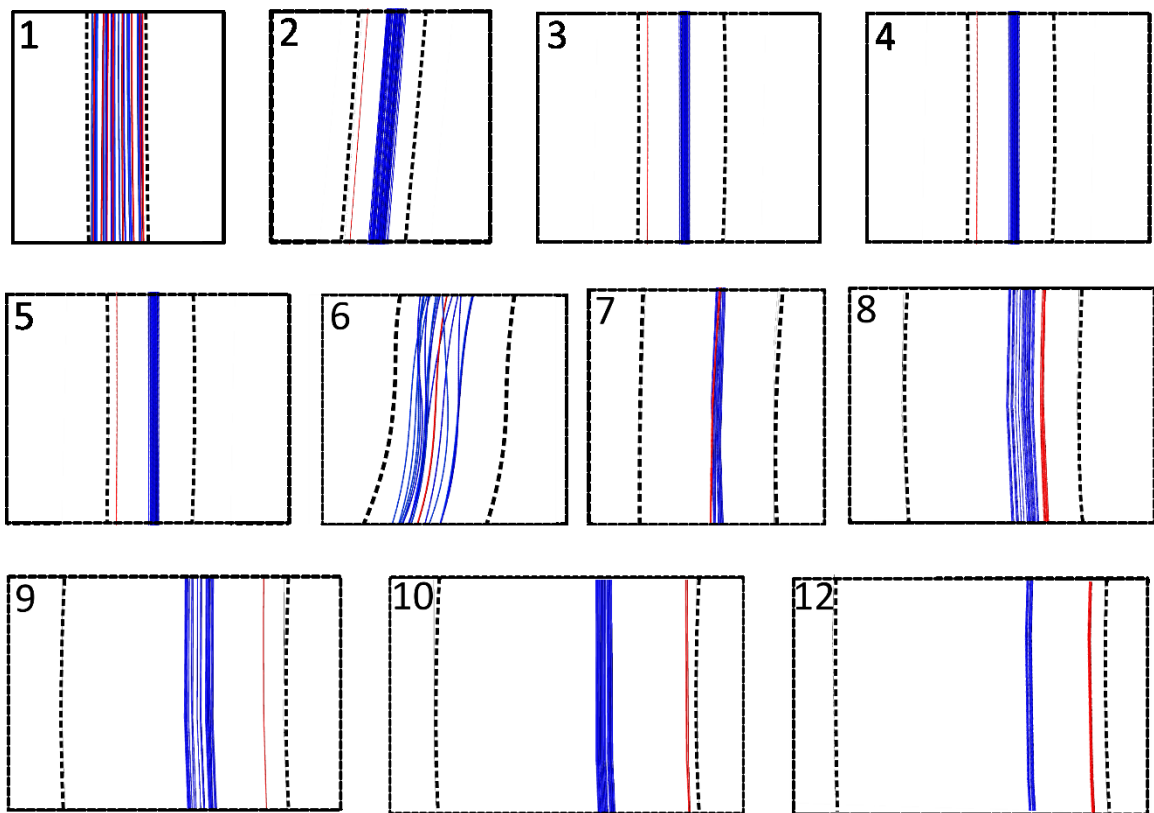


Figure 3-22 Simulated particle trajectories for  $4.5\mu\text{m}$  (blue) and  $9.94\mu\text{m}$  (red) flowing through the device at a flow rate of  $700\mu\text{L}/\text{min}$ .

From the simulation result at  $700\mu\text{L}/\text{min}$  it is observed that the particles were evenly dispersed throughout the channel near the inlet. After the first turn, the large  $9.94\mu\text{m}$  particles are focused but the smaller  $4.5\mu\text{m}$  particles remain unfocused. As the flow progresses towards the center, the streak width of the larger particles decreases because particles have found equilibrium positions. However, the bandwidth of small particles is still large because small particles are affected more by Dean vortex. When the particles enter the center S-junction, the streak width is pushed by the Dean Drag

force and inertial lift from the both walls. This helps in compacting the bandwidth as mentioned by Seo et al.[38]. After the central S-junction, the particles enter into the 2<sup>nd</sup> half of the spiral channel. At the outer spiral turns, because of reducing  $1/R$  and increasing channel width, the Dean velocity is relatively smaller and so is the Dean force. Therefore the inertial lift force can more easily be balanced by the Dean Drag force. Hence, the particle is more likely to find equilibrium positions and get focused. This explains why the bandwidth of small particle streaks gradually reduces, and the separation distance gradually increases in the consequent coil turns (position 8, 9, 10 and 11).

### 3.3 Simulation result at high flow rate

In order to test whether the proposed device works at higher flow rate and higher Reynolds numbers, simulation was also carried out at a flow rate of  $1700\mu\text{L}/\text{min}$  ( $\text{Re}_c=250$ ). Five differently sized particles were introduced into the simulation. Particles were introduced normal to the inlet surface; at every node of an element, one particle of each size was released. The wall boundary conditions were perfectly elastic with a coefficient of restitution 1. The results are shown in figure 3-23.

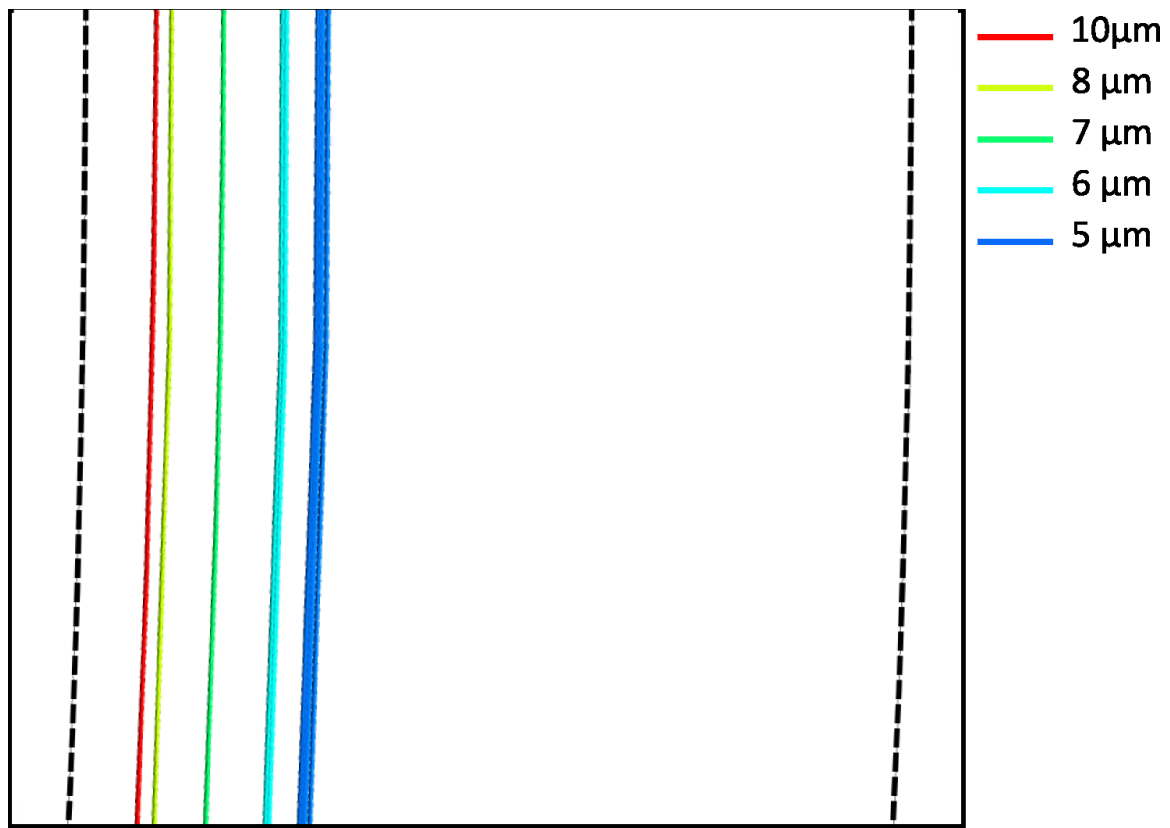


Figure 3-23 Particle streamline of five different particles of diameter ranging from 5 $\mu\text{m}$ , 6 $\mu\text{m}$ , 7 $\mu\text{m}$ , 8 $\mu\text{m}$  and 10 $\mu\text{m}$  (the colors are shown to the right) at flow rate 1700 $\mu\text{L}/\text{min}$  at the outlet of the differential Fermat spiral channel.

Figure 3-23 shows that at 1700 $\mu\text{L}/\text{min}$  at the outlet particle streak width is widest for the smallest 5 $\mu\text{m}$  particles. As the particle size gets bigger, the streamline shifts toward the inner wall and the streak width reduces. Even though, the streak width of some particles is wide but they are distinct from each other. This indicates if more and more particles were added (11 $\mu\text{m}$ , 12 $\mu\text{m}$  etc.) they will also shift closer to the inner wall while

maintaining a distinctive clear streamline. This ensures the separation of multiple streamlines of particles at higher flow rate.

## CHAPTER IV

### EXPERIMENTAL DEMONSTRATION

#### 4.1 Overview

In this chapter, the fabrication, experimental setup, testing and results of the proposed device are discussed. The experiment results, coupled with the numerical simulation confirmed the effectiveness of the differential Fermat Spiral microchannel as an efficient particle separation device. This chapter also details the fabrication procedure of the device and explains the experimental setup and the methodologies of obtaining the result.

#### 4.2 Device Microfabrication

The spiral microchannel was fabricated using standard lithography method, consisting of the following major steps:

#### 4.2.1 Fabrication of SU-8 mold

The microchannel master mold was fabricated using SU-8 2025 (MicroChem Corp.) The master mold was firstly fabricated using standard soft lithography[77,78] technique on a silicon wafer. The 2-D geometry of the microchannel was drawn in AutoCAD and then the design is sent out to CAD/ART services of Outputcity to print the photo mask.

Figure 4-1 shows an image of the photomask.

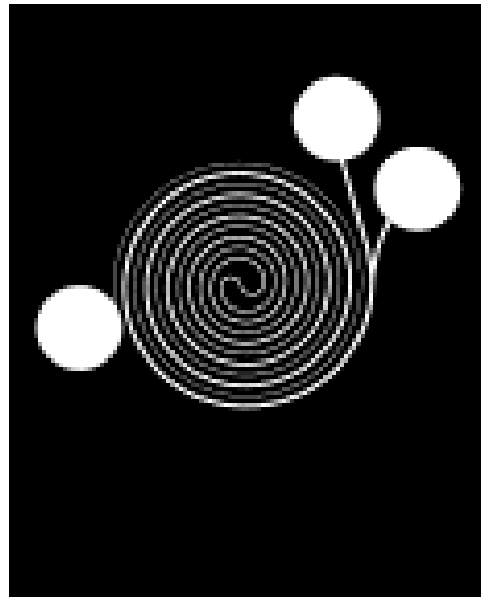


Figure 4-1 Printed photolithography mask of the design.

The mold was transferred onto Silicon wafer using SU-8 2025 and a photomask. The step by step process for SU-8 microchannel mold preparation is described below and illustrated in figure 4-2:

- i. A 4inch silicon wafer is cleaned on piranha solution (1 HF: 1 H<sub>2</sub>O<sub>2</sub>)
- ii. After the piranha cleaning of the wafer it is then rinsed with water, blow dried and baked at 150°C for one hour.
- iii. After baking is complete, the wafer is then cooled down to room temperature.
- iv. SU-8 2025 is then poured on top of the silicon wafer on a spinner.
- v. The spinner is set to accelerate from zero to 1500 rpm and then allowed to spin at 1500 rpm for 30 seconds.
- vi. After spinning is complete, the wafer is placed on a flat surface for ten minutes
- vii. Before exposing to UV light, the wafer is soft baked for three minutes at 65°C and 6 minutes at 95°C
- viii. After the soft baking, the wafer is then allowed to cool down to room temperature.
- ix. The wafer is then exposed to UV light for 16 seconds with the photomask placed on top of the wafer.
- x. After the exposure, the wafer is then baked again at 65°C for one minute and 95°C for 6 minutes.
- xi. Once the wafer is cooled down from post soft baking, the wafer is put on SU-8 developer for 3~6 minutes followed by a rinse with isopropyl alcohol.
- xii. As the mold is blow dried, it is then hard baked at 150°C for 24 hours.

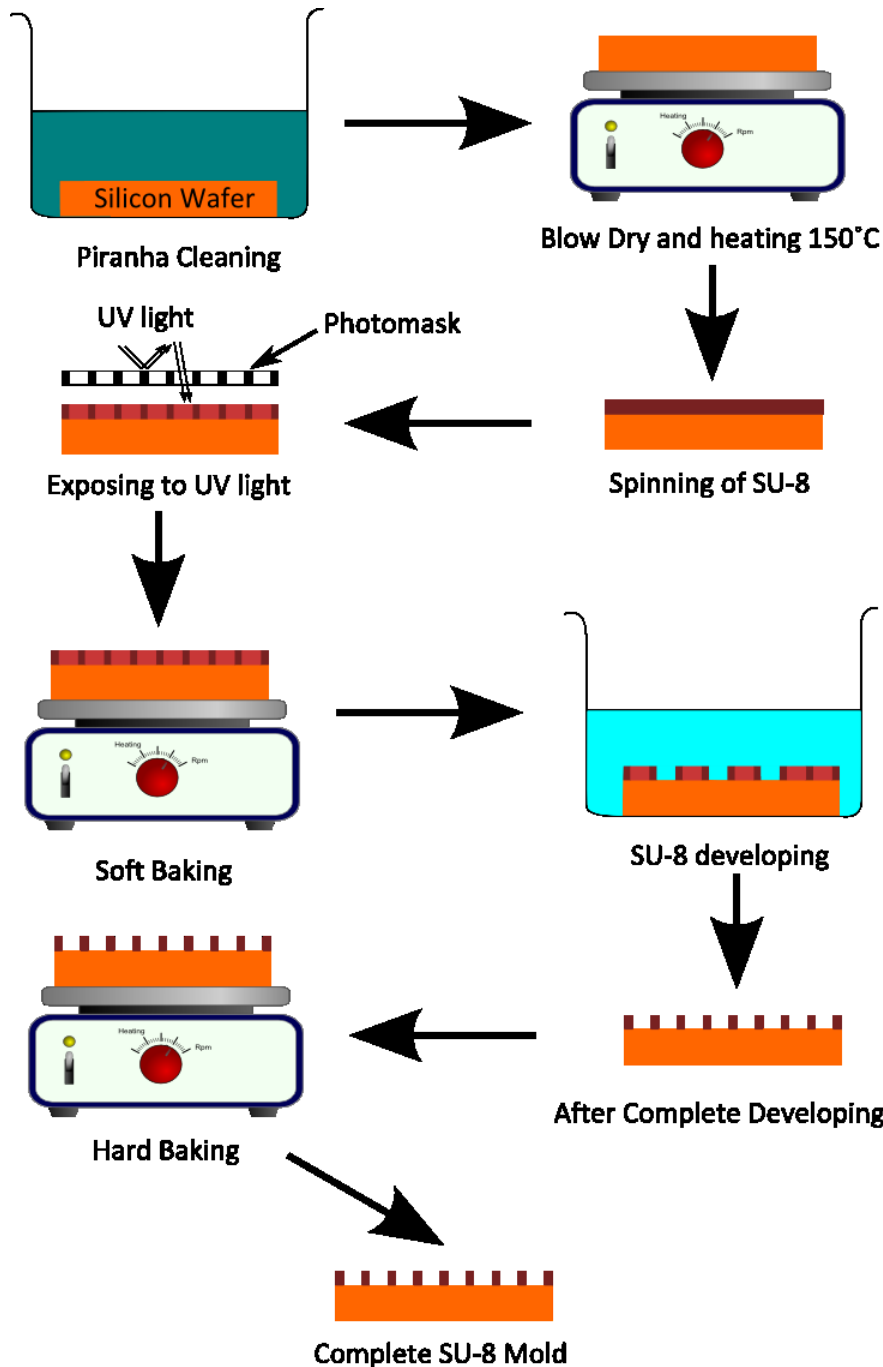


Figure 4-2 SU-8 patterning flow diagram of a silicon wafer. This patterned SU-8 mold will act as a die for PDMS mold

#### 4.2.2 Fabrication of PDMS microchannel

The flow process for fabricating the PDMS-Glass microchannel is presented in figure 4-3.

Polydimethylsiloxane (PDMS) elastomer is mixed in 10:1 ratio with curing agent (Slygard 184, Dow Corning) and poured on top of the SU8 mold. The PDMS on silicon is then degassed for three hours and cure at 70° C to create a PDMS mold. After cooling down, PDMS mold is peeled off from the SU8 mold. Next the inlet and outlet reservoirs are punched using Harris Uni-Core 2mm micro-punch.

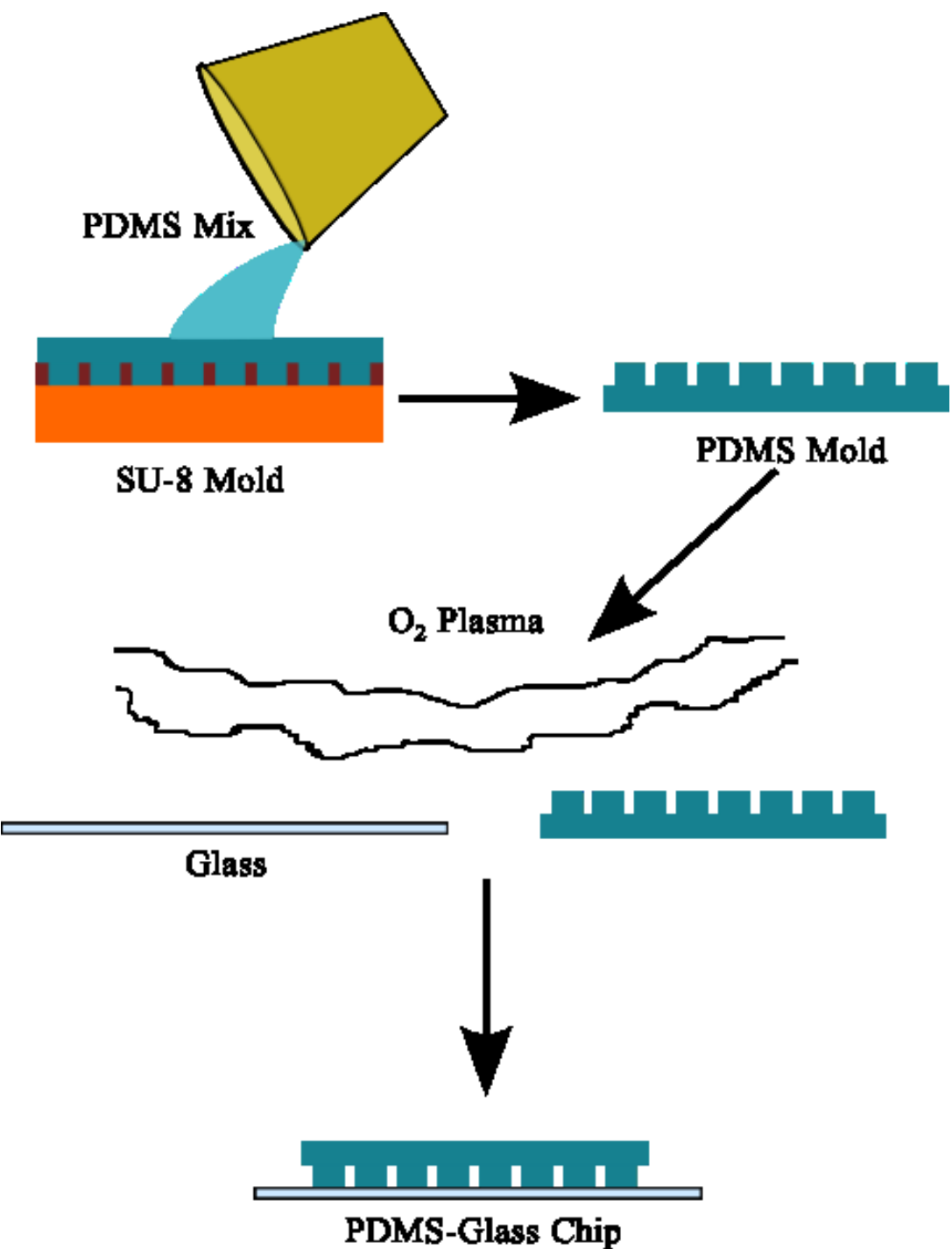


Figure 4-3 PDMS-Glass chip fabrication

#### 4.2.3 Plasma bonding of PDMS-Glass substrate

The PDMS microchannel and glass substrate are both exposed to Oxygen plasma for 50 seconds with pre-cleaned glass slides (VWR Labshop). The microchannel is then aligned on top of the glass slide using methyl alcohol. The process schematic is shown in figure 4-3. After that they were heated at 70° C for 24 hours to finalize the microchannel fabrication. Once the fabrication process is complete, necessary tubing and syringes are connected to the device. Figure (4-4) shows a microscopic picture of the completed microchannel before tubings are connected..

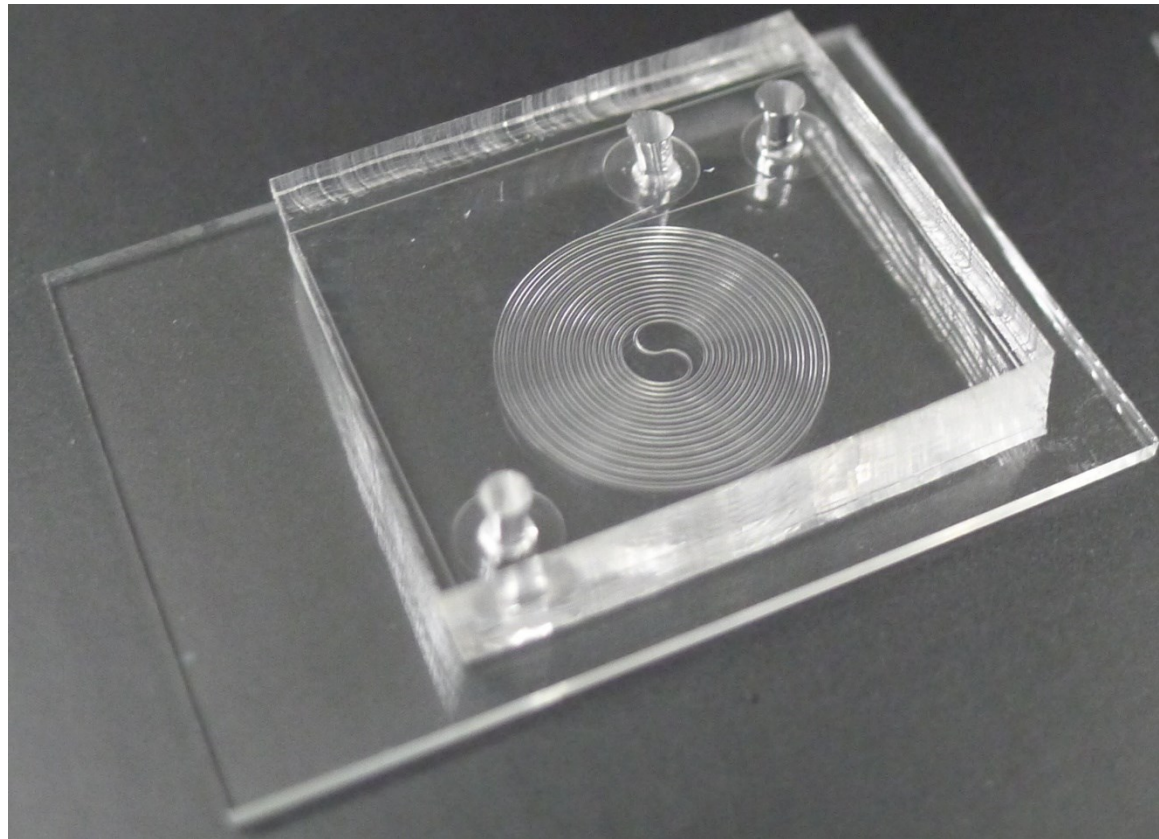


Figure 4-4 Image of fabricated devices before connecting necessary tubing and syringe pumps. Inlet and bifurcated outlet are shown.

After the device fabrication is complete, a microscopic image at different location of the device is captured with an optical microscope and a camera is attached to the microscope. The images are presented in figure 4-5.

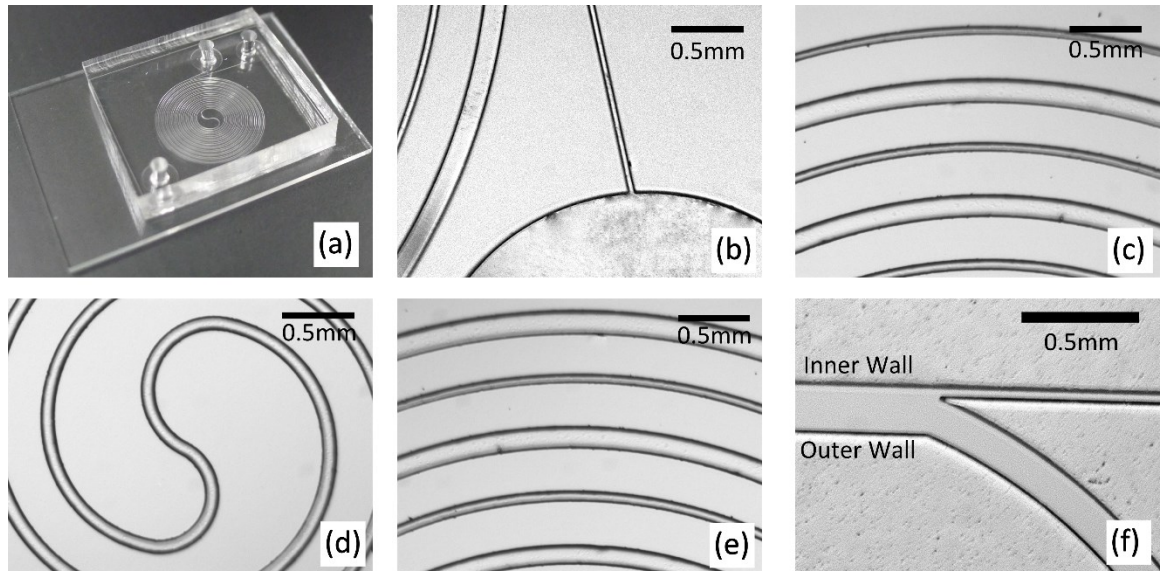


Figure 4-5 Image of the devices. (a) Device overview at full scale (b) Near the inlet reservoir (c) at the first half of the channel (d) at the center S-junction (e) at the second half of the spiral (f) at the bifurcated outlet

### 4.3 Experiments

Once the device is complete, sample is prepared, syringes are loaded with a syringe pump and connected to the device and tested for target flow rate. The details about how the sample is prepared are described in section 4.3.1 and how the device is setup for the experiment is described in 4.3.2. Subsequently, the acquired experimental results are presented and discussed in section 4.3.3

#### 4.3.1 Sample preparation

Fluorescent envy green micro-particles of  $9.94\mu\text{m}$  are bought from Bang Laboratories, and  $4.6\mu\text{m}$  blue microparticles are bought from Polysciences Inc. They are used to test the microchannel for particle separation. The mixture of the two particles (approximately  $1\times10^5$  particles/mL) with DI water is taken into a vial. The mixture is ultrasonicated at  $30^\circ\text{C}$  for one hour. After the sonication, the sample is then loaded in the syringe. After removing unnecessary bubble from the syringes, it is then loaded on a syringe pump (KD scientific).

#### 4.3.2 Experimental setup

Once the syringe pump is driven at the desired flow rate ( $700\mu\text{L}/\text{min}$ ) the mixture starts to flow through the reservoir into the microchannel. A two minutes of settling time is allowed for the flow to reach steady state. Once the flow became steady, the Fluorescence images are captured using an inverted microscope (Olympus IX71) equipped with a 12-bit digital camera (Q Imaging). Captured images are analyzed with freely available public domain ImageJ[79] software.

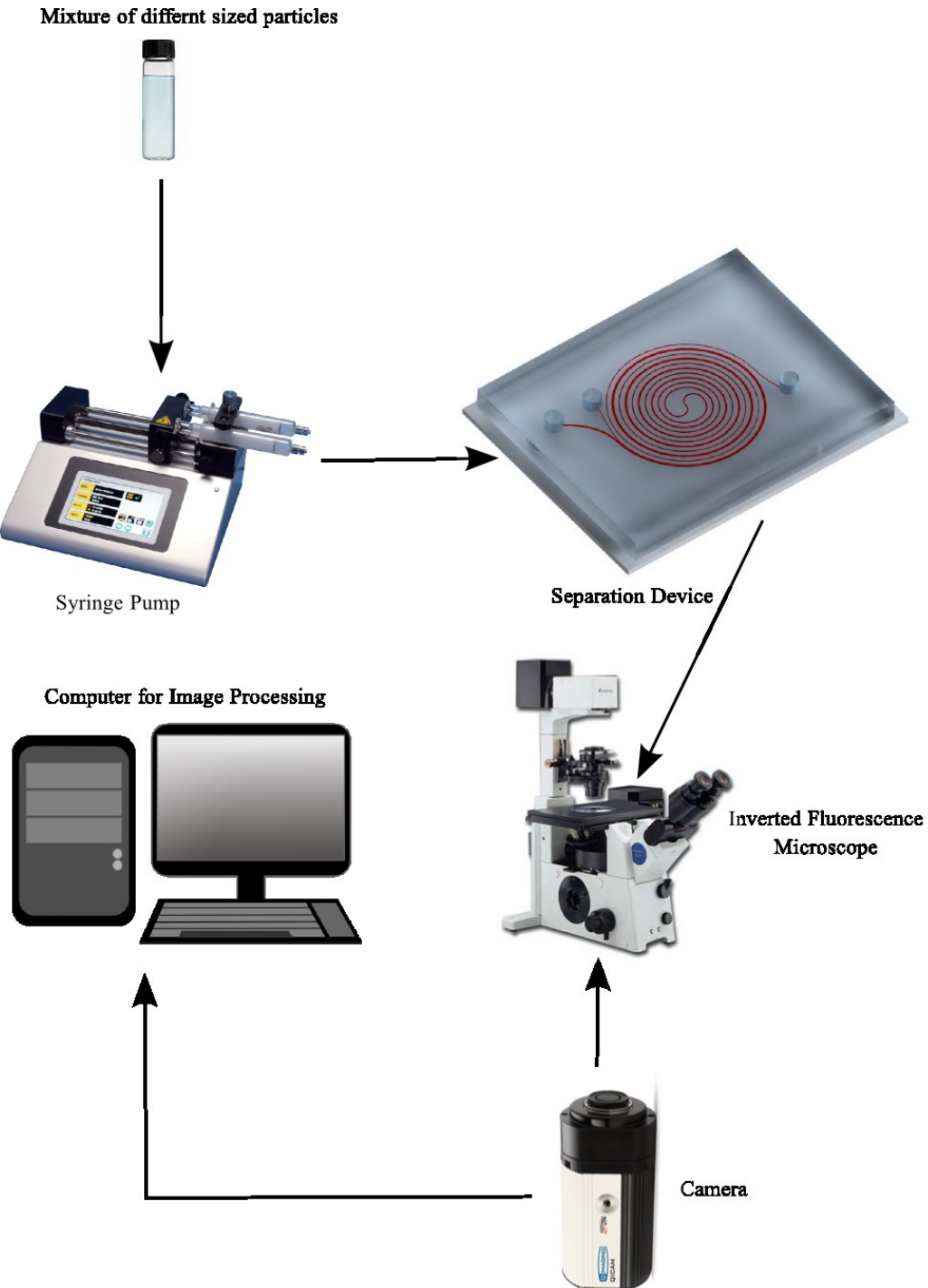


Figure 4-6 Experimental setup of the particle separation process

#### 4.3.3 Experimental results

The fluorescence images are taken at locations specified according to figure 3-21. The result is presented in figure 4-7. All the corresponding numerical results are placed below the experimental images to compare.

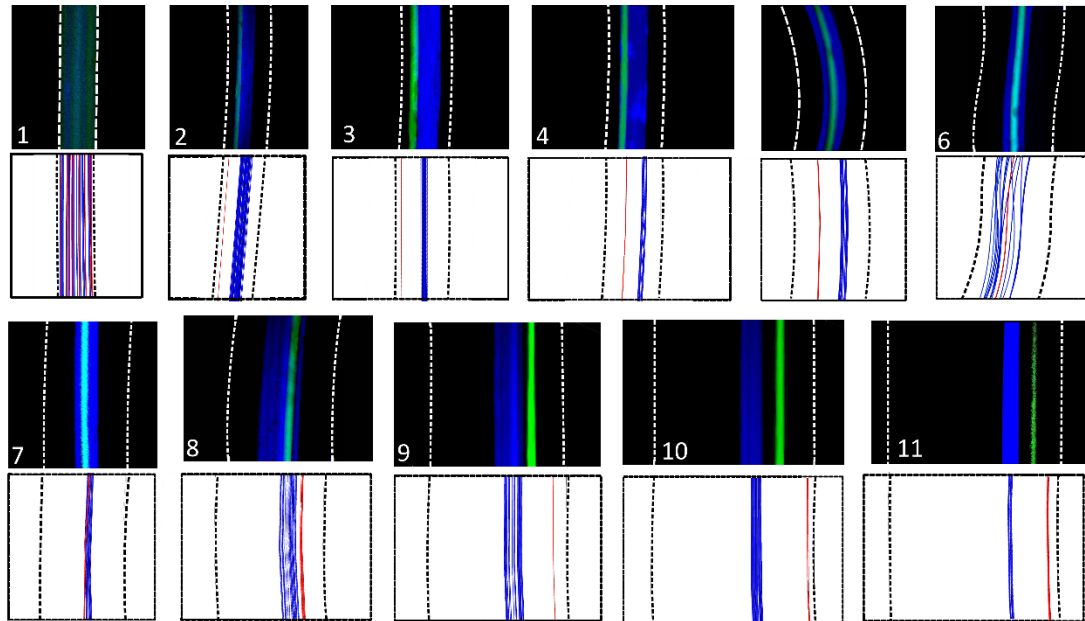


Figure 4-7 Experimental result presented with numerical simulation at different location of microchannel.

Figure 4-7 shows that two differently sized microparticles are evenly distributed at the inlet. As the particles proceeded towards the center junction, large  $9.94\mu\text{m}$  particles tend to get focused near the inner wall (see images 2-4), as observed by other researchers[37,53,69,72,75].  $4.5\mu\text{m}$  particles were more easily to follow the streamlines of Dean vortex[20,35,80,69,72]; as the flow progresses to the center, small particles also tended to find the equilibrium positions, but with a wider bandwidth (images 2- 4).

Along the flow direction, the controlled increment in Dean Drag force helps in maintaining the force balance without causing the breakdown of focused streak of large particles because of the use of gradually increasing channel width. Next, particles enter the S-junction at the center. In the 1st half circle, particles are focused in the streaks near the inner wall. At the 2nd half circle of the S-junction, the outer wall became the inner wall particle streaks are focused again toward the new inner wall. This helps in mitigating the dispersive effect of particles and assist in compacting the particle streak bandwidths,[39] as shown in images 6 and 7. After passing the S-junction, in the 2nd spiral microchannel, the Dean number decreases as a result of decreasing curvature and increasing channel width, causing a decrease in Dean number and Dean drag force[69,72,75]. Because of the reduced Dean effect becoming weak, the streak bandwidth of  $4.5\mu\text{m}$  particle, which were affected more by the Dean effect, gradually decreases along the flow direction, while the  $9.94\mu\text{m}$  particle streak remains the same (see images 8 to 11). At position 9, the two particle streaks are separated because of the different lateral equilibrium positions for different sized particles. At position 9, 10 and 11, the two streaks are completely separated with gradually increased separation distance. From the figure 4-7, it is evident that all the numerical and experimental results are in good agreement.

To find out the bandwidths of two particle streaks and the separation distance between them the fluorescence intensity is calculated via a line scan of the two fluorescent image captured at the position 11 neat the outlet using ImageJ (see Figure 4-8). The particle streak bandwidth is  $35\mu\text{m}$  and  $12\mu\text{m}$  for  $4.5\mu\text{m}$  and  $9.94\mu\text{m}$  particles, and the distance

between the two streaks (center to center) is approximately  $35\mu\text{m}$ . In comparison, Sun et al.[5] reported  $\sim 40\mu\text{m}$  separation distance between  $5\mu\text{m}$  and  $15\mu\text{m}$  particle streaks using a twelve-turn Fermat spiral microchannel a wider channel width of  $300\mu\text{m}$  at a lower flow rate ( $\sim 450\mu\text{L}/\text{min}$ ). It is expected that with the microchannel design a larger separation distance can be achieved if a larger channel width and channel length is used.

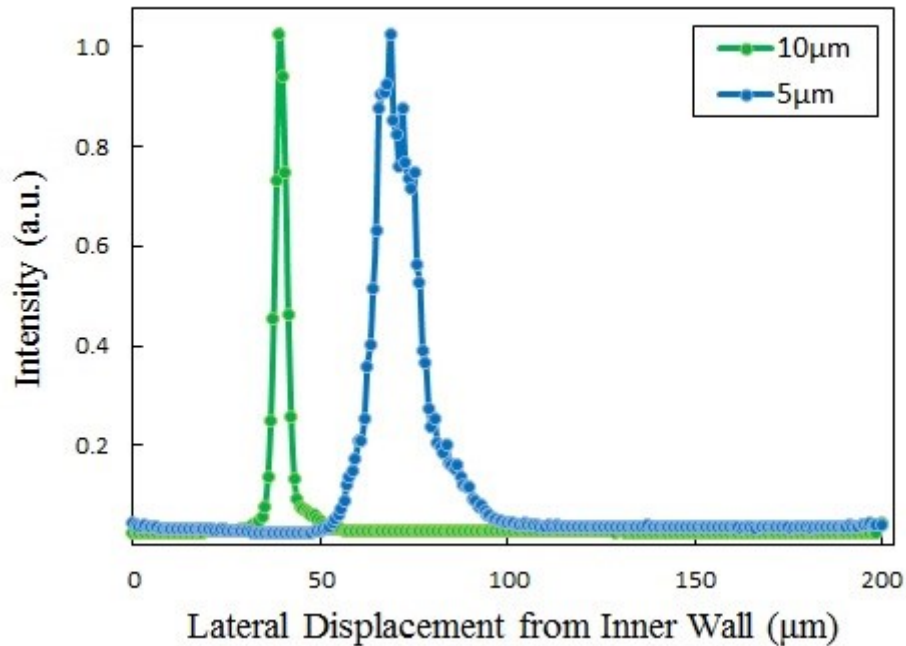


Figure 4-8 Line scan at the outlet of a differential Fermat spiral microchannel. The blue lines represent the streams of  $4.5\mu\text{m}$ , and the green lines represent the streams of  $9.94\mu\text{m}$  particles.

The simulation results are in good agreement with the experimental results at almost all observed locations of the microchannel, indicating that the numerical method can

accurately predict the particle trajectories. In order to prove the channel's particle separation capability at higher Reynolds numbers, next, numerical analysis was conducted at a flow rate of 1700  $\mu\text{L}/\text{min}$  ( $\text{Re}=250$ ). Note that the microchannel was made of PDMS bonded to the glass, which typically cannot withstand a high pressure [81] at a flow rate higher than 700 $\mu\text{L}/\text{min}$ . Mixture of different sized microparticles 5 $\mu\text{m}$ , 7 $\mu\text{m}$ , 8 $\mu\text{m}$ , 10 $\mu\text{m}$ , and 10 $\mu\text{m}$  was introduced in the inlet. Particle trajectories from the numerical work are shown in Figure 3-234-94-9, which shows all particles form distinct streaks with no overlap. The separation distance between the 10 $\mu\text{m}$  and 5 $\mu\text{m}$  particles was approximately 37 $\mu\text{m}$ . The separation distance can be larger if more spiral turns were used[20]. This result demonstrates that the present microchannel has the capability of separating microparticles with 1 $\mu\text{m}$  diameter difference at a high Reynolds number ( $\text{Re}=250$ ).

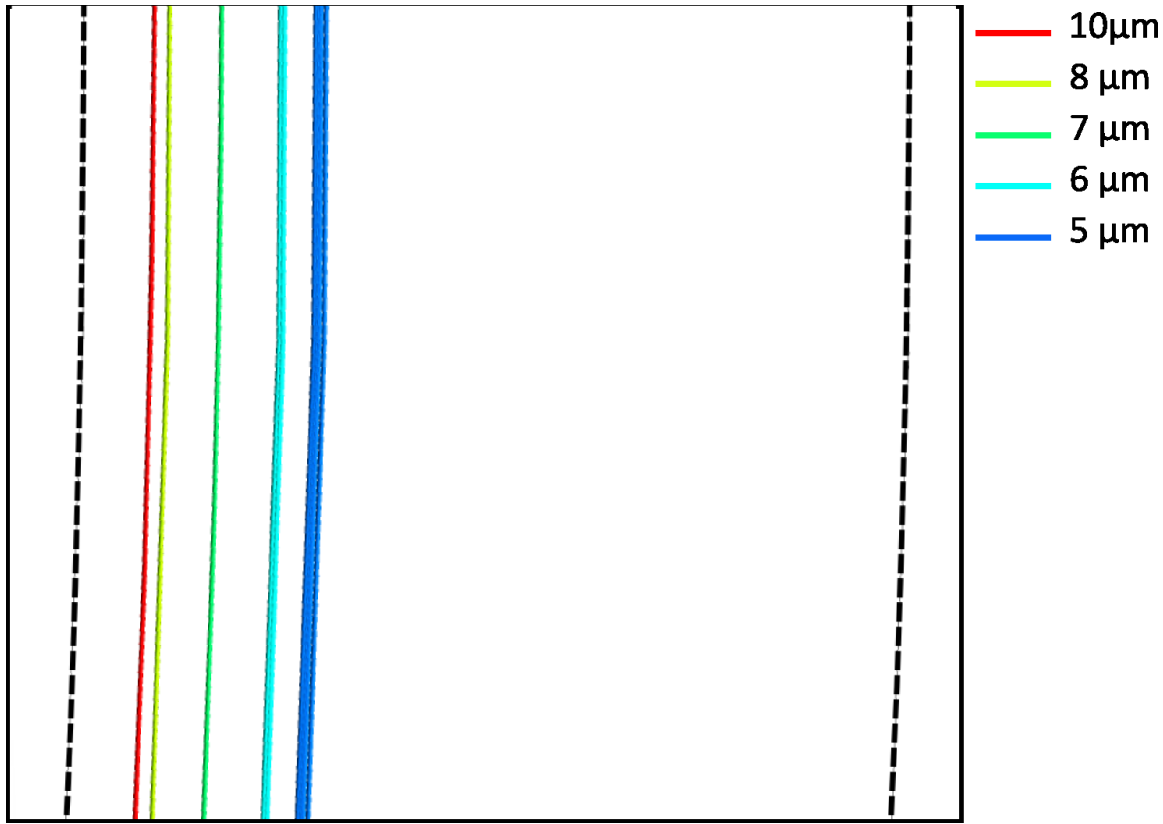


Figure 4-9 Simulation result of mixture of five different sized diameter particles.

The above experimental and numerical work demonstrates the differential Fermat spiral microchannel with variable channel width is able to focus and separate microparticles as small as 4.5  $\mu\text{m}$  by size with high resolution and high throughput. Compared to the conventionally used Archimedean spiral microchannel, the use of differential Fermat spiral enables narrower particle streak bandwidth by taking the advantage of the variable channel width and the central S-shaped features at the center. Compared to the spiral microchannels with constant cross section, the use of the present spiral microchannel with gradually increasing channel width avoids sharp increase of Dean

drag force, which avoid breakdown of focused particle streaks, helps in narrowing the bandwidth of small particles at higher flow rates and higher Reynolds numbers.

The widely accepted notion for particle focusing is that the particle diameter to hydraulic diameter ratio ( $a_p/D_h$ ) in other words particle confinement ratio should be greater than 0.07[18,44]. While the minimum hydraulic diameter of the fabricated channel is 56  $\mu\text{m}$ , the minimum diameter of particles that can be focused by the present microchannel is approximately 4 $\mu\text{m}$ . To focus or separate smaller particles, the channel dimension can be reduced, but this may also cause the clogging of channels by large particles, and the decrease in separation distance of particle streaks.

To increase the separation distance between the two particle streams, increasing the number of spiral turns would be helpful as different researchers has observed the migration of particles towards the channel center[20,69]. Also, as reported by Martel et al.[72] depending on particle confinement ratio, focusing position is different. Therefore a careful selection in channel height for target particle could increase the separation distance between two streams.

## 4.4 Future work

Particle separation is currently one of the most talked areas in bio-microfluidics region.

A successful demonstration of particle separation using a differential Fermat Spiral microchannel is presented in this thesis. Due to the leakage problem, the thesis lacks the experimental results at high flow rate such as  $1700\mu\text{L}/\text{min}$ . Also, the final goal of any particle separation device is the bio-particle sorting, separation and biological assessments. Therefore there are numerous areas where the future work can be focused. In the following two sections, these scopes are discussed, and a tentative guideline is elaborated.

### 4.4.1 Bioparticle separation

The differential Fermat spiral device has proved effective and efficient for polystyrene microspheres. The separation at higher flow rate ( $\sim 700\mu\text{L}/\text{min}$ ) was experimentally demonstrated. It was also numerically demonstrated that the device is capable of working at flow rate ( $\sim 1700\mu\text{L}/\text{min}$ ). Next the device can be tested with biological specimens such as blood cells. The biological cells widely vary in dimensions. If the effective separation of the cells are required, tradeoff between flow rate and separation efficiency needs to be considered. Also, the blood is a non-Newtonian fluid and particles suspended in blood serum might act differently than a DI water-polystyrene system.

Besides, the variation of the channel width from inlet to outlet might be an area of future studies. By what gradient the area should be varied is yet to be discovered. Investigations of how the force ratio changes and how the particle focusing dynamics behaves with different varying area should help design devices with higher flow rate and throughput.

#### 4.4.2 TPE-Glass microfluidic system.

The device is characterized on a PDMS-Glass substrate. The pressure that the system can withstand is erratic[81], difficult to predict and vary rapidly depending on the curing condition. Hence, an alternative system that is capable of withstanding higher pressure. Thermosetting polymer elastomer (TPE) might be a good option to fabricate such system that is reported to withstand 150psi[81].

In an attempt to explore the feasibility of TPE, fabrication effort was performed to develop a TPE-glass system. The most favorable procedure among several available techniques[77,78,81,82] is described below:

Unlike PDMS, TPE is hard and not flexible. Therefore preparation of TPE mold out of the silicon wafer is impossible. Instead, a PDMS mold is prepared as die pattern. The preparation of pattern die is similar to standard PDMS mold preparation. Next the TPE solution is prepared (figure 4-10)

- i. TPE is prepared by mixing 10g of resin (Reichhold) with 0.25g cross linker Styrene monomer(Sigma-Aldrich) and 0.1g of photo initiator (2,2-dimethoxyphenylacetophenone).
- ii. Next three drops (~0.09g) of MEKP is added to the mixture and the mix is stirred at 2500 rpm on a vacuum mixer to avoid mix-up of air bubbles.
- iii. Following the vacuum mixing, the solution is then poured into the PDMS mold.
- iv. Necessary steel rods are placed at locations where microfluidic fittings are to be inserted.
- v. The mixture is then exposed to UV light for 15 mins (15W 365nm UV bulbs)
- vi. After UV cure, the PDMS is then peeled off, and both TPE and glass slide is exposed to oxygen plasma.
- vii. The TPE chip is then aligned on top of the glass slide and kept at room temperature for 12 hours to create bonding.

The chip fabrication is successful but when the particle mixture ran through the microchannel, the spacing between the adjacent channels leaked because of insufficient spacing between them. The spacing between the channels can be increased, to improve the design so that the bonding become stronger. After successful fabrication of TPE-Glass device, particle separation data at high flow rate would be available. However, after several unsuccessful attempts the procedures required more attention and is subsequently postponed because of insufficient time.

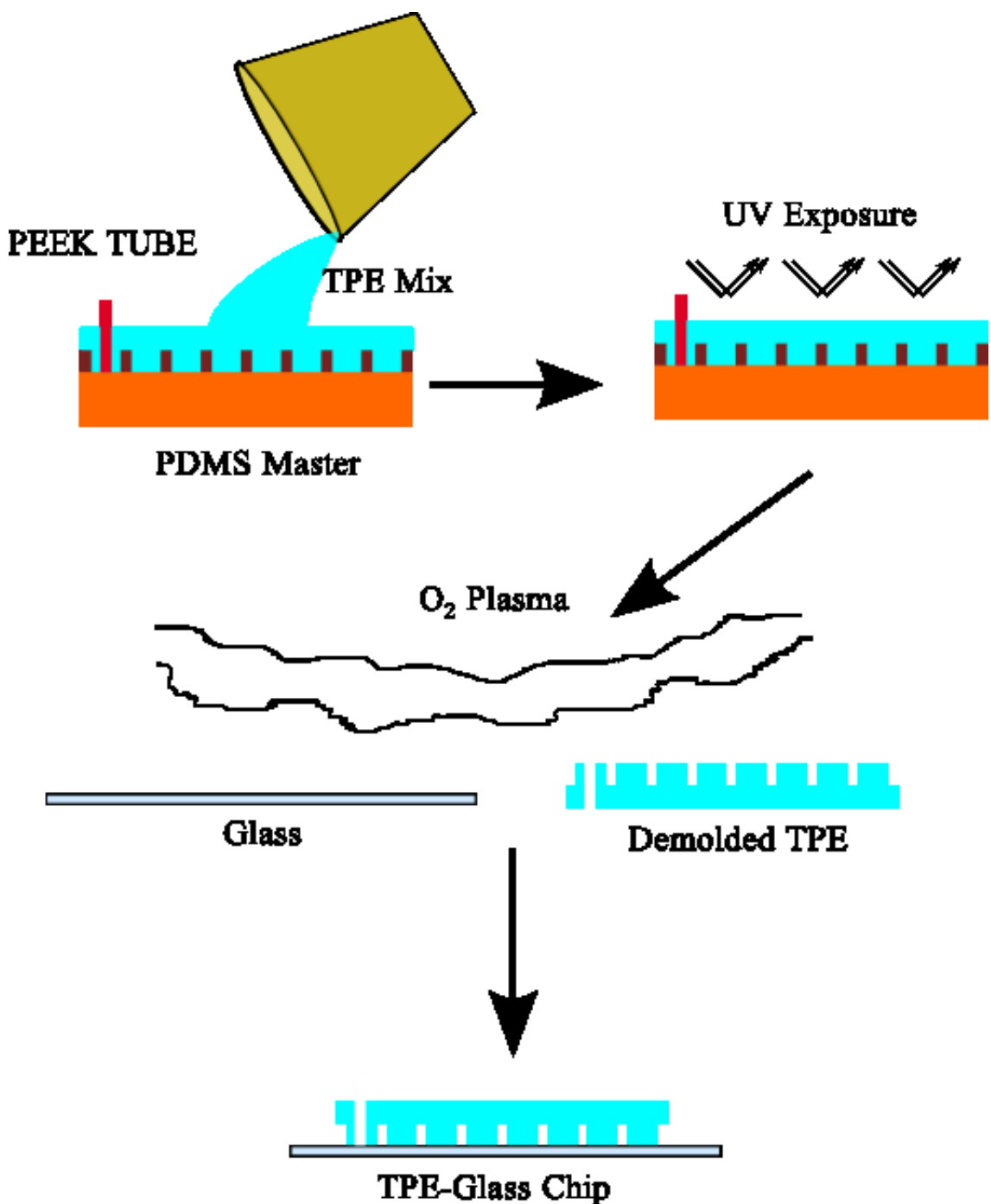


Figure 4-10 TPE Glass microchip fabrication flow chart.

## CHAPTER V

### CONCLUSION

In this work, a differential Fermat's spiral microchannel with gradually increasing channel width for high throughput microparticle separation is presented. Compared to the conventional Archimedean spiral microchannels with constant cross section, the use of the present spiral microchannel with gradually increasing channel width mitigates sharp increase of Dean drag force, which avoid breakdown of focused particle streaks, helps in narrowing the bandwidth of small particles at higher flow rates and higher Reynolds numbers. The use of the S-shape junction at the center of the microchannel mitigates against dispersion and diffusion effects of particle motions and also assists in compacting the bandwidth of focused particle streaks. Experiments showed that the microchannel can successfully separate 4.5  $\mu\text{m}$  and 9.94  $\mu\text{m}$  microparticles at a flow rate of 700  $\mu\text{L}/\text{min}$  ( $\text{Re} = 90$ ); this flow rate is nearly double the flow rate of the recently reported double spiral microparticle separator[5,70]. The particle stream bandwidth was 35  $\mu\text{m}$  and 12  $\mu\text{m}$ , the separation distance between the two particles streams was 35  $\mu\text{m}$ .

The device was attempted to be tested at a flow rate higher than 700 $\mu$ L/min to demonstrate the functionality at even higher flow rate. Unfortunately, at a flow rate higher than 700 $\mu$ L/min the pressure built up in the microchannel exceeded the pressure limit that PDMS-Glass system can withstand, [81] causing the leakage problem. To prove the microchannel's capability for particle separation, the microfluidics system is simulated using the modeling software package ANSYS at higher flow rate. Numerical results showed that the DFS particle separator can work at even higher flow rate (1700 $\mu$ L/min) and a Reynolds number of 250; distinguishable streams of 5, 7, 8, 9 and 10 $\mu$ m particles are formed at the outlet. Hence, the device is expected to function at 1700 $\mu$ L/min for a mixture of five different particles with high separation efficiency.

While the smallest particles used in the experiments were 4.5 $\mu$ m in diameter, particles smaller than 4.5 $\mu$ m can also be separated if the channel height is designed smaller such that for the particle confinement ratio falls above 0.07.. Furthermore, the separation distance between the two particle streaks can be achieved by increasing number of spiral turns and adjusting the particle confinement ratio as observed by Martel et al[72].

With the advantages of narrower focused particle stream, larger separation distance, free-of clogging, and its capability of separating microparticles at large Reynolds numbers with higher resolution, this passive particle separation has potentials to be

used in a variety of biomedical and lab-on-a-chip applications such as cellular analysis, clinical diagnostics and microbiological processes.

## BIBLIOGRAPHY

- [1] Wei Hou H, Gan H Y, Bhagat A A S, Li L D, Lim C T and Han J 2012 A microfluidics approach towards high-throughput pathogen removal from blood using margination *Biomicrofluidics* **6** 024115–024115–13
- [2] Wu Z, Willing B, Bjerketorp J, Jansson J K and Hjort K 2009 Soft inertial microfluidics for high throughput separation of bacteria from human blood cells *Lab. Chip* **9** 1193
- [3] Zare R N and Kim S 2010 Microfluidic Platforms for Single-Cell Analysis *Annu. Rev. Biomed. Eng.* **12** 187–201
- [4] Nivedita N, Ligrani P and Papautsky I 2012 Spiral inertial microfluidic devices for continuous blood cell separation *SPIE MOEMS-MEMS* p 82510R–82510R
- [5] Sun J, Li M, Liu C, Zhang Y, Liu D, Liu W, Hu G and Jiang X 2012 Double spiral microchannel for label-free tumor cell separation and enrichment *Lab. Chip*
- [6] Tsukamoto M, Taira S, Yamamura S, Morita Y, Nagatani N, Takamura Y and Tamiya E 2009 Cell separation by an aqueous two-phase system in a microfluidic device *Analyst* **134** 1994–8
- [7] Czechowska K, Johnson D R and van der Meer J R 2008 Use of flow cytometric methods for single-cell analysis in environmental microbiology *Curr. Opin. Microbiol.* **11** 205–12
- [8] Xia N, Hunt T P, Mayers B T, Alsberg E, Whitesides G M, Westervelt R M and Ingber D E 2006 Combined microfluidic-micromagnetic separation of living cells in continuous flow *Biomed. Microdevices* **8** 299–308
- [9] Cheng I F, Froude V E, Zhu Y, Chang H C and Chang H C 2009 A continuous high-throughput bioparticle sorter based on 3D traveling-wave dielectrophoresis *Lab Chip* **9** 3193–201
- [10] Akagi T and Ichiki T 2008 Cell electrophoresis on a chip: what can we know from the changes in electrophoretic mobility? *Anal. Bioanal. Chem.* **391** 2433–41

- [11] Guldiken R, Jo M C, Gallant N D, Demirci U and Zhe J 2012 Sheathless Size-Based Acoustic Particle Separation *Sensors* **12** 905–22
- [12] Shi J, Ahmed D, Mao X, Lin S C., Lawit A and Huang T J 2009 Acoustic tweezers: patterning cells and microparticles using standing surface acoustic waves (SSAW) *Lab. Chip* **9** 2890–5
- [13] Morijiri T, Sunahiro S, Senaha M, Yamada M and Seki M 2011 Sedimentation pinched-flow fractionation for size- and density-based particle sorting in microchannels *Microfluid. Nanofluidics* **11** 105–10
- [14] Srivastav A, Podgorski T and Coupier G 2012 Efficiency of size-dependent particle separation by pinched flow fractionation *Microfluid. Nanofluidics* 1–5
- [15] Fan L-L, He X-K, Han Y, Du L, Zhao L and Zhe J 2014 Continuous size-based separation of microparticles in a microchannel with symmetric sharp corner structures *Biomicrofluidics* **8** 024108
- [16] Zhang J, Yan S, Sluyter R, Li W, Alici G and Nguyen N-T 2014 Inertial particle separation by differential equilibrium positions in a symmetrical serpentine micro-channel *Sci. Rep.* **4**
- [17] Matsuda M, Yamada M and Seki M 2011 Blood cell classification utilizing hydrodynamic filtration *Electron. Commun. Jpn.* **94** 1–6
- [18] Bhagat A A S, Kuntaegowdanahalli S S and Papautsky I 2008 Continuous particle separation in spiral microchannels using dean flows and differential migration *Lab. Chip* **8** 1906
- [19] Di Carlo D, Edd J F, Irimia D, Tompkins R G and Toner M 2008 Equilibrium Separation and Filtration of Particles Using Differential Inertial Focusing *Anal. Chem.* **80** 2204–11
- [20] Russom A, Gupta A K, Nagrath S, Carlo D D, Edd J F and Toner M 2009 Differential inertial focusing of particles in curved low-aspect-ratio microchannels *New J. Phys.* **11** 075025
- [21] Yoon D H, Ha J B, Bahk Y K, Arakawa T, Shoji S and Go J S 2008 Size-selective separation of micro beads by utilizing secondary flow in a curved rectangular microchannel *Lab Chip* **9** 87–90
- [22] Choi S, Song S, Choi C and Park J K 2007 Continuous blood cell separation by hydrophoretic filtration *Lab Chip* **7** 1532–8

- [23] Chen Z, Zhang S, Tang Z, Xiao P, Guo X and Lu Z 2006 Pool-dam structure based microfluidic devices for filtering tumor cells from blood mixtures *Surf. Interface Anal.* **38** 996–1003
- [24] Sethu P, Sin A and Toner M 2006 Microfluidic diffusive filter for apheresis (leukapheresis) *Lab. Chip* **6** 83–9
- [25] Zhu L, Zhang Q, Feng H, Ang S, Chau F S and Liu W T 2004 Filter-based microfluidic device as a platform for immunofluorescent assay of microbial cells *Lab Chip* **4** 337–41
- [26] Pamme N 2007 Continuous flow separations in microfluidic devices *Lab. Chip* **7** 1644–59
- [27] Rutledge E M, Wilding L P and Elfield M 1967 Automated particle-size separation by sedimentation *Soil Sci. Soc. Am. J.* **31** 287–8
- [28] Wang X-B, Yang J, Huang Y, Vykoukal J, Becker F F and Gascogne P R 2000 Cell separation by dielectrophoretic field-flow-fractionation *Anal. Chem.* **72** 832–9
- [29] Khoshmanesh K, Nahavandi S, Baratchi S, Mitchell A and Kalantar-zadeh K 2011 Dielectrophoretic platforms for bio-microfluidic systems *Biosens. Bioelectron.* **26** 1800–14
- [30] Dean W R 1928 Fluid Motion in a Curved Channel *Proc. R. Soc. Lond. Ser. Contain. Pap. Math. Phys. Character* **121** 402–20
- [31] Hasni A E, Göbbels K, Thiebes A L, Bräunig P, Mokwa W and Schnakenberg U 2011 Focusing and Sorting of Particles in Spiral Microfluidic Channels *Procedia Eng.* **25** 1197–200
- [32] Bhagat A A S, Bow H, Hou H W, Tan S J, Han J and Lim C T 2010 Microfluidics for cell separation *Med. Biol. Eng. Comput.* **48** 999–1014
- [33] Lenshof A and Laurell T 2010 Continuous separation of cells and particles in microfluidic systems *Chem. Soc. Rev.* **39** 1203
- [34] Oakey J, Applegate Jr R W, Arellano E, Carlo D D, Graves S W and Toner M 2010 Particle focusing in staged inertial microfluidic devices for flow cytometry *Anal. Chem.* **82** 3862–7
- [35] Kuntaegowdanahalli S S, Bhagat A A S, Kumar G and Papautsky I 2009 Inertial microfluidics for continuous particle separation in spiral microchannels *Lab. Chip* **9** 2973

- [36] Lee W C, Bhagat A A S, Huang S, Van Vliet K J, Han J and Lim C T 2011 High-throughput cell cycle synchronization using inertial forces in spiral microchannels *Lab. Chip* **11** 1359
- [37] Xiang N, Chen K, Sun D, Wang S, Yi H and Ni Z Quantitative characterization of the focusing process and dynamic behavior of differently sized microparticles in a spiral microchannel *Microfluid. Nanofluidics* 1–11
- [38] Seo J, Lean M H and Kole A 2007 Membraneless microseparation by asymmetry in curvilinear laminar flows *J. Chromatogr. A* **1162** 126–31
- [39] Seo J, Lean M H and Kole A 2007 Membrane-free microfiltration by asymmetric inertial migration *Appl. Phys. Lett.* **91** 033901
- [40] Guan G, Wu L, Bhagat A A, Li Z, Chen P C Y, Chao S, Ong C J and Han J 2013 Spiral microchannel with rectangular and trapezoidal cross-sections for size based particle separation *Sci. Rep.* **3**
- [41] Park J-S, Song S-H and Jung H-I 2009 Continuous focusing of microparticles using inertial lift force and vorticity via multi-orifice microfluidic channels *Lab. Chip* **9** 939
- [42] Kersaudy-Kerhoas M, Dhariwal R and Desmulliez M P Y 2008 Recent advances in microparticle continuous separation *IET Nanobiotechnol.* **2** 1–13
- [43] Sollier E, Rostaing H, Pouteau P, Fouillet Y and Achard J-L 2009 Passive microfluidic devices for plasma extraction from whole human blood *Sens. Actuators B Chem.* **141** 617–24
- [44] Carlo D D, Irimia D, Tompkins R G and Toner M 2007 Continuous Inertial Focusing, Ordering, and Separation of Particles in Microchannels *Proc. Natl. Acad. Sci.* **104** 18892–7
- [45] Gregoratto I, McNeil C J and Reeks M W 2007 Micro-Device for Rapid Separation of Suspensions for Use in Micro-Total-Analysis-Systems ( $\mu$ TAS) *ASME Conf. Proc.* **2007** 1079–85
- [46] Kuntaegowdanahalli S S, Bhagat A and Papautsky I 2009 Continuous multi-particle separation using deterministic focusing in spiral microchannels *Solid-State Sensors, Actuators and Microsystems Conference, 2009. TRANSDUCERS 2009. International Solid-State Sensors, Actuators and Microsystems Conference, 2009. TRANSDUCERS 2009. International* pp 2139 –2142
- [47] Bhagat A A S, Kuntaegowdanahalli S S and Papautsky I 2008 Enhanced particle filtration in straight microchannels using shear-modulated inertial migration *Phys. Fluids* **20** 101702

- [48] Kagalwala T E, Zhou J and Papautsky I 2011 Continuous Size-Based Separation of Microparticles in Straight Channels
- [49] Hansson J, Karlsson J M, Haraldsson T, Brismar H, van der Wijngaart W and Russom A 2012 Inertial microfluidics in parallel channels for high-throughput applications *Lab. Chip* **12** 4644
- [50] Nieuwstadt H A, Seda R, Li D S, Fowlkes J B and Bull J L 2010 Microfluidic particle sorting utilizing inertial lift force *Biomed. Microdevices* **13** 97–105
- [51] Zhou J, Giridhar P V, Kasper S and Papautsky I 2013 Modulation of aspect ratio for complete separation in an inertial microfluidic channel *Lab. Chip* **13** 1919
- [52] Dutz S, Hayden M E, Schaap A, Stoeber B and Häfeli U O 2012 A microfluidic spiral for size-dependent fractionation of magnetic microspheres *J. Magn. Magn. Mater.* **324** 3791–8
- [53] Xiang N, Chen K, Dai Q, Jiang D, Sun D and Ni Z Inertia-induced focusing dynamics of microparticles throughout a curved microfluidic channel *Microfluid. Nanofluidics* **1**–11
- [54] Wu L, Guan G, Hou H W, Bhagat A A S and Han J 2012 Separation of Leukocytes from Blood Using Spiral Channel with Trapezoid Cross-Section *Anal. Chem.* **121012151628004**
- [55] Lim E J, Ober T J, Edd J F, McKinley G H and Toner M 2012 Visualization of microscale particle focusing in diluted and whole blood using particle trajectory analysis *Lab. Chip* **12** 2199
- [56] Whitesides G M 2006 The origins and the future of microfluidics *Nature* **442** 368–73
- [57] Stott S L, Hsu C-H, Tsukrov D I, Yu M, Miyamoto D T, Waltman B A, Rothenberg S M, Shah A M, Smas M E, Korir G K and others 2010 Isolation of circulating tumor cells using a microvortex-generating herringbone-chip *Proc. Natl. Acad. Sci.* **107** 18392–7
- [58] Yu M, Ting D T, Stott S L, Wittner B S, Ozsolak F, Paul S, Ciciliano J C, Smas M E, Winokur D, Gilman A J and others 2012 RNA sequencing of pancreatic circulating tumour cells implicates WNT signalling in metastasis *Nature*
- [59] Miyamoto D T, Lee R J, Stott S L, Ting D T, Wittner B S, Ulman M, Smas M E, Lord J B, Brannigan B W, Trautwein J and others 2012 Androgen receptor signaling in circulating tumor cells as a marker of hormonally responsive prostate cancer *Cancer Discov.* **2** 995–1003

- [60] Stott S L, Lee R J, Nagrath S, Yu M, Miyamoto D T, Ulkus L, Inserra E J, Ulman M, Springer S, Nakamura Z and others 2010 Isolation and characterization of circulating tumor cells from patients with localized and metastatic prostate cancer *Sci. Transl. Med.* **2** 25ra23–25ra23
- [61] Asmolov E S 1999 The inertial lift on a spherical particle in a plane Poiseuille flow at large channel Reynolds number *J. Fluid Mech.* **381** 63–87
- [62] Segre G and Silberberg A 1962 Behaviour of macroscopic rigid spheres in Poiseuille flow Part 2. Experimental results and interpretation *J. Fluid Mech.* **14** 136–57
- [63] Segré G and Silberberg A 1961 Radial Particle Displacements in Poiseuille Flow of Suspensions *Publ. Online 21 January 1961 Doi101038189209a0* **189** 209–10
- [64] Cox R G and Hsu S K 1977 The lateral migration of solid particles in a laminar flow near a plane *Int. J. Multiph. Flow* **3** 201–22
- [65] Matas J-P, Morris J F and Guazzelli Élisabeth 2004 Inertial migration of rigid spherical particles in Poiseuille flow *J. Fluid Mech.* **515** 171–95
- [66] Di Carlo D 2009 Inertial microfluidics *Lab. Chip* **9** 3038
- [67] Ookawara S, Higashi R, Street D and Ogawa K 2004 Feasibility study on concentration of slurry and classification of contained particles by microchannel *Chem. Eng. J.* **101** 171–8
- [68] Ookawara S, Street D and Ogawa K 2006 Numerical study on development of particle concentration profiles in a curved microchannel *Chem. Eng. Sci.* **61** 3714–24
- [69] Martel J M and Toner M 2012 Inertial focusing dynamics in spiral microchannels *Phys. Fluids* **24** 032001
- [70] Sun J, Liu C, Li M, Wang J, Xianyu Y, Hu G and Jiang X 2013 Size-based hydrodynamic rare tumor cell separation in curved microfluidic channels *Biomicrofluidics* **7** 011802
- [71] Nivedita N, Ligrani P and Papautsky I 2012 Spiral inertial microfluidic devices for continuous blood cell separation 82510R–82510R
- [72] Martel J M and Toner M 2013 Particle Focusing in Curved Microfluidic Channels *Sci. Rep.* **3**
- [73] Geng Z, Ju Y, Wang W and Li Z 2012 Continuous blood separation utilizing spiral filtration microchannel with gradually varied width and micro-pillar array *Sens. Actuators B Chem.*

- [74] Martel J M 2014 Particle Focusing in Microchannels
- [75] Martel J M and Toner M 2014 Inertial Focusing in Microfluidics *Annu. Rev. Biomed. Eng.* **16** 371–96
- [76] Morsi S A and Alexander A J 1972 An investigation of particle trajectories in two-phase flow systems *J. Fluid Mech.* **55** 193–208
- [77] Lei W 2004 Development and applications of hard microstamping
- [78] Steigert J, Haeberle S, Brenner T, Müller C, Steinert C P, Koltay P, Gottschlich N, Reinecke H, Rühe J and Zengerle R 2007 Rapid prototyping of microfluidic chips in COC *J. Micromechanics Microengineering* **17** 333
- [79] Schneider C A, Rasband W S and Eliceiri K W 2012 NIH Image to ImageJ: 25 years of image analysis *Nat. Methods* **9** 671–5
- [80] Nivedita N and Papautsky I 2013 Continuous separation of blood cells in spiral microfluidic devices *Biomicrofluidics* **7** 054101
- [81] Sollier E, Murray C, Maoddi P and Di Carlo D 2011 Rapid prototyping polymers for microfluidic devices and high pressure injections *Lab. Chip* **11** 3752–65
- [82] Vickers J A, Dressen B M, Weston M C, Boonsong K, Chailapakul O, Cropek D M and Henry C S 2007 Thermoset polyester as an alternative material for microchip electrophoresis/electrochemistry *ELECTROPHORESIS* **28** 1123–9

## APPENDIX

### User Defined Function

```
/* UDF for computing the lateral displacement of particle suspended in fluid flow*/
#include "udf.h"

#include "mem.h"      /* cell indexing header */
#include "dpm.h"      /* particle properties even though declared in the macro
arguments */

#include <math.h>

DEFINE_DPM_BODY_FORCE(asmolov_lift,p,i)

{

/* declaration of variables */

double w, Dh, Ufx, Ufy, Ufz, Gx, Gy, Gz, rho, a, Fx, Fy, Fz, FL, c_height, c_length,
c_volume, side, height, width, f_height_total, Renx, Reny, Renz, crDh, mu, aUfx, aUfy,
aUfz, Clx, Cly, Clz;

cell_t c = P_CELL(p); /* the cell initialization in which the particle is present*/
Thread *t = P_CELL_THREAD(p); /* thread initialization */

c_volume = C_VOLUME(c,t);

c_height = 0.00001; /* these values varies depending upon mesh cell sizes*/
```

```

c_length = 0.00015; /* these values varies depending upon mesh cell sizes*/

side = c_volume/(c_height*c_length); /* calculating the width of mesh cell for Dh
calculations*/
height = 0.00005;
width = 12*side;

Dh = 4*(height*width)/(2*(height+width));

crDh = pow(c_volume, (1./3.));

mu = 0.001003;

rho = C_R(c,t);
Ufx = C_U(c,t);
Ufy = C_V(c,t);
Ufz = C_W(c,t);

aUfx = fabs(Ufx);
aUfy = fabs(Ufy);
aUfz = fabs(Ufz);

/* local Reynolds number calculation*/
Renx = (rho*aUfx*crDh)/mu;
Reny = (rho*aUfy*crDh)/mu;

```

```

Renx = (rho*aUfz*crDh)/mu;

if(Renx<15.)
    Clx = 0.5;
else
    Clx = 3.4368*(pow(Renx, -0.714));

if(Reny<15.)
    Cly = 0.5;
else
    Cly = 3.4368*(pow(Reny, -0.714));

if(Renz<15.)
    Clz = 0.5;
else
    Clz = 3.4368*(pow(Renz, -0.714));

Gx = (Ufx)/Dh;
Gy = (Ufy)/Dh;
Gz = (Ufz)/Dh;

a = P_DIAM(p);           /* particle diameter */

Fx = Clx*rho*pow(Gx,2)*pow(a,4);
Fy = Cly*rho*pow(Gy,2)*pow(a,4);
Fz = Clz*rho*pow(Gz,2)*pow(a,4);

```

```
if (i==0)
    FL = (Fy+Fz);      /* resultant of shear rate tensor*/
else if (i==1)
    FL = (Fx+Fz);
else if (i==2)
    FL = Fx+Fy;
else
    FL = 0;

return (FL/P_MASS(p));
}
```